2022

Filtration and Adsorption Performance of Activated Carbon Fiber: Applications for Respiratory Protection

Margaret C. Summers
University Of Alabama At Birmingham

FILTRATION AND ADSORPTION PERFORMANCE OF ACTIVATED CARBON FIBER: APPLICATIONS FOR RESPIRATORY PROTECTION

by

MARGARET C. SUMMERS

CLAUDIU LUNGU, COMMITTEE CHAIR
JO ANNE BALANAY
EVAN FLOYD
JONGHWA OH
PATRICK O'SHAUGHNESSY
KRISTINA ZIEROLD

A DISSERTATION

Submitted to the graduate faculty of The University of Alabama at Birmingham,
in partial fulfillment of the requirements for the degree of
Doctor of Philosophy

BIRMINGHAM, ALABAMA

2022

FILTRATION AND ADSORPTION PERFORMANCE OF ACTIVATED CARBON FIBER: APPLICATIONS FOR RESPIRATORY PROTECTION

MARGARET C. SUMMERS

ENVIRONMENTAL HEALTH SCIENCES

ABSTRACT

Activated Carbon Fiber (ACF) is an adsorbent material that can be used to remove volatile organic compounds (VOCs) from the air. Unlike granular adsorbents that are currently used in organic vapor respirators, ACF is a self-supporting fiber structure that can be tailored into non-woven forms and can potentially be used to support particulate filtration. While ACF-containing respirators first appear in patent literature in the 1980s, the use of ACF in respiratory protection has not been widely considered in the PPE market in the intervening years.

To develop the concept of an ACF-containing N95 that offers particulate filtration in addition to nuisance-level or short-term VOC protection, the filtration and adsorption behavior of three "off-the-shelf" ACFs (ACFF 1200, ACFF 1800, and ACFF 2000) was determined using flow conditions and challenge concentrations that are relevant to respiratory protection devices. In order to describe ACF properties that are relevant to adsorption, each ACF was characterized in terms of specific surface area, limiting micropore volume, bulk density, characteristic energy of adsorption, and equilibrium adsorption capacity. ACF performance was also compared to performance of a thin carbon adsorbent that is currently used in nuisance odor particulate respirators. We found that ACFF 1200, the lowest surface area ACF used by our laboratory, had greater 10% breakthrough times for a 200 ppm challenge of toluene, hexane and MEK (respectively) than the nuisance odor adsorbent from a commercially available respirator (3M™ 2097).

Our filtration studies indicate that ACF can be predictably layered to yield greater filtration efficiency; however, in their current form, the ACFs used by our laboratory likely pose too great a pressure drop to be used as the exclusive filtration medium in an N95 respirator when tested according to NIOSH standard test protocol. In general, these results suggest that ACF is best suited as an adjunct to, rather than the primary means of filtration in an N95 respirator.

In conclusion, our studies demonstrate that ACF has properties (i.e., high specific surface area (m^2/g), high adsorption capacity, and rapid adsorption kinetics) that make it a good candidate for use in thin, N95-style respirators for nuisance-level VOCs.

Keywords: Activated carbon fiber, adsorption, filtration, personal protective equipment

ACKNOWLEDGMENTS

First of all, thanks so much to my Academic Advisory Committee for their patience and flexibility with me while I've dealt with life, work, and circumstances over the past several years. I would especially like to acknowledge the following people for their support:

- Dr. Claudiu Lungu, my academic advisor, who gave me the opportunity to pursue a great new career 6 years ago.
- Dr. Jonghwa Oh, who is always a source of practical help and an excellent teacher.
- Dr. Patrick O'Shaughnessy and University of Iowa for serving on my committee and arranging filter testing of my materials at the State Hygienic Laboratory at the University of Iowa. Also thanks to Ridwan Nahar and Dr. Adam Hauser at the Department of Physics, University of Alabama in Tuscaloosa, for allowing me to use their new Apreo scanning electron microscope.
- Committee Members Dr. Evan Floyd, Dr. Kristina Zierold, and Dr. Jo Anne Balanay for their helpful comments during the preparation of my dissertation.
- Fellow graduate students Jake Shedd, Adam Nored, Jordan Roberts, Bunmi Dada, and Nathan Chen for their moral support and encouragement.
- The entire Department of Environmental Health Sciences, but *especially* Paulisha Holt, Allyn Holliday, Tara Fields, and Julie Brown.

This research was funded by National Institute of Occupational Safety and Health (NIOSH) Grant #5T42OH008436-17.

TABLE OF CONTENTS

Page

LIST OF TABLES

LIST OF FIGURES

LIST OF ABBREVIATIONS

(Entries are listed alphabetically)

ACF	Activated carbon fiber
ACFF	Activated carbon fiber felt
APR	Air purifying respirator
BET	Brunauer-Emmett-Teller
CAS	Chemical Abstract Service number
CFR	Code of Federal Regulations
CMD	Count median diameter
D-R	Dubinin-Radushkevich Equation
FFR	Filtering facepiece respirator
GAC	Granular activated carbon
GSD	Geometric standard deviation
HEPA	High efficiency particulate absorbing filter
HVAC	Heating, ventilation and air conditioning
IARC	International Agency for Research on Cancer
LPM	Liters per minute
MEK	Methyl ethyl ketone

mm H_20	Millimeters of water gauge
MMD	Mass median diameter
MPPS	Most penetrating particle size
N95	Refers to N-series respirator (not resistant to oil aerosol)
NaCl	Sodium Chloride
NIOSH	National Institute for Occupational Safety and Health
OSHA	Occupational Safety and Health Administration
OV	Organic Vapor
P100	Refers to P-series respirator (resistant to oil aerosol)
PAN	Polyacrylonitrile
PEL	Permissible Exposure Limit
PPMV	Parts per Million Concentration
PPMB	Parts per Billion Concentration
qF	Quality factor
RPD	Respiratory Protection Device
SEM	Scanning electron microscope
TLV	Threshold Limit Value
TWA_{8hour}	8-Hour Time Weighted Average
VOC	Volatile organic compound
WJ	Wheeler-Jonas Equation
WPS	wide-range particle spectrometer

CHAPTER 1

INTRODUCTION

Activated carbon in the granular form is the most common adsorbent for vapor phase volatile organic compounds (VOCs) in respirator cartridges.[1] However, activated carbon in the fiber form (ACF) has properties that make it a potential alternative adsorbent in the context of worker respiratory protection. Unlike a loose, granular adsorbent, ACF is easy to contain and is less prone to dust attrition than granular activated carbon (GAC).[2] The fibrous nature of ACF suggests the ability to participate in particulate filtration as well as VOC capture,[3] and at least one design for a combined vapor and particulate respirator cartridge that incorporates polyacrylonitrile-derived ACF has been patented to date.[4] If incorporated into a filtering face-piece respirator (FFR), ACF may also have applications as a short-term escape respirator for both organic vapors and particulates.

An advantage of ACF over GAC is related to the typical pore structure of ACF. Many ACFs possess high surface areas (up to and exceeding 2000 m^2/g) and correspondingly high adsorption capacities, often expressed as mass of chemical adsorbed versus mass of sorbent.[2] In comparison to granular and powdered activated carbon, ACF tends to derive a greater proportion of its internal surface area specifically from micropores, making it an excellent potential adsorbent for organic vapor at

occupationally-relevant concentrations (ppmv-level concentrations). [5] The micropores of ACF also tend to be distributed directly on the surface of the fiber, meaning that contaminants diffusing through the adsorbent follow a shorter path to a potential adsorption site, and adsorption happens at a rapid pace. Rapid adsorption is a significant property in scenarios where the residence time between an adsorbent and a challenge contaminant is extremely short; one such scenario might occur during the passage of contaminated air through a facepiece or cartridge respirator.

In theory, the dual function of ACF (for both VOC adsorption and particulate filtration) suggests a potential for use in a respiratory protection device like an N95-style FFR. We hypothesized that ACF is capable of functioning as a dual air-purifying element against both particulates and VOCs. To investigate this hypothesis, this research characterized several types of commercially-available ACFs in terms of adsorption capacity and filtration efficiency. Additionally, our proposed research developed methods to examine the interaction between these two air-purifying mechanisms in a dynamic scenario.

Specific Aims

1. To determine the adsorption capacities of activated carbon fibers for representative VOCs at occupationally-relevant exposure concentrations. Three ACF candidate materials (ACFF 1200, ACFF 1800, and ACFF 2000) were selected based on high reported surface area and ready availability. Breakthrough curves were generated for three challenge contaminants (toluene, hexane and methyl ethyl ketone; representing aromatic, aliphatic, and polar VOCs, respectively). A graph of breakthrough time as function of

ACF bed weight was used to determine adsorption capacities of each ACF configuration (milligrams adsorbate/gram sorbent).

2. To further characterize two of the laboratory's ACF materials (ACFF 1800 and ACFF 2000) using the Dubinin-Radushkevich (D-R) isotherm equation. The D-R isotherm equation was used to estimate equilibrium adsorption capacities for the three challenge contaminants (toluene, hexane, and methyl ethyl ketone). These calculated capacities were compared with the experimental capacities determined in Aim 1. Kinetic rate coefficients for each ACF-adsorbate combination were also determined using a semi-empirical equation. Estimates of 10% breakthrough times for each ACF-adsorbate combination were then obtained by using equilibrium adsorption capacities and calculated kinetic rate coefficients as inputs in the Wheeler-Jonas equation.
3. To characterize the filtration efficiencies of commercially-available ACFs against a sodium chloride (NaCl) test aerosol. The overall goal of Aim 3 is to characterize ACFF 1200, ACFF 1800, and ACFF 2000 as a mechanical filters of solid particles. Each ACF type underwent a particulate filtration challenge using flow conditions relevant to respiratory protection applications (i.e., 10 cm/s face velocity). Initial particulate filtration efficiency as a function of bed depth was assessed in tandem with pressure drop measurements for each ACF type. Experimental filtration efficiency was compared with predicted filtration efficiency at multiple layers. Filtration efficiency testing of selected N95 media was also performed as a positive standard.

4. To compare ACF adsorption and filtration performance with that of a carbon-containing adsorbent from a nuisance odor respirator (3M™ 2097). ACFF 1200 was selected for comparison with the nuisance odor adsorbent based on similar depth, pressure drop, and bulk properties. Using the methods developed in Aim 1, 3M™ 2097 breakthrough curves for toluene, hexane and MEK were obtained, and 10% breakthrough times were compared with those of ACFF 1200. Using the methods identified in Aim 3, filtration efficiency and overall filter quality factor of the adsorbent from the 3M™ 2097 respirator were determined compared with those of the ACFF 1200 media.

Significance

This research brings innovation to the field of occupational health and industrial hygiene by investigating the adsorption and filtration performance of activated carbon fiber (ACF) media in the context of worker respiratory protection. ACF has properties such as high specific surface area (m^2/g) and rapid adsorption kinetics that make it a candidate for use in thin, N95-style respirators for organic vapors. A lightweight adsorbent such as ACF, if incorporated into an N95-style respirator, could potentially provide nuisance-level VOC protection in a physical form that is accessible to workers and consistent with OSHA's voluntary use provisions for facepiece respirators. The research presented in this manuscript represents an initial attempt to characterize ACF media for this particular application.

CHAPTER 2

BACKGROUND AND REVIEW OF LITERATURE

Respiratory Protection Overview

The fundamental purpose of a respiratory protection device (RPD) is to protect the wearer from hazardous concentrations of airborne contaminants and/or oxygen deficient atmospheres. In general, respirators accomplish these tasks by purifying breathing air through some mechanism or by supplying purified air to the wearer. When used correctly and in combination with administrative and engineering controls, the use of respirators can prevent exposure to concentrations of airborne chemicals above recognized safe limits. An overview of the topic of respiratory protection, to include regulatory context, a description of several types of respirators and associated air-purifying mechanisms, respirator performance testing, and trends in occupational respirator use, follows below.

Regulatory Context: 29 CFR 1910.134

The Occupational Safety and Health Administration (OSHA) governs the use of respirators in the workplace through 29 CF 1910.134, the Respiratory Protection Standard.[6] Through 29 CFR 1910.134, OSHA encourages employers to maintain workplace exposure to air contaminants at safe levels by means of engineering controls.

Only when this is not possible or feasible should respiratory protection be used to reduce exposures. [7]

When respirators are required, the Respiratory Protection Standard provides a structured approach to their management and use, helping to ensure that respirators are appropriate to the hazard; that employees are fit tested and trained on proper respirator use and limitations; and that respirators are maintained and stored in a manner that provides some reasonable assurance of proper function. The selection of an appropriate respiratory protection device is made by taking into account the nature and concentration of the airborne contaminant, its including physical, chemical, and toxicological properties.[1] The selection of an appropriate respirator must also account for the function and limitations of the respirator itself, to include assigned protection factors, filtration efficiency, resistance to oil-based aerosols, and/or service life information, as applicable.

Regulatory Context: Respirator Voluntary Use

OSHA has also created provisions for the voluntary use of respiratory protection in the workplace, as outlined in Appendix D of the Respiratory Protection Standard. Voluntary use provisions guarantee the right of employees to wear respiratory protection even in the event that workplace exposures are below OSHA's Permissible Exposure Limit (PEL) concentrations. Appendix D of OSHA's Respiratory Protection Standard states the following:

"*Respirator use is encouraged, even when exposures are below the exposure limit, to provide an additional level of comfort and protection for workers."*[7]

Occupational epidemiology has shown that exposure to airborne contaminants in the workplace can have a variety of health effects, including, but not limited to, pneumoconiosis-like syndromes caused by the inhalation of particulate matter, hypersensitivity reactions related to the inhalation of particulate matter and/or organic vapors, and various short and long term health effects, including both acute toxicity syndromes and carcinogenesis.[8,9] Additionally, evidence suggests that some chemical and particulate exposures can exert negative health effects at concentrations below recognized exposure limits,[10–12] a fact that is openly acknowledged by OSHA in the following statement:

"*Many PELs have not been updated since 1971, and current scientific data suggests that, in many instances, the outdated PELs are not sufficiently protective of worker health*."

The current PEL for styrene is one such example of an outdated exposure limit.[13] Styrene is a common precursor chemical used in the composites industry. Styrene exposure can be associated with short-term central nervous system effects like headache, drowsiness, and delayed reaction time.[14] The OSHA PEL for styrene (100 ppm) was lowered to a more protective limit (50 ppm) in 1989. However, the 1989 PEL was vacated in 1992 after legal objections; the 100 ppm PEL was reinstated and exists today. The current Threshold Limit Value (TLV®) for styrene is 5 times lower (20 ppm) than the OSHA PEL. Despite evidence of styrene's harmful acute and chronic effects, including its classification as a possible human carcinogen (Group 2B) by the International Agency for Research on Cancer (*IARC*), workplace exposure to styrene under 100 ppm $TWA_{8\ hour}$ could technically be classified as "nuisance-level exposure"

from a regulatory perspective. Accordingly, such an exposure demonstrates a scenario where an employee may justifiably elect to wear a respirator on a voluntary basis.

Particulate Respirators

Particulate respirators protect the wearer against dust, fumes, and mists. To function, particles are drawn across a filter medium by the negative pressure that results from inhalation and subsequently removed from the airstream by a combination of filtration mechanisms. Particulate respirators are also referred to as "non-powered air purifying particulate respirators" and are classified by NIOSH according to their filtration efficiency (i.e., 95-, 99-, and 100-series) and resistance to oil-based aerosols (N, R, and P series). For example, an N95 respirator is so classified because it is *not* resistant to degradation from oil aerosols and demonstrates ≥ 95% filtration efficiency when tested with a sodium chloride (NaCl) aerosol under a set of standard test conditions. Particulate respirators commonly exist as filtering facepiece respirators (FFRs), in which the filter medium is integral to the body of the respirator (i.e., N95 respirators). They may also be used as components of respirator cartridges (i.e., P100 cartridges) for half- or full-face respirator assemblies.

Overview of Filtration

The performance of a filter system for a particular challenge aerosol can be predicted based on several input factors, which include particle size, linear velocity through the filter, filter depth, filter surface characteristics, and filter fiber diameter.[15] The overall performance of a filter system results from the combined action of several

mechanisms, each of which predominate at different particulate size ranges and/or flow conditions. Three common filtration mechanisms are described below:

Impaction. Impaction occurs when a particle deviates from the flowing airstream (in accordance with the particle's inertia), making contact with the filter. Because impaction is driven by inertial forces, filtration by impaction increases with increased particle size, density, and speed. [15]

Interception. When particles moving in a streamline flow around filter components, they can be removed from the airstream by interception: particle capture that occurs when the distance between the center of the particle and the fiber surface come within one particle radius of each other. Unlike impaction, intercepted particles do not deviate from their streamlines. In general, the probability of filtration by interception increases with increasing particle diameter. [15]

Brownian Diffusion. Small particles which are not governed by inertial or gravitational forces are removed from the airstream by Brownian diffusion. Filtration by diffusion occurs when particles come into contact with the filter through random diffusive motion and are removed from the airstream. Diffusive motion tends to increase with decreasing particle size and increasing temperature. The probability of filtration by diffusion is also enhanced by low air velocity through a filter. [16]

Most Penetrating Particle Size. Each filtration mechanism has a particle size range for which it is most effective, and there is a narrow range of particle sizes at which no single filtration mechanism predominates (Figure 1).[17] This means that each filter system has a diameter of minimum efficiency; i.e., a particle size range where filtration efficiency

exists at a relative minimum. This diameter is known as the Most Penetrating Particle Size (MPPS). The identification of the MPPS has implications for filter performance testing because it represents a "worst case condition," from which the efficiency of a filter at other size ranges can be assumed to be more favorable.

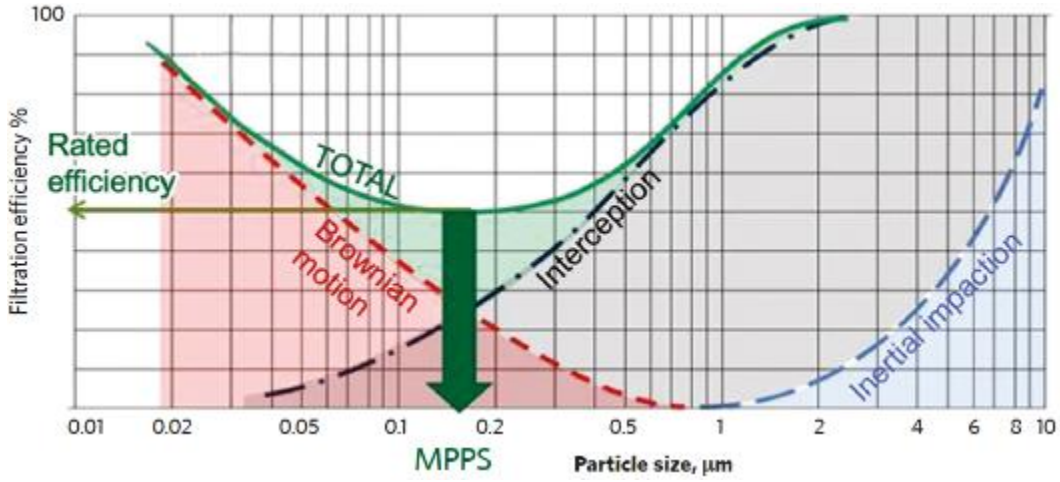

Figure 1. Filtration efficiency curves for several common filtration mechanisms, illustrating their relationship with the diameter of minimum efficiency.

Overview of Filtration Testing

Requirements for the performance testing of non-powered air purifying particulate respirators are found in 42 CFR 84.[18] There are nine total respirator types in this class (i.e., combinations of N,R,P and 95, 99, 100 series respirators). N95 respirators are tested with sodium chloride (NaCl) aerosols that have a count median diameter (CMD) of 75±20 nm and a geometric standard deviation of 1.86. A NaCl test aerosol with this count distribution has a corresponding mass median aerodynamic diameter (MMAD) of 347 nm, within the general range of the MPPS for many filter types.[19] N95 respirators are tested at a flow rate of 85 LPM. N95 performance testing relies on a measurement system called light-scattering photometry to determine upstream and

downstream aerosol concentrations in accordance with NIOSH Method TEB-APR-STP-0059.

Organic Vapor Respirators

Chemical Cartridge Respirators can be used to remove gases and vapors from an airstream. Organic vapor (OV) respirators are a subset of this respirator type. OV respirators often consist of half- or full-face elastomeric facepiece with cartridge or cannister style attachments. The basic structure of an OV cartridge is made up of a loose adsorbent material (granular activated carbon) that is packed within a rigid housing. Inside the respirator cartridge, the GAC is usually supported at the inlet and outlet by course particulate filters, which hold the GAC in place and prevent the migration of small sorbent particles/dusts.

Adsorption

Granular activated carbon removes gases and vapors from an airstream through the process of adsorption. Adsorption occurs as the result of a weak physical attraction (Van der Waals force) between a gas-phase molecule and a solid surface. As such, adsorption is dependent on temperature, pressure, the surface geometry of the adsorbent, and the chemical properties of the adsorbate.[20] Adsorbents are typically highly porous materials. This property is reflected in the specific surface area of the adsorbent, which in some cases can exceed 2000 m^2/gram. For a gas-phase molecule to be adsorbed, it must travel through the carrier air stream to the surface of the adsorbent (interparticle diffusion), diffuse through the boundary layer at the surface of the adsorbent (film diffusion), and eventually migrate through the pore structure to an appropriate adsorptive

site (intraparticle diffusion).[2] Intraparticle diffusion tends to be the rate limiting step for most granular activated carbons (GAC), which contain a combination of micropores (less than 2 nm pore width), mesopores (between 2-50 nm pore width), and macropores (greater than 50 nm pore width).[2] The scientific literature has fully described the tendency of micropores to fill preferentially in ambient air environments and low VOC concentrations, due in large part to the combined attractive force exerted by the narrow pore walls of micropores.[21]

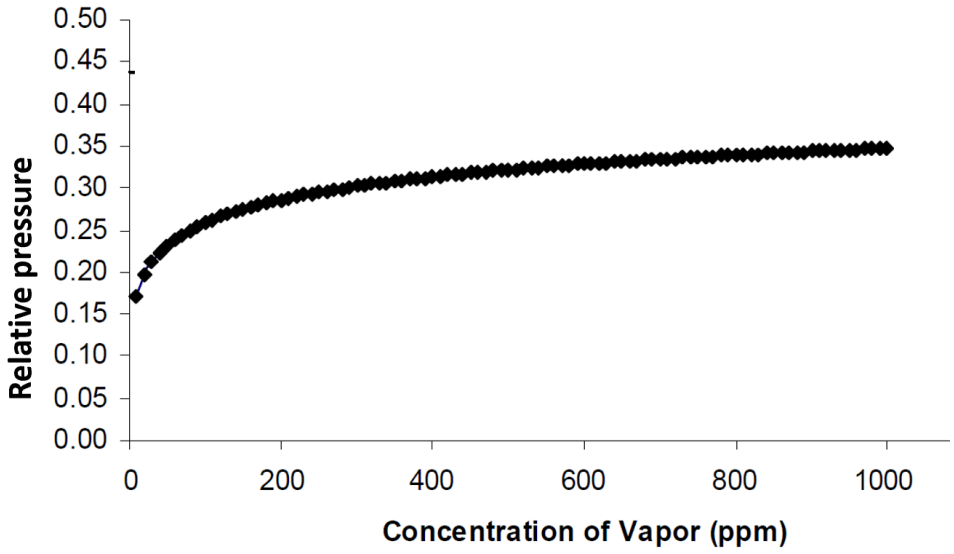

Figure 2. An example of a Type I Isotherm Plot

The relationship between a vapor's concentration (or relative pressure) and the amount of vapor adsorbed by a porous material at a given temperature is known as an isotherm. Isotherms are often used to characterize adsorbent-adsorbate systems. The isotherm depicted in Figure 2 is characteristic of an adsorbent with a large percentage of micropores. The Dubinin-Radushkevich Adsorption Isotherm Equation is

a commonly applied model for predicting adsorption capacities of organic vapors on ordinary commercial activated carbons as well as activated carbon fibers.[22]

Equation 1.[23]

$$W_e = W_o d_L \exp\left(-\left(\frac{RT \cdot \ln(P_0/P)}{\beta E_0}\right)^2\right)$$

where W_e = equilibrium adsorption capacity (g adsorbate/g carbon)
W_o = limiting micropore volume (cm^3/g carbon)
d_L = liquid density of the adsorbate (g/cm^3)
T= air temperature (K)
R = gas constant
P_0=saturation pressure
P=relative pressure of adsorbate
T = air temperature (K)
β = affinity coefficient of the adsorbate
E_0 = characteristic energy (kJ/mol)

Examination of the D-R isotherm equation can provide some insight into the factors that impact the adsorption capacity of a carbon for a particular adsorbate. First, it is clear that a lower saturation vapor pressure for an adsorbate will yield a higher value of W_e; meaning that, as a general rule, less volatile compounds are more strongly adsorbed than more volatile compounds within the same chemical class.[24] Another important parameter related to capacity is W_o, the micropore space. The micropore space is an indication of the total volume available for adsorption. Occlusion of the micropore space in granular activated carbons (as occurs when GACs are extensively functionalized) has been associated with drastic reductions in adsorption capacity. [24]

Organic Vapor Respirator Performance Testing

Organic vapor cartridges are tested by performing "breakthrough tests," a controlled experiment wherein the adsorbent is challenged with a contaminated airstream

while downstream concentrations are measured. Breakthrough occurs when adsorption sites on the carbon become increasing occupied by adsorbate molecules and the challenge contaminant can be detected downstream of the adsorbent. Most breakthrough curves for packed carbon beds exhibit a characteristic S-shape (Figure 3), and breakthrough curves can be visually inspected to yield information about the adsorbent. For example, a breakthrough curve with a steep slope indicates a low resistance to mass transfer that is characteristic of highly microporous adsorbents.

The requirements for the testing of organic vapor respirators for occupational use are found in 42 CFR Part 84.207.[18] Organic vapor chemical cartridges are typically tested with a 1000 ppm challenge contaminant (carbon tetrachloride) at a flow rate of 64 LPM or 32 LPM, depending on whether the cartridge is used singly or in pairs. The maximum allowable breakthrough is 5 ppm, and the minimum time to reach 5 ppm breakthrough is 50 minutes.

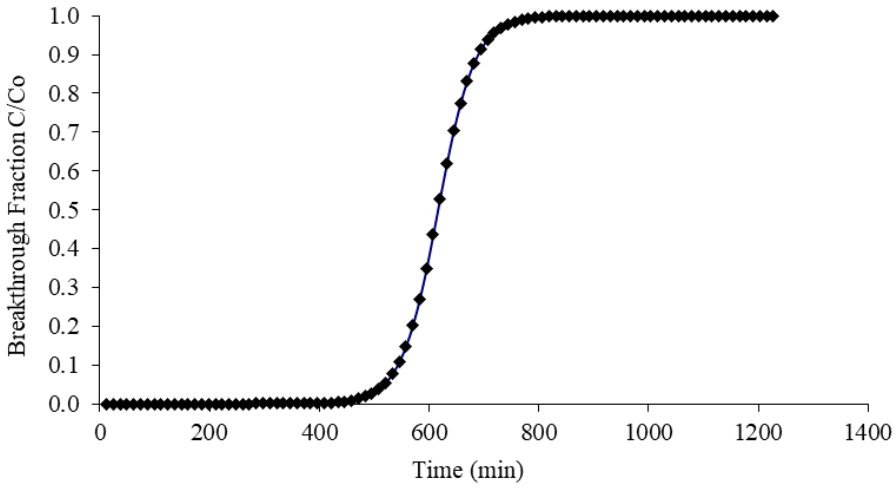

Figure 3. Example of an organic vapor breakthrough curve.

Dual Particulate and Organic Vapor Respirators

Based on the complexity of many workplace exposures, the use of both particulate and gas-phase respirators is sometimes indicated. Exposure to a complex mix of airborne contaminants occurs in a variety of workplaces: these workplaces can include industrial settings in which workers are exposed to both solvent vapors and liquid aerosols that may result from the use of spray coatings, adhesives, and cleaning solvents; healthcare settings in which workers may be exposed to infectious aerosols, potent pharmaceutical compounds, VOC-containing surgical smoke, and vapor-phase disinfectants;[25,26] and a variety of law enforcement and first responder settings. For example, during the 2018 wildfire season in California, many private citizens and first responders were exposed to not only combustion gases like carbon monoxide and hydrogen cyanide, but also particulate matter and volatile organic compounds.[27]

No disposable or re-usable respirator is capable of providing protection against all possible airborne contaminants; however, options currently exist for combined particulate and vapor filtration.[1] Organic vapor respirator cartridges that fit elastomeric half-face or full-face respirators typically consist of granular activated carbon housed within a plastic filter assembly and sandwiched between several layers of non-woven material. The non-woven components may consist of polypropylene or glass fiber; this element serves to contain the granular media and provide some measure of particulate filtration. Other organic vapor cartridge arrangements consist of a pleated glass-fiber filter upstream of the carbon bed that provides P100-level particulate filtration; in such arrangements, the upstream aerosol filter acts as a physical barrier to prevent solid and liquid particles from being deposited on the carbon bed, and the downstream carbon bed can then adsorb gas-

phase volatile species, as well as any volatiles that might evaporate from the solid or liquid droplets captured by the aerosol filter.[24] While these respirator assemblies are effective, they may pose drawbacks in the form of weight, and bulk. These properties have an impact on the wearer's perception of comfort; user comfort is strongly associated with consistent and proper respirator use.[28,29]

FFRs that support nuisance-level organic vapor adsorption *in addition to* particulate filtration are also available. One example of such a device is the 3M™ 8514 N-95 Particulate Respirator, which consists of a thin carbon-containing layer sandwiched between an electrostatically-treated polypropylene body. The carbon layer is a fibrous non-woven web that has been impregnated with activated carbon powder. In the context of respiratory protection, no certification of performance exists for nuisance level organic vapor adsorption (although these devices may be certified with regard to their ability to capture particulates; i.e., given a NIOSH N-, P-, R-, 95-100 rating). The physical form of the adsorbent within these nuisance-level respirators raises a concern: because carbon particles are suspended in a non-woven matrix, significant void space can exist between each particle. This creates the possibility for carbon-free channels in the adsorbent matrix, meaning that a challenge contaminant may pass through the sorbent media without physically contacting the sorbent.[30] These void spaces are clearly visible when a sample of the media is transilluminated (Figures 4-5). The shallow depth and low total carbon weight of the adsorbent layer in nuisance-level respirators could also contribute to rapid breakthrough of organic vapors when these devices are subjected to the challenging use conditions. In a 2012 study, a 3M™ 8247 facepiece respirator subjected to a 20 ppm xylene challenge demonstrated almost immediate contaminant breakthrough under

simulated use conditions, suggesting that a minimum amount (or “critical bed weight”) of carbon may be necessary to improve breakthrough times for this respirator type.[25]

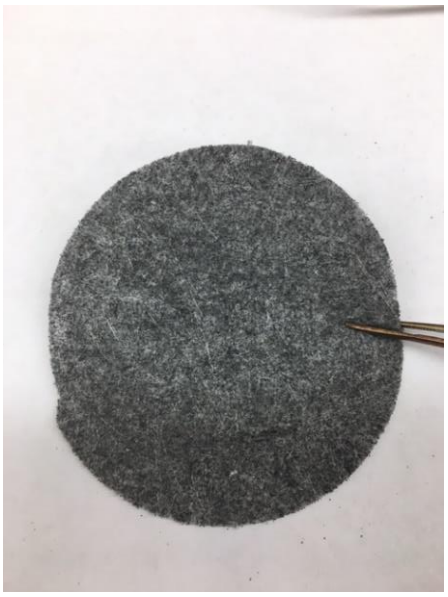

Figure 4. Nuisance adsorbent media extracted from a 3M™ 2097 P100 pancake filter.

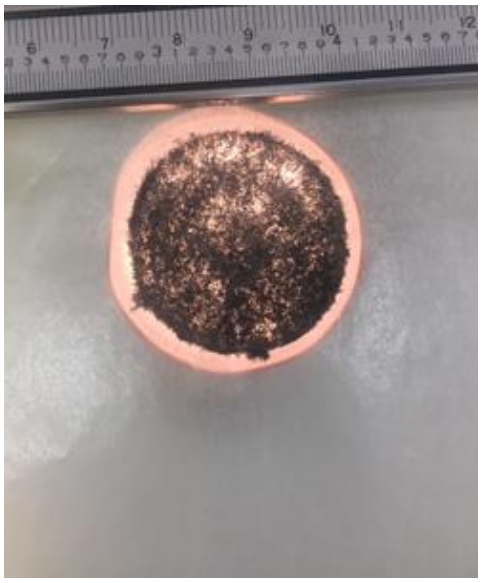

Figure 5.. Nuisance adsorbent media from 3M™ 2097 P100 pancake filter, transilluminated to demonstrate void spaces and unequal distribution of the carbon within the polypropylene matrix.

Activated Carbon Fiber

As previously described, activated carbon in the granular form serves as the most common adsorbent for vapor phase volatile organic compounds in respirators; however, activated carbon in the fiber form has several properties that make it a possible alternative to granular activated carbon in certain respiratory protection applications.[31]

Activation Process

Activated carbon fiber is produced by first heating an organic precursor fiber to high temperatures in an inert atmosphere; the remaining material undergoes a second thermal treatment in the presence of an oxidizing atmosphere, usually steam or carbon dioxide. It is during this step that micropores are formed.[32] The activation stage is responsible in part for creating an extensive pore structure on the surface of the fiber. Increasing the duration of the activation process produces an ACF with larger specific surface area and greater pore volume.[2] On the other hand, a short activation process produces an ACF with less surface area and narrower pore widths.

Precursors

Common ACF precursors include phenolic resin, polyacrylonitrile and viscose rayon fibers[5]. The identity of the ACF precursor material can ultimately have an impact on adsorption behavior.[33] For example, ACF produced with polyacrylonitrile (PAN) has high degree of nitrogen inclusions; this makes PAN-derived ACF well-suited to adsorb polar molecules.[34]

Review of Literature

Adsorption isotherms for a wide variety of ACF-adsorbate systems have been modeled and described experimentally in the context of engineering, HVAC, and pollution prevention applications[34–36]. With *specific* reference to respiratory protection, far fewer studies exist. Balanay et al[37] determined adsorption capacities for phenolic resin-derived ACFs of varying forms and surface areas, using toluene as a representative volatile organic compound (VOC). She demonstrated that an ACF with a specific surface area of 1500 m^2/g exhibited greater adsorptive capacity (429 ± 0.01 mg/g) for toluene than a granular adsorbent with a higher specific surface area of 1800 m^2/g (392 ± 0.02 mg/g).

Rochereau *et al* speculated that the fibrous form of ACF may support particulate filtration as well as VOC capture,[38] and at least one design for a combined vapor and particulate respirator cartridge that incorporates polyacrylonitrile-derived ACF has been patented to date.[39]

With regard to filtration, a study by Hindmarsh[40] examined the filtration performance of pitch-derived ACF media using a salt aerosol (MMD of 0.6μm). A single 25 mg ACF filter disk (11 cm diameter, depth 2.5 cm) was able to effectively filter 99.5% (by mass) of a sodium chloride aerosol when challenged at a flow rate of 30 LPM. However, pressure drop across this particular ACF configuration was found to be prohibitively high at 75 mm H_20. Research by Lorimier[41] examined the filtration performance of commercially available rayon-derived ACF for alumina particles (MMD 0.37 μm) under experimental conditions that were meant to approximate flow rates, temperature, and relative humidity inside a heating, ventilation and air conditioning

(HVAC) unit. ACF felts demonstrated a high initial filtration efficiency (74%) with a low associated pressure drop (under 210 Pa). However, researchers used a face velocity (37 cm/s) far greater than might be expected with normal breathing patterns across an N95 or cartridge style respiratory protection device.

A study by Hayashi et al[42] examined filtration efficiency of a cellulose-derived ACF for NaCl (MMD 0.5 μm) aerosols at a fixed face velocity of 0.05 m/s. Researchers found that experimental measures of pressure drop on clean filters and for cake filtration matched well with theoretically predicted values, and potential uses for ACF in waste incinerators, boilers, and bag filters were suggested. Once again, this study was conducted without specific regard to respiratory protection.

Gaps in the Literature and Research Direction

Few studies have been performed with regard to the adsorption and filtration behavior of ACF using test conditions that are relevant to respiratory protection. Additionally, we could find no studies that evaluated the performance of ACF against the thin adsorbent media currently used in nuisance OV respirators, as described above. Previous doctoral research in our laboratory described the adsorption capacity and critical bed depths of several ACFs types, using granular activated carbon as a measure of comparison.[37,43,44] This dissertation advances that work in several ways: We tested several ACF types against representative OVs at occupationally relevant concentrations. We also evaluated pressure drop and filtration performance of off-the-shelf ACFs, identifying maximum possible bed depths for use in respiratory protection devices. Finally, we compared the filtration and adsorption performance of ACF with that of a

nuisance OV adsorbent and developed an experimental set-up for simultaneous adsorption and filtration testing of ACF media.

CHAPTER 3

DETERMINATION OF ACTIVATED CARBON FIBER ADSORPTION CAPACITY FOR SEVERAL COMMON ORGANIC VAPORS

Introduction

In the United States, an estimated 5 million workers are required to wear respirators on a regular basis.[6] Unmitigated exposure to airborne contaminants in the workplace can result in a variety of health effects, including, but not limited to, interstitial lung disease related to the inhalation of particulate matter, hypersensitivity reactions related to the inhalation of particulate matter and/or organic vapors, and various short and long term health effects, including both acute toxicity syndromes and cancer.[8]

Workers who are exposed to airborne contaminants above permissible exposure limits (PELs) may require the use of respiratory protection. Based on the complexity of many workplace exposures, the use of both particulate and gas-phase respirators is often indicated.[1] Exposure to a complex mix of airborne contaminants occurs in a variety of workplaces: these workplaces can include industrial settings in which workers are exposed to both solvent vapors and liquid aerosols that may result from the use of spray coatings, adhesives, and cleaning solvents; healthcare settings in which workers may be exposed to infectious aerosols, potent pharmaceutical compounds, VOC-containing

surgical smoke, and vapor-phase disinfectants;[25,26] and a variety of law enforcement and first responder settings.[27]

While no single disposable or re-usable respirator is capable of providing protection against all possible airborne contaminants, several options currently exist for combined particulate and vapor filtration.[1] Organic vapor respirator cartridges that fit elastomeric half-face or full-face respirators typically consist of granular activated carbon (GAC) housed within a plastic filter assembly and sandwiched between several layers of non-woven material, which serves to contain the granular media and provide some measure of particulate filtration.

GAC removes contaminants from the air through adsorption. Adsorption occurs as the result of a weak physical attraction (Van der Waals force) between a gas-phase molecule (adsorbate) and a solid surface (adsorbent). Because adsorption is a physical process, it is highly dependent on the surface characteristics of the adsorbent, and particularly on surface area.[23] The high surface area of GAC stems from the activation process, which imparts an extensive pore structure to the adsorbent. Within the resulting pore structure, pores less than 2 nm in width (micropores) are the most favorable sites for adsorption, due in large part to the combined attractive force exerted by the narrow pore walls of micropores on the adsorbate molecule.[2] Both the total surface area and the microporosity of the adsorbent are indications of the total volume available for adsorption and can be directly related to the overall performance of the adsorbent.[5] Conventional organic vapor respirators that rely on GAC adsorbents are effective, but may pose drawbacks in the form of weight and bulk of the assembly. These properties have an

impact on the wearer's perception of comfort; user comfort is strongly associated with consistent and proper respirator use. [29,28]

In the context of workplace safety, activated carbon in the fiber form (ACF) represents a potential alternative adsorbent for respiratory protection devices. ACFs are made from polymer fibers that have been carbonized at high temperatures and subsequently activated with carbon dioxide or steam.[32] ACF is highly porous and tends to derive a greater proportion of its internal surface area from micropores than GAC. ACF microporosity is also concentrated at the fiber surface, shortening gas diffusion distances and promoting rapid adsorption.[45] This kinetic profile facilitates adsorption in scenarios where the residence time between an adsorbent and a challenge contaminant is short, as might occur during the passage of contaminated air through a thin facepiece or cartridge respirator.[25] ACF also tends to retain the physical form of the precursor fiber and unlike GAC, can be fabricated into self-supporting woven and non-woven forms. ACF in the non-woven form (i.e., felt) suggests the potential for a filtration medium that is capable of supporting both adsorption and particulate filtration applications.[46]

Several studies have investigated the use of ACF for indoor air quality applications related to both particulate filtration and adsorption.[41,47] Additionally, adsorption behavior for a wide variety of ACF-adsorbate systems have been modeled and described experimentally in the context of engineering, HVAC, and pollution prevention applications.[42,47,48] However, with specific reference to respiratory protection, far fewer studies exist. Hindmarsh et al fabricated pitch-based non-woven ACF mats and tested their ability to adsorb a non-polar VOC (4000 mg/m^3 hexane) under both dry and humid conditions; however, certain elements of test conditions in this study (i.e., flow rate

through the media) were not reflective of respirator use conditions.[49] Balanay et al[43] showed that an ACF with a specific surface area of 1500 m^2/g exhibited greater adsorptive capacity (429 ± 0.01 mg/g) for toluene than a granular adsorbent with a higher specific surface area of 1800 m^2/g (392 ± 0.02 mg/g) using a flow rate of 64 LPM (approximating the respiratory rate during moderate levels of exertion), thereby demonstrating the viability of this medium in respiratory protection applications. Pending further characterization and testing, specific ACF configurations could potentially be incorporated into N95-style respirators to be used in the event of accidental or intentional release of harmful gases and particulate matter in public spaces or public transportation. Thin ACF-based respirators that protect against both VOCs and particulate matter for short periods of time could be stored in public spaces and deployed in emergency situations. Additionally, the use of a thin, ACF-based adsorbent in an N95-style respirator could provide protection against low concentration VOC exposures (i.e., "nuisance odor" applications) in the workplace or home environment.

With both workplace and emergency use applications in mind, we determined the adsorption capacities of commercial ACFs for several representative organic vapors at occupationally relevant exposure concentrations. Adsorption capacity, defined as milligrams adsorbate per gram adsorbent, can be related to media breakthrough time through descriptive models, has implications for the estimation of respirator service life in future studies and applications.[22,50] Additionally, we performed laboratory characterization of ACF types in terms of surface area and micropore volume, with the aim of quantifying characteristics known to be significant to media capacity. Finally, this study identifies ACF depths that meet a specified performance criteria (i.e., adsorbent bed

depth corresponding to maximum acceptable pressure drop, and breakthrough time in minutes at maximum acceptable pressure drop) when presented with use conditions similar to those of a typical facepiece respirator.

Methods

The materials and methods used to complete this Aim are described in the sub-headings below.

ACF Selection

Three high surface area ACFs were assessed: two rayon-derived ACFs [ACFF 1800 and ACFF 2000; Bonding Chemical Co., Katy, TX.], and one PAN-derived ACF [ACFF 1200, CeraMaterials, Dingmans Ferry, PA]. Properties of the ACF media are listed in Table 1. The numbers 1200, 1800, and 2000 refer to the manufacturer-reported surface area of each material in m^2/gram. Surface chemistry plays a role in the behavior of an ACF-adsorbate system, and adsorption can vary based on the precursor material and activation conditions[5]. For example, PAN- derived ACFs, which have a relatively high concentration of nitrogen- and oxygen-containing surface groups, tend to show an enhanced adsorption of polar VOC species at low concentrations in comparison to other ACF types.[51] The "off-the-shelf" ACFs selected for this study are intended to reflect a variety of precursor materials, surface areas and media bulk properties.

Table 1. ACF Media Characteristics.

Media Name	Precursor	Reported Surface Area (m^2/gram)	Single Layer Depth (cm)
ACFF 2000	Rayon	2000	0.30

Media Name	Precursor	Reported Surface Area (m^2/gram)	Single Layer Depth (cm)
ACFF 1800	Rayon	1800	0.30
ACFF 1200	PAN	1200	0.25

ACF Characterization

To obtain surface area measurements and micropore characterization, ACF media underwent nitrogen adsorption at 77K using a Micromeritics ASAP 2020 Physisorption Analyzer (Micromeritics Corp, Norcross, GA). Total specific surface area and average pore diameter of ACFs were determined by the BET method. BET (Brunauer-Emmett-Teller) theory describes the adsorption of gas particles onto a solid surface based on the assumption of multimolecular adsorption. The BET method is often used by convention to estimate the surface area of microporous carbons.[23]

Challenge contaminants

Three organic vapors which could conceivably be encountered in the workplace or home environment were selected for use in this experiment. Toluene, Hexane and Methyl Ethyl Ketone (MEK) are representative *aromatic*, *aliphatic* and *polar organic* hydrocarbons, respectively. These challenge contaminants are commonly used in solvents, paints and coatings. Acute exposure to MEK (*IARC Group 2B*) is most commonly associated with irritation of the upper respiratory tract[52], while acute exposure to toluene (*IARC Group 3*) and hexane (*not classified by IARC*) may result in nervous system depression.[53,54] Relevant properties of the challenge contaminants are listed in Table 2. In each breakthrough study, a uniform challenge concentration of 200 ppm was

used. This concentration was deemed occupationally-relevant, as it is *equal to* or *less than* the OSHA Permissible Exposure Limit (PEL) for each contaminant.

Table 2. Challenge Contaminant Properties.

Challenge Contaminant	Chemical Class	OSHA PEL	Acute Health Effects
Toluene	Aromatic	200 ppm	Vapors irritate the eyes and upper respiratory tract; exposure can cause dizziness, headache, and neurological impairment
Hexane	Aliphatic	500 ppm	Irritation of respiratory tract, cough, mild depression, cardiac arrhythmias
Methyl Ethyl Ketone	Polar	200 ppm	Vapors irritate the eyes, nose and throat

Experimental Set-Up

A diagram of the test set-up is shown in Figure 6. The dynamic adsorption chamber is a two-piece stainless steel vessel that opens to allow placement of the test media within a 4-cm internal diameter filter holder. Sections of test media are backed with a layer of non-woven polypropylene and a stainless steel mesh to prevent shedding of the material. The test rig was maintained at a temperature of 25 ºC and RH of 30% by ambient air-conditioning system (Assay Technology, Livermore, CA), which provided clean conditioned air to the test rig at the desired flow rate. Flow rate was monitored in

real-time with a downstream mass flow meter. A flow rate of 7.5 LPM was employed for all experiments; for the chamber dimensions, this flow rate corresponds to a face velocity of 10 cm/s at the test media surface. This face velocity was selected because it approximates the face velocity experienced by a filtering facepiece respirator (FFR) with an average surface area of 100 cm^2 when subjected to moderate airflow (64 LPM).[18] FFR surface area varies based on style (i.e., cup, duckbill, flat-fold) and respirator manufacturer. For simple cup-style respirators, areas as small as 59 cm^2 and as large as 150 cm^2 have been reported. For the purposes of this experiment, an approximate surface area of 100 cm^2 was selected based on these ranges. A flow rate of 64 LPM was selected as it corresponds to the ventilatory rate at moderate exertion; 64 LPM is also the flow rate used to certify the performance of organic vapor respirator cartridges per 42 CFR Part 84.207.[18]

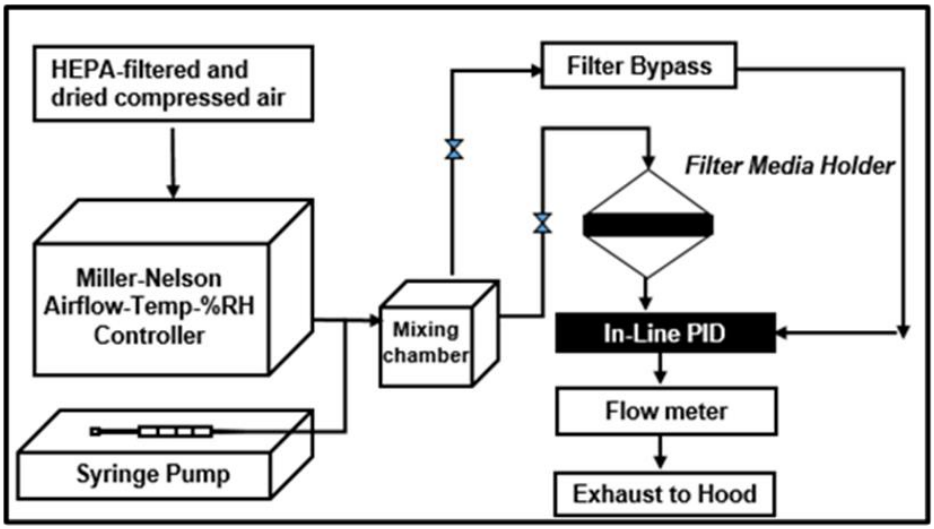

Figure 6. Simplified experimental set-up.

The VOC challenge was generated by evaporating liquid into the conditioned airstream via a motor-driven syringe pump (Chemyx, Inc, Stafford, TX) and an injection

port. The vaporized liquid was mixed thoroughly with clean air within the test rig to generate the desired concentration. The challenge VOC concentrations were measured in real-time by a photoionization detector (Baseline MOCON, Lyons, CO), and were fixed at 200±5 ppm.

Breakthrough Experiments

ACF samples were placed in the test chamber and challenged with a VOC-containing airstream, as described above. Downstream challenge concentrations were monitored with a photoionization detector and the time at ($\frac{C_0}{C_x}$) = 0.10 (breakthrough concentration of 10%) was recorded. For each ACF-adsorbate pair (3 ACF types x 3 adsorbates), the 10% breakthrough was assessed for at least three different bed depths, each corresponding to consecutive single layers of filter media. A single trial was performed for each bed depth.

Data Analysis

The Wheeler-Jonas (WJ) equation, a semi-empirical model of breakthrough time, was used to describe the performance of ACFs under dynamic use conditions. The WJ equation, which has been successfully applied to the adsorption behavior of granular activated carbon (GAC) and activated carbon fiber (ACF) packed beds,[55] has the following form when expressed in terms of breakthrough time:

Equation 2.[55]

$$t_{b=} \frac{W_e W}{C_0 Q} - \frac{W_e \rho_b}{C_0 k_v} \cdot \ln\left(\frac{C_0}{C_x}\right)$$

Where t_b = breakthrough time (min)
W_e = kinetic adsorption capacity (g/g)
W=weight of adsorbent (g)
C_0=inlet concentration (g/cm^3)

C_x =outlet concentration (g/cm^3)
Q =volumetric flow rate (cm^3/min)
k_v = rate constant of adsorption (min^{-1})
ρ_b = density of the packed bed (g/cm^3)

For each ACF-adsorbate pair, 10% breakthrough time (t_b) versus bed weight (W, a function of bed depth) was plotted (Figures 2 – 10). From the plot, the adsorption capacity (W_e) of the material was determined using the WJ equation, as follows:

Equation 3. $W_e = \text{slope} \cdot C_0 \cdot Q$

Where W_e = kinetic adsorption capacity
C_0 = inlet concentration
ρ_b = packed bed density
W = ACF weight
Q = volumetric flow rate

Pressure Drop Measurement

Pressure drop refers to the resistance across a filtration media in mm H_20 during inhalation or exhalation. Constraints associated with pressure drop are a limiting factor on ACF bed depth, and by extension, the total mass of carbon that can be incorporated into any ACF-containing respirator. Per 42 CFR Part 84.203, pressure drop for organic vapor respirators is not to exceed 40 mm H_2O when measured at a flow rate of 85 LPM.[18] A TSI VelociCalc (Shoreview, MN) with differential pressure probes was used to measure pressure drop across each ACF configuration, so that the maximum permissible bed depth within the allowable range of pressure drop could be identified. Based on the density of each ACF material, maximum bed depths were expressed in terms of total carbon weight (W). This relationship allowed estimation of 10% breakthrough times for

each maximum permissible bed depth using the t_b vs W plots described above (Figures 7-15).

Performance Criteria

Per 42 CFR Part 84.207, organic vapor chemical cartridges are typically tested with a 1000 ppm CCl_4 (carbon tetrachloride) challenge at a flow rate of 64 LPM or 32 LPM, depending on whether the cartridge is used singly or in pairs. The maximum allowable breakthrough is 5 ppm, and the minimum time to reach 5 ppm breakthrough is 50 minutes.[18] For the purposes of this study (which uses 200 ppm rather than 1000 ppm, and the challenge contaminants toluene, hexane, and MEK rather than CCl_4), a "successful" adsorption trial has been defined any ACF depth that does not demonstrate immediate breakthrough and that is sufficient to prevent 5 ppm breakthrough for at least 150 minutes under the experimental conditions. This modified performance criterion is based on a rule-of-thumb that states if a challenge concentration is reduced by a factor of 10, the service life of a chemical cartridge should increase by a factor of 5.[56] Applying this relationship to a 200 ppm contaminant challenge yields a service life of 150 minutes This performance criteria is intended to identify any ACF configurations that could potentially be considered for full-shift use scenarios against PEL-level contaminants.

Results

Surface area analysis confirms that each of the tested ACFs have exceptionally high specific surface areas when measured by the BET method (Table 4). Both ACFF 1800 and ACFF 2000 have measured surface areas below the reported nominal surface areas (1541 m^2/g vs. 1800 m^2/g and 1903 m^2/g vs 2000 m^2/g, respectively), possibly

reflecting quality control issues with these particular "off-the-shelf" products. Results of surface area analysis reveal that each ACF type is highly microporous; however, the lowest surface area ACF presents the highest degree of microporosity by volume (ACFF 1200, 72.96% microporosity by volume). The ACF with the highest measured surface area has the lowest percentage of micropores by volume (ACFF 2000, 35.71%). This suggests that for ACF adsorbents, there may be a point of diminishing return related to increases in surface area. For example, the literature suggests that with increasing degrees of activation (corresponding to higher surface areas), there can be etching and widening of the adsorbent's pore structure at the expense of microporosity. [5,21]

Table 3. Results of ACF Surface Area Analysis

Parameters	ACFF 1800	ACFF 2000	ACFF 1200
Nominal surface area (m^2/g)	1800	2000	1200
BET Surface Area (m^2/g)	1541.34	1903.55	1205.97
Micropore area (m^2/g)	1056.14	838.89	1015.25
% Micropore by area	68.52	44.06	78.70
Pore Volume (cm^3/g)	0.69	0.90	0.58
Micropore Volume (cm^3/g)	0.41	0.32	0.42
% Micropore by volume (cm^3/g)	59.51	35.71	72.96
Pore Size (nm)	1.80	1.91	1.82

Breakthrough time experiments by layer (Figures 7-15) indicate that ACFF 2000 has the highest adsorption capacity for toluene (380 mg/g), followed by ACFF 1800 and ACFF 1200 (344 mg/g and 249 mg/g, respectively). A similar trend was observed for hexane: adsorption capacity varied directly with media surface area (220 mg/g; 195 mg/g;

and 145 mg/g for ACFF 2000, ACFF 1800, and ACFF 1200, respectively). ACFF 1200 showed the highest adsorption capacity for the polar adsorbate MEK (165 mg/g), followed by ACFF 1800 and ACFF 2000 (168 mg/g and 146 mg/g, respectively) (Tables 4-6).

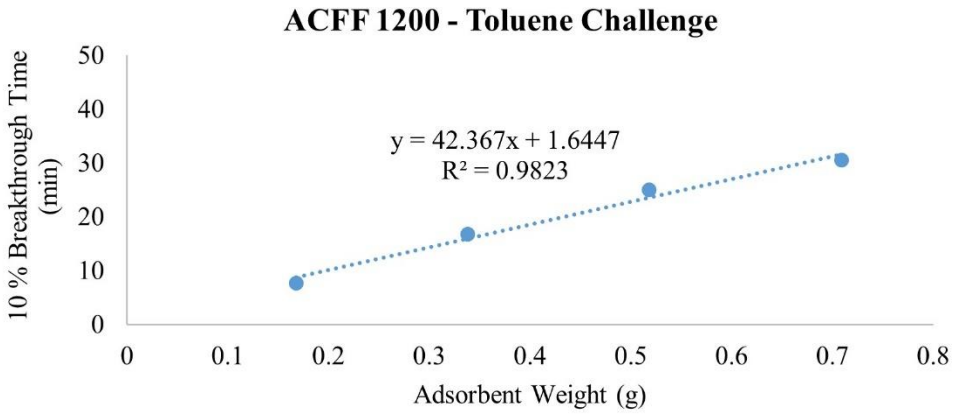

Figure 7. ACFF 1200 Toluene Breakthrough Time vs. Adsorbent Weight

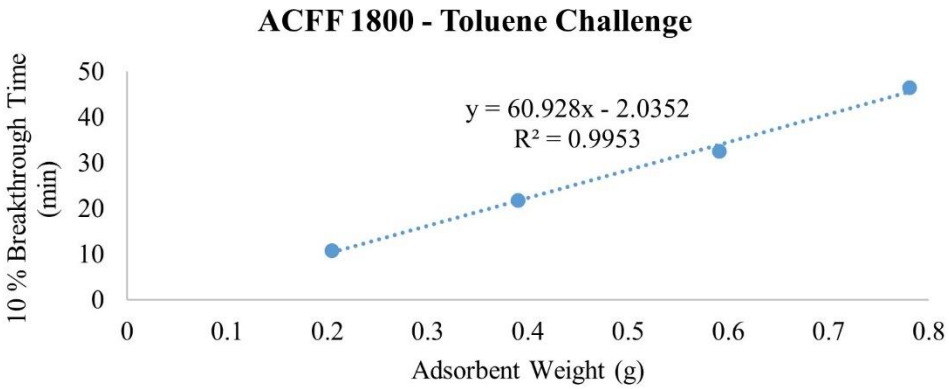

Figure 8. ACFF 1800 Toluene Breakthrough Time vs. Adsorbent Weight

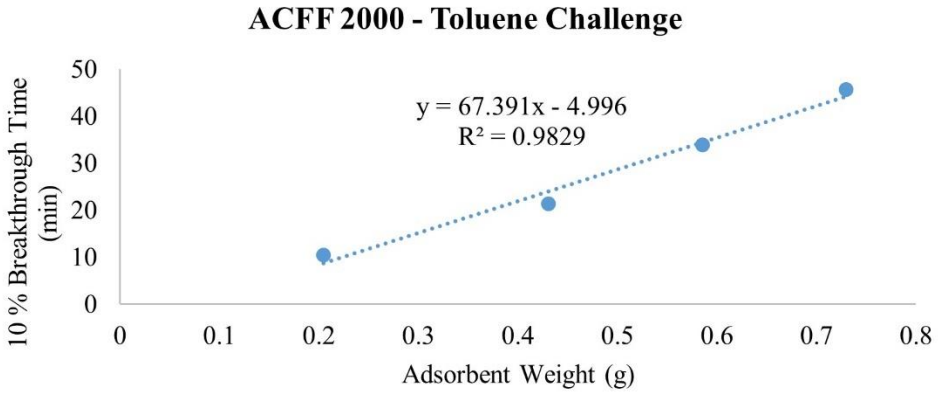

Figure 9 ACFF 2000 Toluene Breakthrough Time vs. Adsorbent Weight

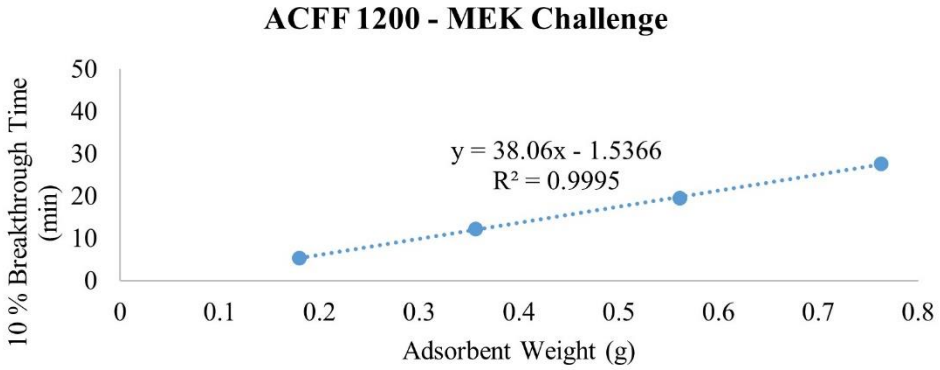

Figure 10. ACFF 1200 MEK Breakthrough Time vs. Adsorbent Weight.

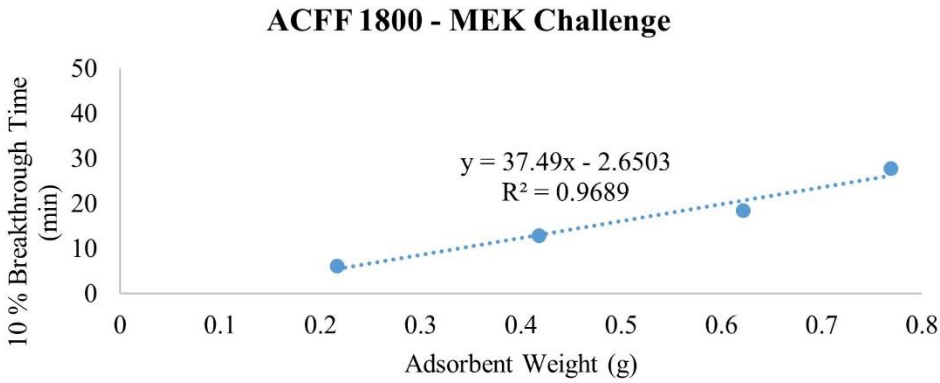

Figure 11. ACFF 1800 MEK Breakthrough Time vs. Adsorbent Weight

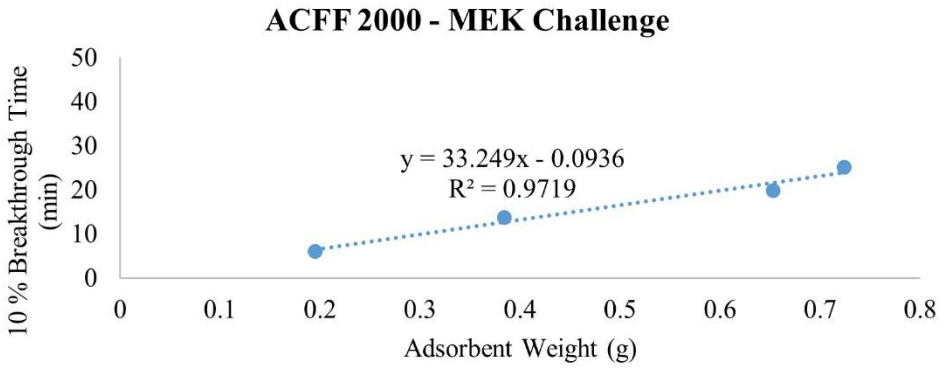

Figure 12. ACFF 2000 MEK Breakthrough Time vs. Adsorbent Weight

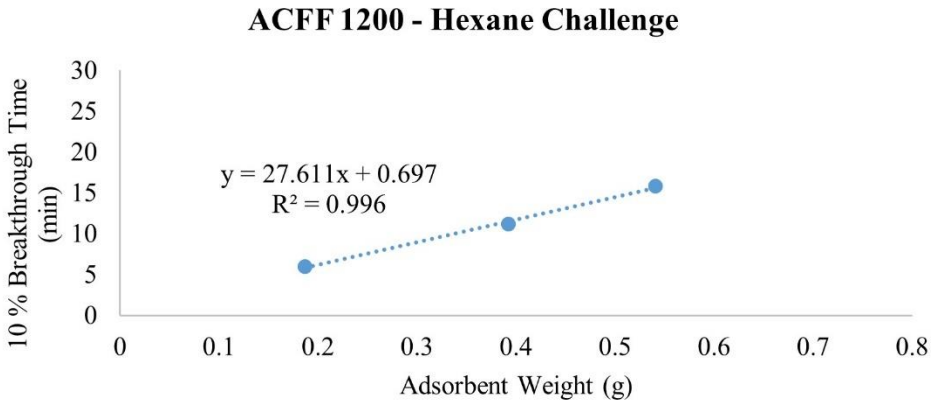

Figure 13. ACFF 1200 Hexane Breakthrough Time vs. Adsorbent Weight.

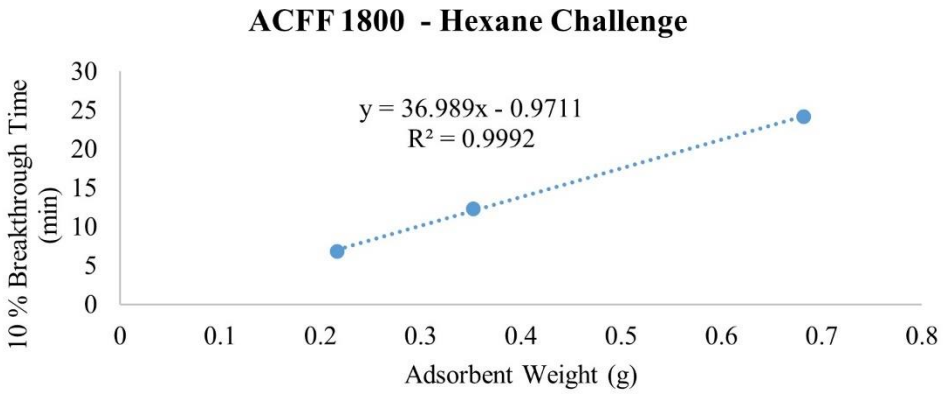

Figure 14. ACFF 1800 Hexane Breakthrough Time vs. Adsorbent Weight.

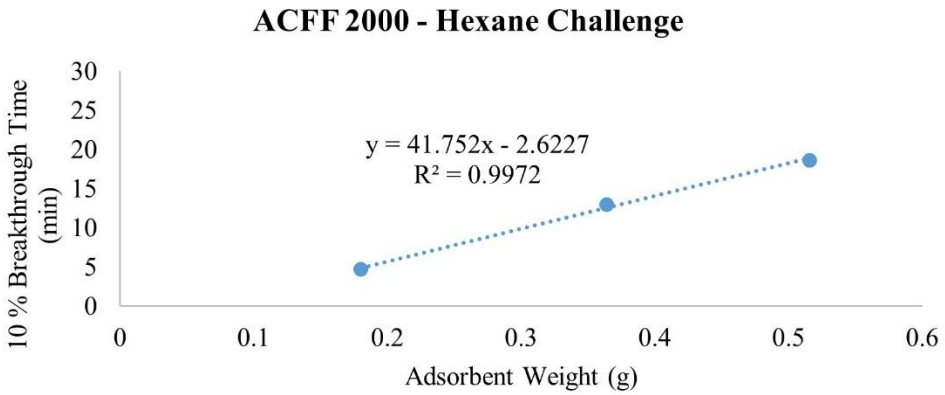

Figure 15. ACFF 2000 Hexane Breakthrough Time vs. Adsorbent Weight.

Table 4. Breakthrough Experiments with 200 ppm Toluene as challenge contaminant.

Adsorbent	Layer	Bed weight (g)	$tb_{10\%}$ (min)	Experimental Capacity (mg/g)
ACFF 1200	1	0.167	7.67	*239.26*
	2	0.338	16.83	
	3	0.518	25.00	
	4	0.708	30.50	
ACFF 1800	1	0.204	10.83	*344.09*
	2	0.390	21.83	
	3	0.591	32.50	
	4	0.780	46.50	
ACFF 2000	1	0.204	10.42	*380.59*
	2	0.430	21.42	
	3	0.585	34.83	
	4	0.729	45.67	

Table 5. Breakthrough Experiments with 200 ppm MEK as challenge contaminant.

Adsorbent	Layer	Bed weight (g)	$tb_{10\%}$ (min)	Experimental Capacity (mg/g)
ACFF 1200	1	0.180	5.33	*168.13*
	2	0.356	12.17	
	3	0.561	19.5	
	4	0.762	27.67	
ACFF 1800	1	0.216	6.17	*165.61*
	2	0.417	12.83	
	3	0.621	18.5	
	4	0.769	27.83	

ACFF 2000	1	0.195	6.00	*146.87*
	2	0.383	13.67	
	3	0.652	19.83	
	4	0.724	25.17	

Table 6. Breakthrough Experiments with 200 ppm Hexane as challenge contaminant.

Adsorbent	Layer	Bed weight (g)	$tb_{10\%}$ (min)	Experimental Capacity (mg/g)
ACFF 1200	1	0.186	6.00	*145.9*
	2	0.392	11.17	
	3	0.540	15.83	
ACFF 1800	1	0.216	6.85	*195.5*
	2	0.352	12.33	
	3	0.681	24.17	
ACFF 2000	1	0.180	4.70	*220.70*
	2	0.364	13.00	
	3	0.515	18.67	

For pressure drop measurements, ACFF 1200 had a maximum bed weight of 2.119 grams (i.e., maximum bed weight within the stated pressure drop requirement of 40 mm H_20); this corresponds to a maximum bed depth of 8 layers (2.140 cm). ACFF 1800 and 2000 had maximum bed weights of 1.399 and 1.312 grams, respectively. (Table 7). These correspond to maximum bed depths of 4 layers (1.553 cm and 1.550 cm, respectively). The weight of each maximum bed depth was used to extrapolate maximum possible 10% breakthrough times for the three analytes using the t_b *vs. W* plots described above (Table 7). For ACFF 1200, maximum predicted 10% breakthrough times are 85.12 minutes, 79.58 minutes, and 56.97 minutes for toluene, MEK, and hexane, respectively. For ACFF 1800, maximum predicted 10% breakthrough times are 71.52 minutes, 42.44 minutes, and 49.79 minutes for toluene, MEK, and hexane, respectively. For ACFF 2000, maximum predicted 10% breakthrough times are 71.61 minutes, 39.56

minutes, and 43.22 minutes for toluene, MEK, and hexane, respectively. These figures highlight the importance of media bulk properties (in this case, density and permeability to airflow) in maximum predicted 10% breakthrough times. In general, ACFF 1200 has a lighter, more spongy structure than ACFF 1800 and ACFF 2000 and could therefore accommodate more layers (i.e., more adsorbent mass) before the 40 mm H_20 pressure drop requirement was exceeded.

Table 7. Maximum ACF bed depths and associated bed weights not in exceedance of 40 mm H_2O when tested at a 10 cm/s velocity airflow. Also included are extrapolated 10% breakthrough times ($T_{b\ 10\%}$) for each maximum bed weight.

Adsorbent	Maximum Bed Depth (cm)	Maximum Bed Weight (mg)	Toluene $T_{b\ 10\%}$ (min)	MEK $T_{b\ 10\%}$ (min)	Hexane $T_{b\ 10\%}$ (min)
ACFF 1200	2.149	2.119	85.12	79.58	56.97
ACFF 1800	1.553	1.399	71.52	42.44	49.79
ACFF 2000	1.550	1.312	71.61	39.56	43.21

Discussion

Adsorption capacity, defined as milligrams sorbate per grams of adsorbent, is useful in ranking the amount of sorbate that can potentially be removed from a contaminated airstream. Although granular activated carbon is the sorbent traditionally used in organic vapor respirators, the adsorption capacity of ACFs for toluene have compared favorably to the adsorption capacity of granular activated carbon for toluene in previous studies.[31,57] The observed differences in adsorption capacity between ACF types noted above may be related to both precursor material and surface area characteristics. For example, the ACF with the highest surface area (ACFF 2000) showed the highest adsorption capacity for aromatic and aliphatic VOC representatives used in this study (toluene and hexane, respectively). Additionally, ACFF 1800 had higher adsorption

capacities for toluene and hexane than ACFF 1200, the lowest surface area material used. However, ACFF 1200 had a much higher capacity for the polar organic VOC (MEK) than did ACFF 2000 (168.13 mg/g vs. 146.17 mg/g). PAN-derived ACFs tend to have a higher concentration of nitrogen- and oxygen-containing species than other conventional ACFs. Because adsorption is a surface phenomenon, such differences in polarity may explain why the ACFF 1200 shows greater capacity for the polar VOC MEK than rayon-based ACFs with greater surface areas. This suggests that some combination of surface chemistry and/or microporosity may be equally as significant as surface area in the adsorption of polar organic molecules onto activated carbon. Unfortunately, this study is limited in that the PAN-based ACF (ACFF 1200) and rayon-based ACFs (ACFF 1800 and ACFF 2000) were not tested at equivalent specific surface areas.

We previously defined a successful adsorption trial as an ACF depth that does not demonstrate immediate breakthrough and that is sufficient to prevent 5 ppm breakthrough for at least 150 minutes under our experimental conditions. ACF configurations that meet this criteria could potentially be considered for full-shift use scenarios against PEL-level contaminants. However, none of the maximum predicted 10% breakthrough times (Table 7) met the stated performance criteria, and 10% breakthrough times at maximum permissible bed depths did not approach full-shift durations: The best case scenarios were 85 minutes (ACFF 1200) for toluene, 79 minutes (ACFF 1200) for MEK, and 57 minutes (ACFF 1200) for hexane.

Based on these results, it is questionable whether an organic vapor N95 could accommodate enough ACF for shift-length protection without causing excessive breathing resistance; however, there is ample opportunity for further research. For

example, the “off-the-shelf” ACFs used in this study were not specifically designed for use in respiratory protection devices. Optimizing media bulk properties (such as fiber diameter and fiber packing density), or possibly blending the ACF with other filtration media to reduce pressure drop may be necessary to fully develop the concept of an organic vapor N95. It would also be interesting to investigate design techniques like respirator pleating to maximize carbon mass within stated pressure drop constraints. Additionally, any such media should also be tested under the more stringent flow conditions for particulate respirators described in 42 CFR Part 84.181 in addition to the flow conditions for organic vapor respirators (42 CFR Part 84.207), as used in this study.

We believe that a more immediate application for ACF would be its potential use in short-term “emergency use” N95 style respirators, or as the adsorbent component of “nuisance odor” N95-style respirators. For example, employees with chemical sensitivity or asthma may desire voluntary use of a lightweight respirator for chemical odors or chemical exposures below OSHA PELs. The incorporation of ACF into a facepiece respirator may be promising for the further reduction of organic vapor concentrations when workplace exposures are already below the permissible exposure limit, and NIOSH currently supports OSHA’s voluntary use provision of respirators for this purpose.

CHAPTER 4

ESTIMATION OF ACTIVATED CARBON FIBER ADSORPTION CAPACITY AND 10% BREAKTHROUGH TIMES USING A PREDICTIVE MODEL

Introduction

Activated carbon fiber has been studied by our laboratory as an alternative to GAC in respiratory protection devices. In this chapter, we calculated equilibrium adsorption capacities of two ACFs using the Dubinin-Radushkevich (D-R) isotherm equation.

To determine carbon breakthrough times (and by extension, respirator service life) *without* experimental data, an isotherm model is generally needed. An isotherm demonstrates the equilibrium behavior of the adsorbent/adsorbate and can be used to estimate the capacity of a microporous carbon for a particular adsorbate. The D-R isotherm equation is the most widely used model for predicting adsorption capacities of activated carbons used in organic vapor respirator cartridges, [58] and it can be used in conjunction with the Wheeler-Jonas equation (described in Chapter 3) to estimate respirator service life. In previously published work by our laboratory, breakthrough data was used to determine capacity by testing ACFs at successive bed depths. However, in order to reduce time and testing efforts, the goal of this Aim is to examine if the D-R equation can be used to predict ACF adsorption capacity and breakthrough times without performing breakthrough experiments.

Methods

ACF Media and Adsorbates

Two rayon-derived ACFs [ACFF 1800 and ACFF 2000; Bonding Chemical Co., Katy, TX.] were assessed in this study. The numbers 1800 and 2000 refer to the surface area of each material in m^2/gram, as reported by the manufacturer and as characterized by our laboratory using the BET method (1541.34 ±96.13 m^2/g and 1903.71 ±65 m^2/g, respectively). ACFF 1800 and 2000 have bulk densities of 0.0785±0.0053 g/cm^3 and 0.00673 ± 0.0024 g/cm^3, respectively; they are similar in depth (0.3 cm) and appearance, and are derived from the same manufacturer and precursor material. Adsorbates toluene, hexane, and MEK were used in breakthrough testing as representatives of aromatic, aliphatic, and polar hydrocarbons, respectively.

Breakthrough Testing

Experimental 10% breakthrough times ($t_{b\ 10\%}$) were determined for each ACF to allow for comparison with predicted values. The experimental set-up used to test ACF breakthrough time has been described previously. In short, ACF samples were placed in the test chamber and challenged with a VOC-containing airstream. Downstream challenge concentrations were monitored with a photoionization detector and the time at $(\frac{C_0}{C_x}) = 0.10$ (breakthrough concentration of 10%) was recorded. The ACFs were tested separately against three adsorbates (toluene, hexane, MEK) and for at least three bed depths, each corresponding to consecutive ACF layers. Test conditions were maintained at 25 ºC and RH of 30% by an ambient air-conditioning system (Assay Technology, Livermore, CA), and a flow rate of 7.5 LPM was employed for all experiments. This flow

rate corresponds to a face velocity of 10 cm/s at the test media surface. This face velocity was selected because it approximates the face velocity experienced by a filtering facepiece respirator (FFR) with an average surface area of 100 cm^2 when subjected to moderate airflow (64 LPM). $t_{b\ 10\%}$ results and corresponding bed weights were tabulated for comparison with predicted $t_{b\ 10\%,}$ as described below.

Adsorption Data

In the absence of experimental data, two carbon parameters (limiting micropore volume, W_o (cm^3/g); and characteristic energy of adsorption, E_o (kJ/mol)) can be used to calculate an equilibrium adsorption capacity in accordance with the D-R equation. These carbon parameters can be obtained from nitrogen adsorption isotherms. Each ACF media underwent nitrogen adsorption (n=3 trials) at 77K using a Micromeritics® ASAP 2020 Physisorption Analyzer (Micromeritics Corp, Norcross, GA). To determine the limiting micropore volume and energy of adsorption, a D-R transform of the N_2 isotherm data was plotted on a logarithmic scale using Micromeritics® MicroActive Reporting software. A linear regression of these data were used to extract W_o and E_o based on the intercept and slope of the regression line, respectively.

Equilibrium Adsorption Capacity for Toluene, Hexane, and MEK

The D-R equation can be extended to many different adsorbates through the addition of an affinity coefficient (β): the ratio of an adsorbate's molecular polarizability to that of a reference adsorbate, most often benzene.[23] We used the D-R equation to calculate the ACFF's equilibrium adsorption capacity at 200 ppm and 298K for each of the three adsorbates (toluene, hexane, MEK) using the carbon parameters W_o and E_0 as

determined above. [59] Input parameters used in our calculations (to include affinity coefficients for each adsorbate) are provided in Table 8.

Equation 4. [23]

$$W_e = W_o d_L \exp\left(-\left(\frac{RT \cdot \ln(P_0/P)}{\beta E_0}\right)^2\right)$$

where W_e = equilibrium adsorption capacity (g adsorbate/g carbon)
W_o = limiting micropore volume (cm^3/g carbon)
d_L = liquid density of the adsorbate (g/cm^3)
T= air temperature (K)
R = gas constant
P_0=saturation pressure
P=relative pressure of adsorbate
T = air temperature (K)
β = affinity coefficient of the adsorbate
E_0 = characteristic energy (kJ/mol)

Table 8. Input Parameters used to calculate ACFF 1800 and ACFF 200 equilibrium adsorption capacities for toluene, n-hexane, and MEK

Adsorbate	Toluene	n-Hexane	MEK
Molecular weight (g/mol)	92.14	86.16	72.11
Liquid Density (g/cm^3)	0.8669	0.6603	0.8054
Benzene Molecular Polarizability	26.259	26.259	26.259
Adsorbate Molecular Polarizability	31.054	29.877	20.681
β (Affinity Coefficient to Benzene)	1.162	1.123	0.806
P_0 in mmHg at 25 ºC	21	124	78

Adsorption Rate Coefficient

In order to predict breakthrough times in the absence of experimental data, some estimate of the adsorption rate coefficient must be made. For each ACF-adsorbate pair, adsorption rate coefficients were determined using the following semi-empirical relationship developed by Lodewyckx and Wood:[60]

Equation 5.

$$k_{v=} 800 \cdot \beta^{0.33} \cdot v_L^{0.75} \cdot d_p^{-1.5} \cdot \sqrt{\frac{W_e}{M_w}}$$

where k_v = adsorption rate coefficient (min-1)
W_e = equilibrium adsorption capacity (g/g), per Equation 1
v_L = linear velocity through filter (cm/s)
d_p= fiber diameter (cm)
Mw = molecular weight of adsorbate (g/mol)

This equation has been successfully applied to ACFs by substituting fiber diameter for particle diameter.[35] Because ACF fiber diameters are much smaller in diameter than GAC particles used in many respirator cartridges (0.10 -0.11 cm),[59] the overall implication of this substitution is a much faster kinetic profile for ACF in comparison to a traditional granular adsorbent. To estimate fiber diameter, each ACFF was visualized at 5000X using an Apreo™ 2 Scanning Electron Microscope (Thermofisher Scientific, Waltham, MA) operated at 20 kV voltage and 0.40 nA current. Values used to calculate ACFF 1800 and ACFF 2000 adsorption rate coefficients are provided in Table 9, below.

Table 9. Input Parameters used to calculate ACFF 1800 and ACFF 2000 adsorption rate coefficients for toluene, n-hexane, and MEK.

Adsorbate	Toluene	n-Hexane	MEK
Molecular weight (g/mol)	92.14	86.16	72.11
β (Affinity Coefficient to Benzene)	1.162	1.123	0.806
Equilibrium Adsorption Capacities (g/g)	0.346	0.183	0.135
ACFF 1800 and 2000 fiber diameter (cm)	*0.001 cm (per SEM images)*		
Linear velocity through filter (cm/s)	*10 cm/s*		

Calculation of Breakthrough Time

The Wheeler-Jonas (WJ) equation, a semi-empirical model of breakthrough time, was then used to predict ACF breakthrough times at ($\frac{C_0}{C_x}$) = 0.10. The WJ equation has been successfully applied to the adsorption behavior of granular activated carbon (GAC)

and ACF packed beds;[55] in our previous study, we used the Wheeler-Jonas equation to determine ACF adsorption capacity based on experimental inputs.

Equation 6. $$t_{b=} \frac{W_e W}{C_0 Q} - \frac{W_e \rho_b}{C_0 k_v} \cdot \ln\left(\frac{C_0}{C_x}\right)$$

Where t_b = breakthrough time (min)
W_e = kinetic adsorption capacity (g/g)
W=weight of adsorbent (g)
C_0=inlet concentration (g/cm^3)
C_x =outlet concentration (g/cm^3)
Q =volumetric flow rate (cm^3/min)
k_v = rate constant of adsorption (min $^{-1}$)
ρ_b = density of the packed bed (g/cm^3)

To predict breakthrough time without experimental inputs, estimates of W_e and k_v were used in Equation 2, along relevant experimental conditions (i.e., 200 ppm challenge concentration; 7.5 L/min flow rate, and a 10% breakthrough target) and carbon bulk properties (ACFF 1800 density 0.0785±0.0053 g/cm;[3] ACFF 2000 density 0.00673 ± 0.0024 g/cm^3). Results were compared with experimental breakthrough times.

Results

Adsorption Data

Isotherm data indicated that ACFF 1800 had an average limiting micropore volume of 0.579 ± 0.044 cm^3/g and characteristic energy of 16.88 ± 0.023 kJ/mol. ACFF 2000 had an average limiting micropore volume of 0.673 ±0.023 cm^3/g and a characteristic energy of 17.25 ± 0.34 kJ/mol. ACFF limiting micropore volumes compare favorably with those of GAC used in commercially available OV cartridges (0.434 – 0.783 cm^3/g). [59]

Table 10. Limiting micropore volume and characteristic energy, as obtained through N_2 adsorption isotherm data.

Parameter	Units	ACFF 1800	ACFF 2000
Limiting Micropore Volume, W_o	cm^3/g	0.579 ± 0.044	0.673±0.023
Characteristic Energy	kJ/mol	17.25±0.34	16.88 ±0.12

Equilibrium Adsorption Capacity and Adsorption Rate Coefficients

W_o and E_o were used to determine each ACF's equilibrium adsorption capacity for toluene, hexane, and MEK at a concentration of 200 ppm using the D-R equation. In all instances, equilibrium capacities for ACFF 2000 were higher than those of the ACFF 1800, based on lower characteristic energy and higher micropore volume input values. SEM images of the ACFs reveal an approximate range of fiber diameters between 8-10 μm, allowing for the calculation of k_v using equation 5.

Table 11. Toluene, Hexane, and MEK equilibrium adsorption capacities and adsorption rate coefficients for ACFF 1800 and ACFF 2000.

Parameter	Units	ACFF 1800	ACFF 2000
$W_{e\ toluene}$	mg/g	346.76	403.03
$W_{e\ n\text{-}hexane}$	mg/g	183.50	213.28
$W_{e\ n\text{-}MEK}$	mg/g	135.83	157.88
$k_{v,\ toluene}$	min^{-1}	9.22E+06	9.94E+06
$k_{v,\ n\text{-}hexane}$	min^{-1}	6.85E+06	7.39E+06
$k_{v,\ n\text{-}MEK}$	min^{-1}	5.71E+06	6.15E+06

Breakthrough Time Calculation

In general, breakthrough time predictions aligned well with our experimental results (Tables 12-14; Figures 16-17). Predicted $t_{b10\%}$ exceeded experimental $t_{b\ 10\%}$ in all but three instances.

Table 12. Comparison of Experimental and Predicted $t_{b\ 10\%,}$ with 200 ppm toluene as the adsorbate.

Adsorbent	Layer	Bed weight (g)	Experimental $t_{b10\%}$ (min)	Predicted $t_{b\ 10\%}$ (min)
ACFF 1800	1	0.204	10.83	*12.69*
	2	0.390	21.83	*24.31*
	3	0.591	32.50	*36.73*
	4	0.780	46.50	*48.53*
ACFF 2000	1	0.204	10.42	*14.60*
	2	0.430	21.42	*30.72*
	3	0.585	34.83	*41.77*
	4	0.729	45.67	*52.05*

Table 13. Comparison of Experimental and Predicted $t_{b\ 10\%,}$ with 200 ppm hexane as the adsorbate.

Adsorbent	Layer	Bed weight (g)	Experimental $tb_{10\%}$ (min)	Predicted $t_{b\ 10\%}$ (min)
ACFF 1800	1	0.216	6.85	*7.66*
	2	0.352	12.33	*12.45*
	3	0.681	24.17	*24.11*
ACFF 2000	1	0.180	4.70	*7.26*
	2	0.364	13.00	*14.68*
	3	0.515	18.67	*20.80*

Table 14. Comparison of Experimental and Predicted $t_{b\ 10\%}$, with 200 ppm MEK as the adsorbate.

Adsorbent	Layer	Bed weight (g)	Experimental $t_{b10\%}$ (min)	Predicted $t_{b\ 10\%}$ (min)
ACFF 1800	1	0.180	5.33	*6.27*
	2	0.356	12.17	*12.09*
	3	0.561	19.5	*17.99*
	4	0.762	27.67	*22.26*
ACFF 2000	1	0.216	6.17	*6.98*
	2	0.417	12.83	*13.72*
	3	0.621	18.5	*23.33*
	4	0.769	27.83	*25.88*

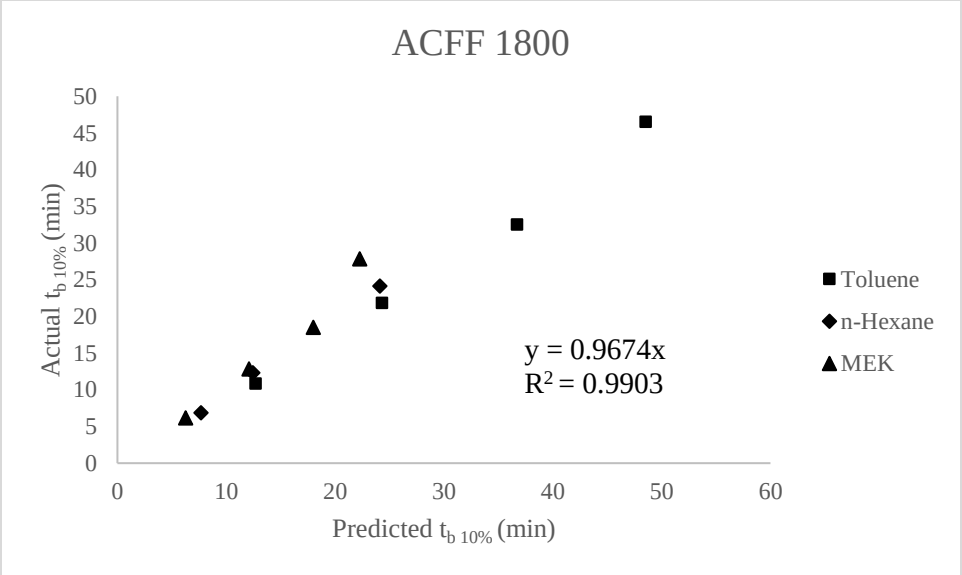

Figure 16. Predicted versus actual 10% breakthrough times for ACFF 1800. A linear least squares slope with a forced zero intercept (0.9674) and squared correlation coefficient (0.9903) have been provided.

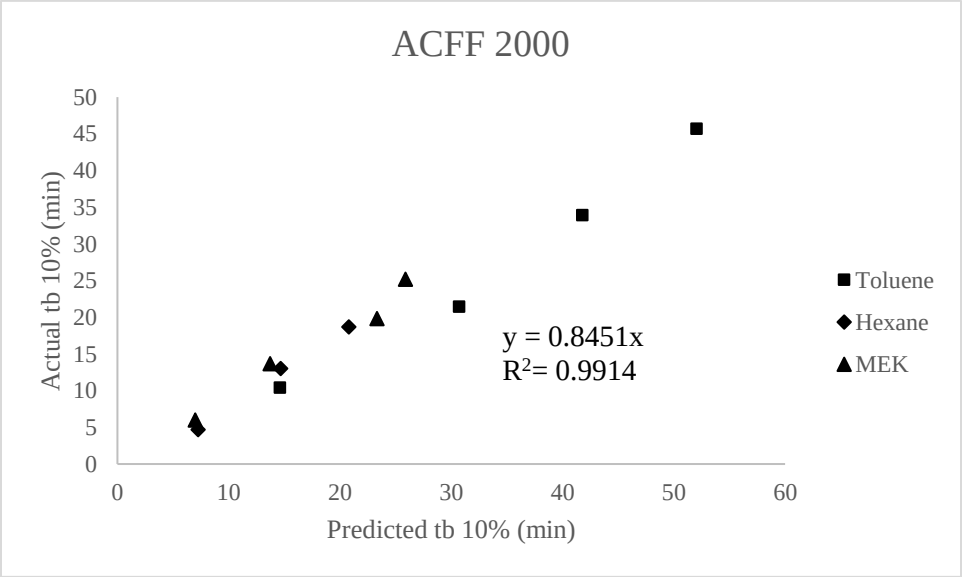

Figure 17. Predicted versus actual 10% breakthrough times for ACFF 2000. A linear least squares slope with a forced zero intercept (0.8451) and squared correlation coefficient (0.9914) have been provided.

Discussion

In this Aim, we estimated ACFF breakthrough times for three organic vapors, using a flow rate and challenge concentration that are relevant to respiratory protection applications. Our method relied on N_2 adsorption and the D-R isotherm equation to estimate a capacity term for each carbon-adsorbate system, and Lodewyckx and Wood's extended rate coefficient equation to estimate a kinetic term (i.e., adsorption rate coefficient). Based on these inputs, the Wheeler-Jonas Equation was then used to predict breakthrough times, which compared favorably with experimental results described in Chapter 3. The above method has been applied extensively to GACs in the context of respirator service life predictions; [56] [61] however, the use of the D-R equation to predict ACF breakthrough times for respiratory protection applications is limited. [31]

In almost all cases, we noticed that the predicted values of breakthrough time were greater than actual breakthrough time. (Several exceptions were noted for ACFF 1800-MEK and ACFF 2000 MEK). In the context of respirator service life prediction, the opposite is generally desirable: a predictive model that underestimates service life may be more protective of worker health. The D-R equation has shown a tendency to overestimate capacity and by extension breakthrough time in previous studies: this was demonstrated through the testing of respirator cartridge breakthrough time for over 30 chemicals at concentrations between 100 and 2000 ppm at Los Alamos National Laboratory.[22] The tendency of the D-R equation to overestimate capacity is believed to be related to uncertainty in the β term. Another known limitation of the D-R isotherm equation is that it does not reduce to Henry's Law at very low concentrations. To address

this concern, it would be useful to repeat the above study at nuisance-level (ppmv-ppmb) concentrations.

This study was limited by lack of statistical analysis examining the relationship between experimental and predicted breakthrough times, as presented in Tables 12-14 and Figures 16-17, although in many cases predicted vs. experimental breakthrough times for ACFF 1800 were within 2 minutes of each other. In future studies, it may be useful to set performance criteria (i.e., ±5% difference) to identify "successful" breakthrough time predictions. Determining the "success" of the predictive model may also be possible by computing the confidence interval of the slopes in Figures 6-7, with a confidence interval that bounds 1.0 indicating no significant difference between predicted and experimental values.

Future research would ideally look at attempt $t_{b10\%}$ prediction under conditions that are more challenging (i.e., higher relative humidity and heat) and/or that encompass a greater range of concentrations (low ppmv and ppmb) and adsorbate classes.

CHAPTER 5

PARTICULATE FILTRATION STUDY OF NON-WOVEN ACTIVATED CARBON FIBER

Introduction

Particulate respirators are commonly used in the workplace to protect the wearer against dust, fumes, and mists. Particulate respirators are also referred to as "non-powered air purifying particulate respirators (APRs)" and are classified by the National Institute of Occupational Safety and Health (NIOSH) according to their filtration efficiency (i.e., 95-, 99-, and 100-series) and resistance to oil-based aerosols (N, R, and P series). Particulate respirators may exist as filtering facepiece respirators (FFRs), in which the filter medium is integral to the body of the respirator (i.e., N95 respirators). They may also be used as components of respirator cartridges (i.e., P100 cartridges) for half- or full-face respirator assemblies.

For non-powered APRs to function, contaminated air is drawn across a filter medium by the negative pressure that results from inhalation. The performance of a filter system for a particular challenge aerosol can be predicted based on several input factors, which include particle size, linear velocity through the filter, filter depth, filter surface characteristics, and filter fiber diameter.[15] The overall efficiency of a filter system results from the combined action of several filtration mechanisms, each of which predominate at different particulate size ranges and/or flow conditions.

Our laboratory has previously investigated activated carbon fiber (ACF) as a potential adsorbent material for use in respiratory protection devices that protect the wearer against organic vapors. Activated carbon fiber is produced when an organic precursor fiber is heated to high temperatures in an inert atmosphere and then exposed to an oxidizing atmosphere, usually steam or carbon dioxide, in a process called "activation." The activation stage is responsible for creating an extensive pore structure on the surface of the fiber that allows for adsorption of organic vapors. During the carbonization and activation stages, the overall form and fiber matrix of the precursor material is preserved. Previous studies have speculated that the self-supporting fibrous form of ACF may participate in particulate filtration as well as organic vapor capture,[38] and at least one design for a combined vapor and particulate respirator cartridge that incorporates ACF has been patented to date.[39]

The filtration performance of ACF has been described in both HVAC and industrial air pollution control technology applications;[35,36,41,62,63] however, filtration performance of activated carbon fibers under use conditions relevant to respiratory protection has not yet been studied. The requirements for the performance testing of non-powered particulate APRs can be found in 42 CFR Part 84.207 and have been adopted by NIOSH in their standard test protocols for N95 respirator certification (NIOSH TEB-STP-APR-0059). This STP has specific requirements for test aerosol characteristics, challenge flow rate and humidity, aerosol measurement, and acceptable performance criteria.[18] Performance testing of ACFs using this test protocol, or other conditions that can be directly related to respiratory protection, has not yet been described in the literature.

To further develop the concept of an ACF-containing respirator that offers particulate filtration in addition to nuisance-level or short-term organic protection, the filtration efficiency of three "off-the-shelf" ACFs were determined using parameters that are relevant to respiratory protection, as described below. ACFs were testing using a benchtop set-up developed in our laboratory, in addition to the NIOSH TEB-STP-APR-0059 protocol for initial filter penetration.

Methods

ACF Media.

Three ACF felts (ACFFs) were selected for this study and are intended to reflect a variety of precursor materials, surface areas and media bulk properties. These ACFFs include two rayon-derived ACFs [ACFF 1800 and ACFF 2000; Bonding Chemical Co., Katy, TX.], and one PAN-derived ACF [ACFF 1200, CeraMaterials, Dingmans Ferry, PA]. The numbers 1200, 1800, and 2000 refer to the surface area of each material in m^2/gram, as reported by the manufacturer and as previously characterized by our laboratory through surface area analysis in Chapters 3 and 4.

Media Characterization

To better visualize ACF felt structure, individual fiber morphology, approximate fiber diameter and degree of fiber uniformity. SEM images were obtained using an Apreo™ 2 Scanning Electron Microscope (Thermofisher Scientific, Waltham, MA) operated at 20 kV voltage and 0.40 nA current. Each ACF felt was visualized at three magnifications (50X, 500X, and 5000X). ACF felts were also characterized in terms of packing density, or (α). Packing density is a unitless ratio of fiber volume to the bulk

volume of a filter medium.[15] In general, this term accounts for void space versus occupied space in a filter material. The impact of packing density on pressure drop and overall filtration efficiency have been well-described.[15] In order to determine packing density, uniform sections (6 cm diameter) of ACFF were cut and weighed (n=8). ACFF thickness was measured using Manostat™ calipers, and the apparent volume and bulk density of each ACFF cutting was determined. A literature derived value for the skeletal density of activated carbon fiber (2.00 g/cm^3)[64] was used in combination with the collected data to determine α, in accordance with Equation 4 below:

Equation 4. $$\text{Solidity } (\alpha) = \frac{\text{filter mass (g)}}{\left(\text{Skeletal Density } \left(\frac{\text{g}}{\text{cm}^3}\right)\right)(\text{Apparent Volume } (\text{cm}^3)}$$

Most Penetrating Particle Size (MPPS) Estimate

Determinations of approximate fiber diameter and packing density allowed for the calculation of most penetrating particle size (MPPS) for each ACF felt under planned test conditions. In accordance with filtration theory, filter systems have a diameter of minimum efficiency at which individual filtration mechanisms perform at a relative minimum. The MPPS varies with experimental conditions related to flow, kinetics, and with certain filter properties, per Equation 5,[17] below:

Equation 5.[17] $$D_{p,min} = 0.885\left(\left(\frac{K}{1-\alpha}\right)\left(\frac{\sqrt{\lambda}\,kT}{\mu}\right)\left(\frac{D_f^2}{u}\right)\right)^{\frac{2}{9}}$$

where $D_{p,\,min}$= minimum efficiency diameter, or most penetrating particle size
K=Kuwubara hydrodynamic factor
α= solidity, or fiber volume fraction of the material
u= face velocity
λ = mean free path of gas molecules (6.65 x 10^{-8} m)

k= Boltzmann's constant
μ = gas viscosity (1.80 x 10^{-5} Pa)
T= absolute temperature

Experimental Set-up

To test media filtration efficiency, a benchtop aerosol generation and measurement system was assembled in our laboratory. A block diagram and photographs of the experimental set-up are provided in Figure 18-20. Key elements of the experimental set-up are described below.

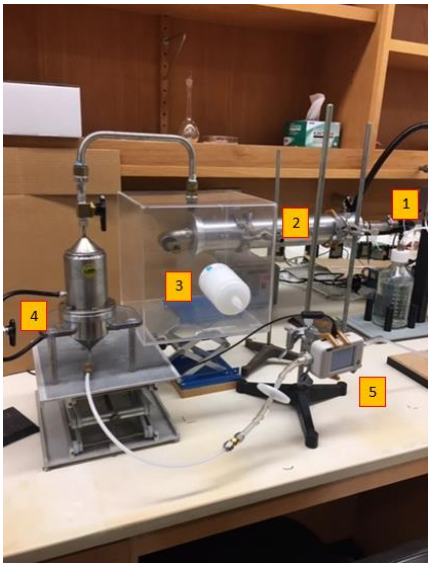

Figure 18. Key elements of experimental set-up (1) Aerosol Generator operated at 20 psi; (2) Charge Neutralizer; (3) Mixing Chamber; (4) Sampling Chamber with upstream and downstream ports to WPS; (5) Downstream flowmeter connected to laboratory vacuum.

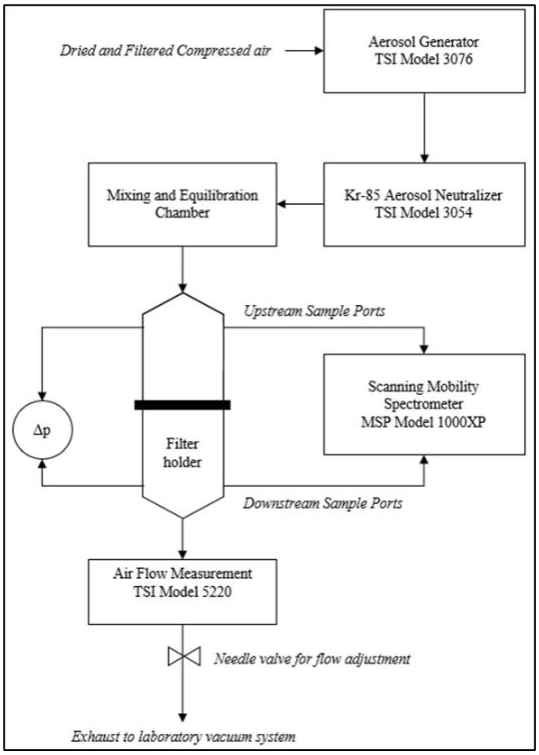

Figure 19. Simplified experimental set-up for particulate filtration efficiency testing of ACF media.

Aerosol Generation and Transmission

To generate a test aerosol, a 4 mg/cm^3 salt solution was added the reservoir of a TSI Model 3076 constant output atomizer (TSI, Shoreview, MN), which was operated at 20 psi using filtered and dried laboratory compressed air. Size distribution measurements (n=4) of the test aerosol show a count median diameter (CMD) of 73.03 nm and geometric standard deviation (GSD) of 1.71 After generation, the aerosol was neutralized with a Kr-85 source (TSI, Shoreview, MN) before entering a mixing and equilibration chamber, where it encountered HEPA-filtered make-up air. The neutralized aerosol was then drawn from the mixing chamber to the sample chamber using a downstream vacuum source.

Filter Sample Chamber

ACFF samples were placed in a stainless steel chamber, which was adapted from previous use by our laboratory in organic vapor breakthrough testing of ACF as described in Chapter 3. The chamber contains upstream and downstream sample ports for aerosol measurement. The upstream and downstream sample ports were fitted with non-conductive silicon tubing of equal length to convey the aerosol from the sample chamber to the aerosol measurement system. The sample chamber also contains upstream and downstream pressure taps that were fitted with hose barbs for connection to a differential pressure sensor (TSI Velocicalc Model 9565). The internal diameter of the chamber is 4 cm with a tapered inlet and an expansion section (>2 internal diameters from the inlet to the filter material) to ensure laminar flow at the face of the test media.

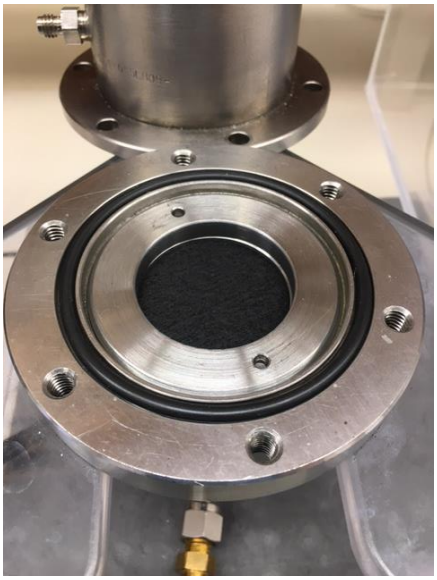

Figure 20. Interior of sample chamber, showing filter holder platform. Filter material (ACFF 1200 pictured above) is held in place between two circular chucks with an internal diameter of 4 cm. A threaded component is tightly fitted on top of the filter media and prevents filter bypass.

Flow conditions

A flow rate of 7.5 LPM was employed for all experiments. For the chamber dimensions, this flow rate corresponds to a face velocity of 10 cm/s at the test media surface. As previously described in Chapter 3, this face velocity approximates the face velocity experienced by a filtering facepiece respirator (FFR) with an average surface area of 100 cm^2 when subjected to moderate airflow (64 LPM).[18] To ensure consistent flow conditions, a flow meter (TSI Multi-meter Model 5200) was placed in-line immediately downstream of the sample chamber. The flow meter has a digital display which allowed for real-time monitoring of sample flow rate. For this experiment, no attempt was made to control temperature or relative humidity beyond ambient conditions.

Aerosol measurement

An MSP brand (Shoreview, MN) Wide Range Particle Spectrometer (WPS)(Model 1000XP) was used to determine aerosol concentrations using a count-based method. The WPS consists of three on-board instruments: a differential mobility analyzer (DMA), a condensation particle counter (CPC), and a laser particle spectrometer (LPS). In our application, the WPS was operated in Scanning Mobility Particle Sizer (SMS) mode. This mode incorporates the input of the CPC and DMA to produce particle count data resolved to discrete size ranges of particles ("bins" or "channels"). The scanning mode reflects a fast cycle time between channels. Because downstream and upstream concentrations were taken successively, not simultaneously, the scanning mode was preferred in order to avoid error associated with any unforeseen temporal shifts in the make-up of the test aerosol. The WPS in SMS mode has a range of measurement of 10-350 nm and a 12-36 channel resolution.

Determination of Filtration Efficiency and Pressure Drop

For each media type, initial penetration and filtration efficiency were determined by performing successive downstream and upstream measurement cycles (n=3). Pressure drop across the media was logged using a TSI DP-Calc micromanometer (TSI, Shoreview, MN). Initial penetration and pressure drop was then performed for N= 2, 3, and 4 layers of media. A single layer of North Brand N95 media (#7130N95S) was also tested as a positive control. For each trial, filter penetration and filter efficiency were determined as follows:

Equation 7.[15] $$\text{Penetration (\%)} = \frac{\text{Particle Concentration Upstream}}{\text{Particle Concentration Downstream}} \text{ x } 100$$

Equation 8 $$\text{Filtration Efficiency (\%)} = 100 - \text{Penetration (\%)}$$

Determination of Quality Factor

Because the tested materials have different bulk properties (i.e., different thicknesses and packing densities), *quality factor* (q_F) was used as a metric of comparison across ACF types. q_F is the ratio of fractional particle capture per unit thickness to pressure drop per unit thickness.[15] It can be expressed as follows:

Equation 9.[15] $$q_F = \frac{\ln\left(\frac{1}{P}\right)}{\Delta p}$$

Where P = fractional filter penetration
Δp = pressure drop (mm H2O)

Depth Filtration

The evolution of pressure drop and filtration efficiency with successive layers of media can be described by Equations 10 and 11,[65] respectively. In general, filter

penetration tends to decrease exponentially with the addition of successive layers, and filter pressure drop tends to be additive with additional layers.

Equation 10.[65] $$\Delta p_{total} = \Delta p_{total} + \Delta p_{total} + \cdots$$

Equation 11.[65] $$\text{Filtration Efficiency}_{total} = 1 - (P_{\text{Layer 1}} \cdot P_{\text{Layer 2}} \cdot \ldots)$$

However, the above equations assume that filters in series behave independently of each other. In reality, non-ideal effects like the development of airflow disturbances and preferential flow pathways can occur at the interface of layered filters.[16] To test the assumptions of layer independence, measured ACF filtration efficiencies at Layers 2-4 were compared with predicted efficiency per Equation 11.

Automated Filter Testing

In addition to benchtop testing performed in our laboratory, ACFF samples were tested for instantaneous filter penetration using an Automated Filter Tester (TSI Model 8130A) at the University of Iowa. Tests were conducted according to instructions for initial penetration as described in NIOSH TEB-APR-STP-0059, a standard test method used to certify N95 respirators in accordance with the performance criteria of 42 CFR 84. Unlike the CPC/DMA combination used in our aerosol measurement system, the TSI Model 8130A uses a light-scattering photometer to measure aerosols. Additionally, the conditions of use for the Automated Filter Testing are also more stringent than criteria used in our laboratory: ACFFs were tested at 85 ± 5% LPM and challenged with 200±5 mg of a NaCl test aerosol. The sample collection time was one minute, and single layers of ACFF were tested in duplicate.

Results

SEM Images and Media Characterization

SEM images appear in Figures 19-27. Images of each ACF type at 50x magnification indicate randomly oriented fibers consistent with a non-woven felt matrix. Magnification at 500X further indicate that fibers of each ACF type are relatively uniform in appearance and diameter. Estimates of fiber diameter were obtained from SEM images at 5000X. All fibers have a ridged appearance and an approximate range of diameters between 8-10 µm. Despite having a different manufacturer and precursor material, ACFF 1200 showed similar appearance and fiber diameter when compared to ACFF1800 and ACFF 2000. Media characterization (Table 15) indicates that ACFF 1200 has the highest bulk density (0.0547 g/cm^3) and packing density (0.0273) of the tested media. Calculation of the MPPS for the given test conditions and media ranged between 435-439 nm.

19 *20* *21*

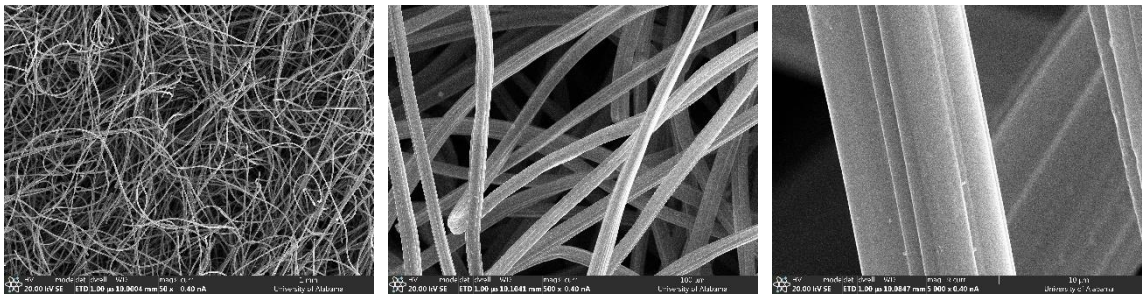

Figures 19-21. ACFF 1200 SEM images at 50X, 500X and 5000X magnification**.**

22 *23* *24*

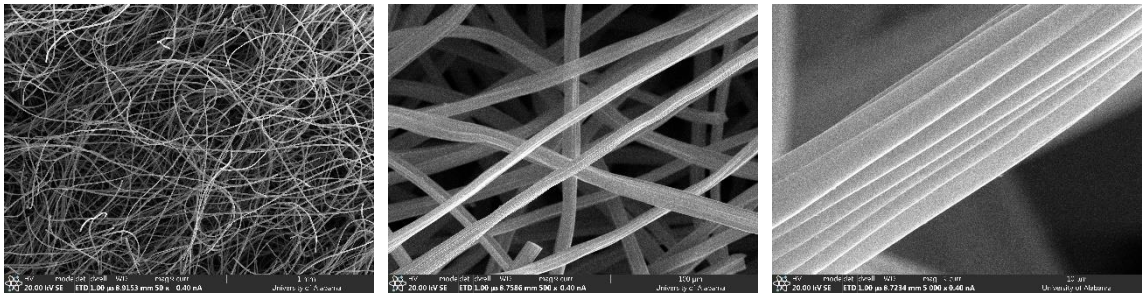

Figures 22-24. ACFF 1800 SEM images at 50X, 500X, and 5000X magnification.

25 *26* *27*

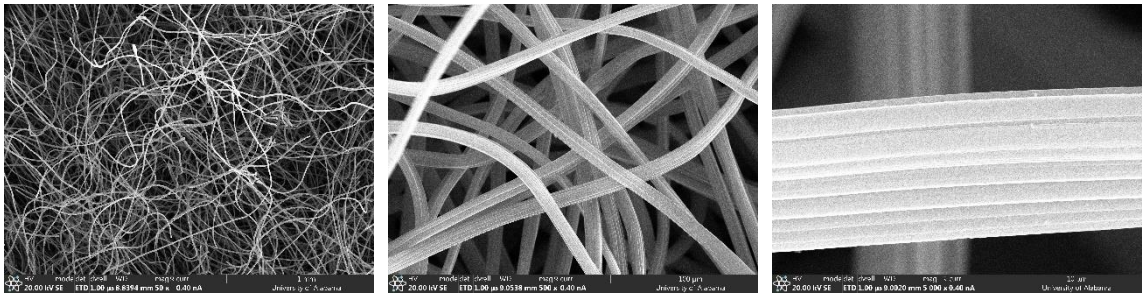

Figures 25-27. ACFF 2000 SEM images at 50X, 500X, and 5000X magnification.

Table 15. Media characterization by fiber diameter, bulk density, and packing density. MPPS for a 10 cm/s face velocity is also shown.

Media Type	Fiber Diameter (μm)	Bulk Density (g/cm^3)	Packing density (α)	MPPS (nm) at 10 cm/s face velocity
ACFF 1200	8-10	0.0547	0.0273	435
ACFF 1800	8-10	0.0520	0.0260	437
ACFF 2000	8-10	0.0488	0.0244	439

Filtration Efficiency and Pressure Drop Testing

A graph of size-resolved filtration efficiency for each media at N=1 layer appears in Figure 28. Although the SMS has a measurement range of 10-350 nm, size bins below the 31.47 nm median channel diameter were excluded from analysis based on low

and inconsistent number concentrations. Visual inspection of filtration efficiency plots for each ACF media shows high efficiency in the diffusion regime that declines with increasing particle diameter. Consistent with calculations of MPPS in Table 8, Figure 28 indicates that our measurement system approaches but does not fully encompass diameters of minimum efficiency for the tested media.

A summary of results for N=1 layer appear in Table 16. For single layer tests, ACFF 1200 (the thinnest media) had the highest initial penetration (43.25%). However, this media showed the lowest pressure drop and highest filter quality factor, indicating bulk properties that are more favorable to filtration than the ACFF 1800 and ACFF 2000. For single layer testing, ACFF 1800 and 2000 showed similar performance (33.16% and 31.78% initial penetration; 5.71 mm H_2O and 5.42 mm H_2O, and 0.019 0.021 mm^{-1} H_2O and 0.021 mm^{-1} H_2O quality factor). As these materials are made by the same manufacturer and with the same precursor material, no significant difference in global filtration efficiency or pressure drop was anticipated between these two media.

Table 16. ACF single layer filtration efficiency at 10 cm/s and using the experimental set-up shown above.

Media Type	Pressure Drop (mm H_2O)	Instantaneous Filter Efficiency (%)	Instantaneous Penetration (%)	Quality Factor (mm H_2O^{-1})
ACFF 1200	3.40	56.75	43.25	0.02513
ACFF 1800	5.71	66.84	33.16	0.01971
ACFF 2000	5.42	68.22	31.78	0.02132

Table 17 shows the results of filtration testing at layers 2-4 of ACFF media. Measured filtration efficiencies are shown with predicted filtration efficiencies, per Equation 11. Under these test conditions, all ACFF media types achieve >95%

particulate filtration efficiency at N=4 layers. Close alignment between measured and predicted filtration efficiencies indicate that ACFF filtration at depth can be reasonably predicted.

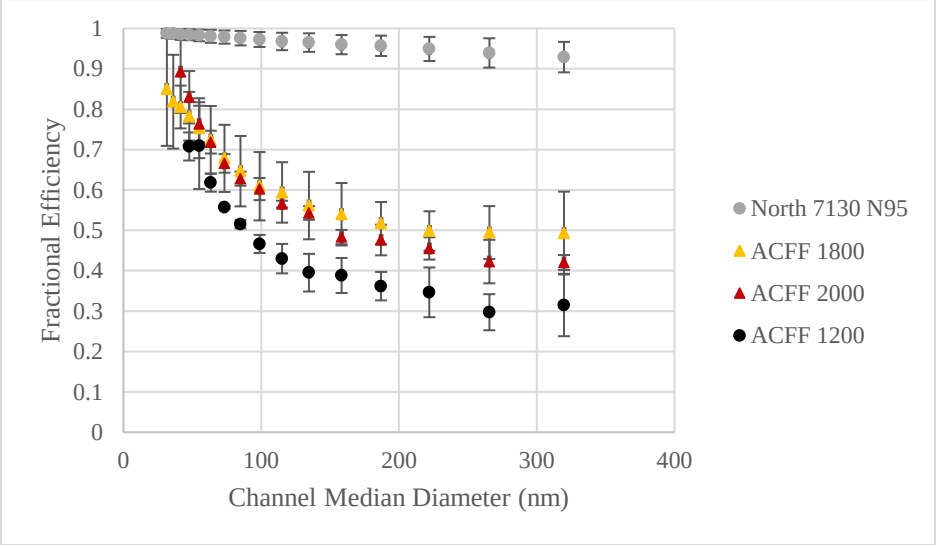

Figure 28. Initial filtration efficiency versus particle diameter for each tested media at a 10 cm/s face velocity and N=1 layer of media. A sample of N95 media was tested as a positive comparison.

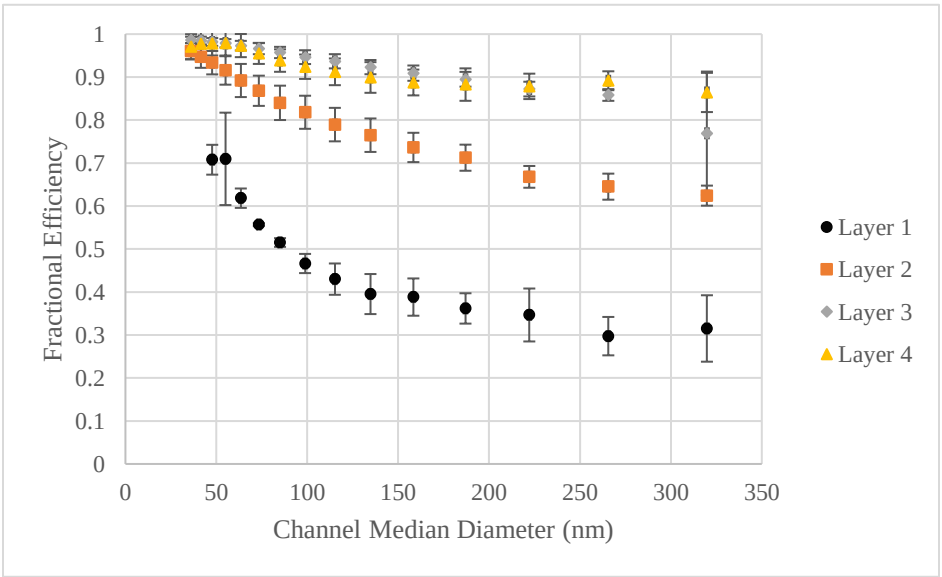

Figure 29**.** ACFF 1200 initial filtration efficiency versus particle diameter at a 10 cm/s face velocity and N=1-4 layer of media.

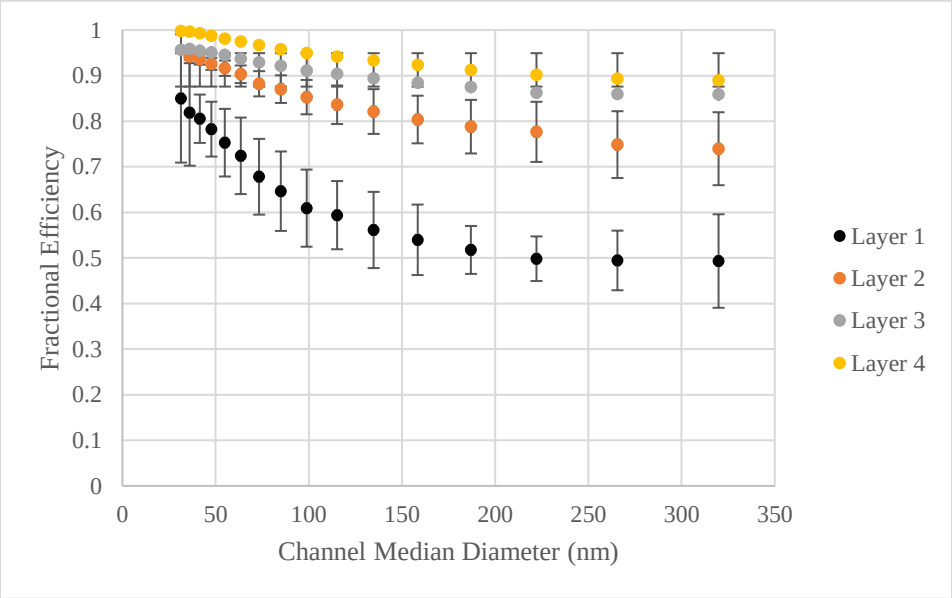

Figure 30. ACFF 1800 initial filtration efficiency versus particle diameter at a 10 cm/s face velocity and N=1-4 layer of media.

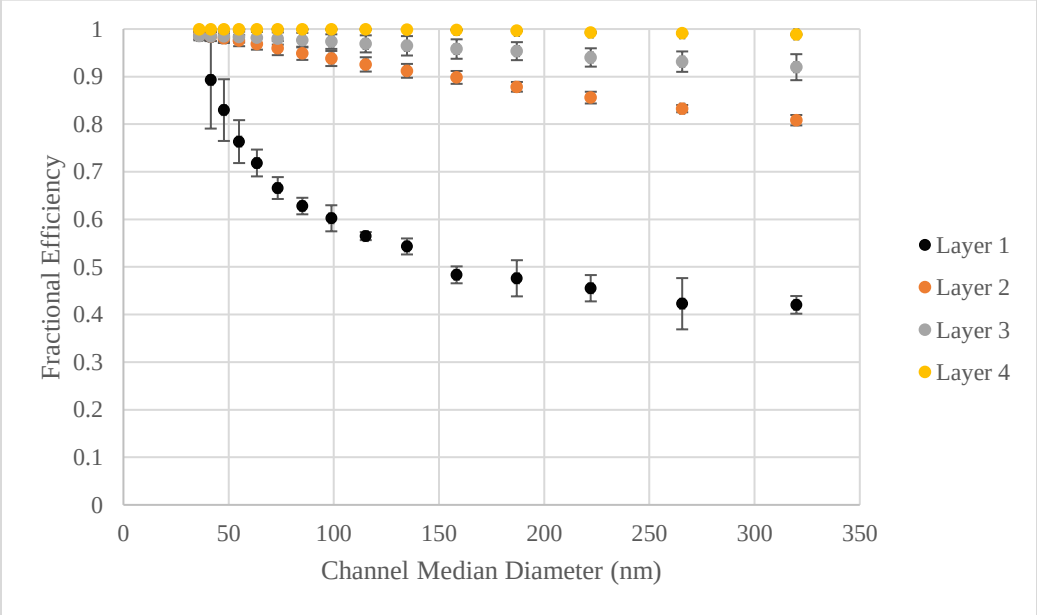

Figure 31**.** ACFF 2000 initial filtration efficiency versus particle diameter at a 10 cm/s face velocity and N=1-4 layer of media.

Table 17. ACF measured and predicted filtration efficiency at layers 2-4. Predicted filtration efficiency is given by $(1-(P^N))*100$, where P is fractional penetration of Layer 1 and N is the number of layers.

Media	Measured Filtration Efficiency (%)	Predicted Filtration Efficiency (%)	Percent Difference
ACFF 1200 Layer 2	84.43	81.29	3.71
ACFF 1200 Layer 3	95.27	91.91	3.53
ACFF 1200 Layer 4	95.51	96.50	-1.04
ACFF 1800 Layer 2	86.62	89.01	-2.76
ACFF 1800 Layer 3	94.00	96.36	-2.51
ACFF 1800 Layer 4	98.53	98.79	-0.26
ACFF 2000 Layer 2	94.77	89.90	5.14
ACFF 2000 Layer 3	97.44	96.79	0.67
ACFF 2000 Layer 4	99.89	98.98	0.91

Automated Filter Testing

Average results (n=2 trials and N=1 layer of media) from the Automated Filter Test trials are shown in Table 18. Instantaneous penetration values obtained using this method were considerably higher (68.662% - 77.393%) than those obtained at our laboratory (31-75% - 43.25%). This difference is most likely due to the 8130A's more challenging flow conditions (85 LPM) and a photometric measuring system that was more likely to interact with the media's predicted MPPS than the count-based system used at our lab.

Table 18. Single layer testing of ACFF media at 85 lpm using a TSI Model 8130 Automated Filter Tester.

Media Type	Pressure Drop (mm H_2O)	Instantaneous Filter Efficiency (%)	Instantaneous Penetration (%)
ACFF 1200	5.395	22.607	77.393
ACFF 1800	7.815	29.586	70.414
ACFF 2000	8.460	31.338	68.662

Table 19. Predicted maximum filtration efficiency within the confines of a 35 mm H_2O inhalation resistance when tested based on single layer filtration efficiency from Table 18.

Media Type	Maximum Bed Depth	Predicted Efficiency at Maximum Bed Depth	Meets N95 Particulate Filtration Criteria?
ACFF 1200	6 Layers (1.5 cm)	79.15%	No
ACFF 1800	6 Layers (1.8 cm)	87.81%	No
ACFF 2000	5 Layers (1.5 cm)	84.73%	No

Discussion

In this study, ACFFs were tested for filtration efficiency using two different test methods. The first method, developed in our laboratory, employed a face velocity of 10 cm/s, which approximates velocity through a 100 cm^2 FFR at a 64 LPM airflow. Based on the diameter of the test chamber in our laboratory, a 7.5 liter per minute flow rate was used to achieve a 10 cm/s face velocity. However, this flow rate and face velocity are both significantly lower than the flow rate and face velocity used in the NIOSH TEB-APR-STP-0059 protocol. Our laboratory determined filtration efficiency using a count-based measurement system. Under the flow conditions described above, ACFF 1200, 1800, and 2000 demonstrated global filtration efficiency >95% when tested at N=4 layers. Additionally, ACFF 1200, 1800, and 2000 measured below 35 mm H_20 pressure drop at N=4 layers.

The second method, based on NIOSH TEB-APR-STP-0059, employed a photometric aerosol measuring system and an 85 LPM flow rate, which equates to a higher face velocity (approximately 14 cm/s) and volumetric flow rate than was used in our experimental set-up. Under these conditions, single layer ACFFs showed initial filtration efficiencies much lower than those demonstrated in our laboratory: between 22.6%-31.34%. Using Equations 10 & 11[65] and the assumption that layers of ACFF

behave independently at depth, we conclude that ACFF in its current form would most likely *not* be capable of achieving > 95% filtration efficiency without exceeding the upper limit on pressure drop for FFRs (35 mm H_2O inhalation resistance). Based on our findings, ACF can be predictably layered to yield greater filtration efficiency; however, in their current form, all ACFFs likely pose too great a pressure drop to be used as the exclusive filtration medium in an N95 respirator when tested according to NIOSH TEB-APR-STP-0059 (Table 19). In general, these results suggest that ACFF is best suited as an adjunct to, rather than the primary means of filtration in an N95 respirator.

Broader conclusions about the suitability of ACFF as a filter media cannot necessarily be concluded on the basis of these tests alone. In our experimental design, "off-the-shelf" ACFFs were used because they were readily available and relatively cost-effective. Because both filtration efficiency and pressure drop vary predictably with modifiable bulk properties like depth, packing density, and fiber diameter, it is possible that an ACFF filter could be tailored for better performance in respiratory applications.

There were several limitations to this study. One clear limitation of this study is that the aerosol measuring system employed by our laboratory did not encompass the MPPS that was modeled for each ACFF based on our estimates of fiber diameter and packing density. Nevertheless, the count-based data collected in our laboratory provided insight into the filtration efficiency of ACFFs for ultrafine particles (<100 nm), which are generally too small to be detected by photometric aerosol measuring systems. In testing single layer ACF filtration efficiency, a sample of N95 media was also tested as a positive comparison. However, the N95 filtration efficiency curve does *not* show the MPPS in the 30-350 nm range, which is atypical for an electret filter.[66] This finding was

unexpected and may cast doubt on the validity of our aerosol measuring system. Additionally, this study made no attempt to assess many of the other factors that could potentially impact the performance of the ACFF media, such as relative humidity, temperature, cyclic airflow, or filter behavior in the presence of liquid aerosol.

The results of Chapter 3 suggest that ACFF may be a good candidate for use in low-level or nuisance odor applications. This study demonstrates the extent to which ACFF participates in filtration under conditions relevant to respiratory protection. Future research would ideally focus on the development of ACFF media that have been specifically tailored for use in RPDs, or that employ a staged approach (i.e., ACFF used as a single component of a multimedia respirator).

CHAPTER 6

COMPARATIVE PERFORMANCE TESTING OF ACTIVATED CARBON FIBER AND A NUISANCE ODOR RESPIRATOR ADSORBENT

Introduction

Volatile organic compounds (VOCs) are frequently encountered in the occupational environment as constituents of solvents and paints; both acute and long-term VOC exposure can pose hazards to human health. In the occupational setting, OSHA's Permissible Exposure Limits (PELs) dictate the acceptable workplace concentrations of airborne contaminants. A "nuisance-level" VOC exposure refers to an exposure below the PEL or other recognized exposure limit. Not all nuisance level VOC exposures are benign: for example, exposure to VOCs that are known respiratory sensitizers can induce airway hyper-reactivity at low to moderate exposure concentrations in susceptible individuals. Although the use of a respirator for nuisance-level exposure may fall outside the traditional scope of the NIOSH Respirator Decision Logic, there are several potential scenarios in which an employee or hobbyist may voluntarily elect to use respiratory protection in the context of a low-concentration VOC exposure, even in the event that the actual exposure exists well below regulatory limits.

Previous work in our laboratory has explored the use of activated carbon fiber in N95 respirators, with one potential application being an N95 respirator that offers

nuisance VOC adsorption for low exposure concentrations. In general, ACF tends to derive a greater proportion of its internal surface area specifically from micropores, making it an excellent potential adsorbent for organic vapor at occupationally-relevant concentrations (ppmv-level concentrations). The micropores of ACF also tend to be distributed directly on the surface of the fiber. This means that contaminants diffusing through the adsorbent follow a shorter path to a potential adsorption site, and adsorption happens at a rapid pace. Rapid adsorption is a significant property in scenarios where the residence time between an adsorbent and a challenge contaminant is extremely short, such as might occur during the passage of contaminated air through a facepiece or cartridge respirator.

Filtering face-piece respirators that support nuisance-level organic vapor adsorption are currently available and marketed for occupational and non-occupational use. An example of such a device is the 3M™ 8214 N95 Particulate Welding Respirator, which consists of a thin carbon-containing layer sandwiched between an electrostatically-treated polypropylene body. The carbon layer consists of a fibrous non-woven web (polypropylene) that has been impregnated with activated carbon powder. These types of sorbent-loaded webs are light-weight and self-supporting. While these devices may be certified with regard to their ability to capture particulates (i.e., given a NIOSH N-, P-, R-, 95-100 rating), no similar certification of performance exists for nuisance level organic vapor adsorption, and the term "nuisance level" can encompass a range of concentrations that spans several orders of magnitude. Additionally the performance of these respirators may be impacted by unequal distribution of the carbon sorbent within

the polypropylene matrix. These media have been shown to experience rapid breakthrough under challenging use conditions.[25]

To further develop the concept of an ACF-containing N95 that offers nuisance OV protection, the performance of an ACF felt relative to that of existing nuisance OV adsorbents should first be established. Accordingly, we compared filtration and adsorption performance of a previously characterized ACF (ACFF 1200) with the adsorbent layer from a nuisance OV respirator by creating breakthrough curves for three representative organic vapors. We also compared each media's morphology and surface area characteristics. To compare the filtration behavior of these media, pressure drop, quality factor and filtration efficiency testing were also performed.

Methods

Nuisance Odor Adsorbent

Commercially-available nuisance OV respirators **(**3M™ P100 Item 2097) served as the source of the carbon-loaded polypropylene filter media. According to 3M™'s product website, the 2097 filter can provide respiratory protection for welding, brazing, torch cutting, metal pouring and soldering operations in the occupational setting. In addition to a reported 99.97% particulate filtration efficiency for oil-based aerosols (0.185±0.020 μm CMD DOP), product information states that this filter type offers "nuisance level relief" from organic vapors that are below the OSHA PEL. The exact carbon content (% by weight) of the media is withheld as proprietary; however, patent literature for similar media show that a carbon concentration of up to 60-90% by mass can be achieved.[30] For the purposes of these experiments, the 3M™ 2097 adsorbent layer

was gently removed by cutting the outer circumference of the pancake filter and gently peeling the adsorbent material away from the other filter elements.

ACF Media

A single PAN-derived ACF [ACFF 1200, CeraMaterials, Dingmans Ferry, PA], previously characterized by our laboratory in Chapters 3 and 4 was chosen because it exhibited the highest filter quality factor and lowest pressure drop of the previously characterized ACF felts. Additionally, preliminary characterization indicated that ACF 1200 *may* have a similar a similar carbon weight per area (grammage) to the 3M™ 2097 adsorbent. [ACFF 1200 grammage 157.14 ± 21.74 g/m^2; total grammage for the 3M™ 2097 media 168.00 ± 9.54. Assuming that 60-90% of the media's basis weight is carbon, the potential carbon grammage range for the 3M™ 2097 Adsorbent is 100.8- 151.2 g/m^2]

Characterization and Performance Testing

Surface Area Analysis, SEM Analysis, Breakthrough Time Testing, Filtration, and Pressure Drop Testing of the ACFF 1200 and the 3M™ 2097 Adsorbent were performed according to the methods previously described in Chapter 3 and 4; however, because the weight of carbon in the 3M™ 2097 adsorbent is not conclusively known, no attempts were made to calculate the media's adsorption capacity. To perform surface area analysis of the 3M™ 2097 adsorbent, a sample of the intact adsorbent layer (polypropylene with embedded carbon) was analyzed. Additionally, the embedded carbon from the adsorbent layer was scraped loose from the media and collected for separate analysis.

Results

SEM Images

SEM images of the ACFF 1200 at 200X magnification (Figure 32) indicate randomly arranged fibers with an approximate diameter of 8-10 µm. Fibers appear to be uniform in appearance and size. In contrast, the 3M™ 2097 adsorbent exhibits a wide range of fiber diameters, consistent with in appearance with melt-blown deposition (Figure 33). Additionally, many of the fibers in the 3M™ 2097 adsorbent appear to be much smaller in diameter than the ACFF 1200 fibers, possibly giving it an advantage as a filter of particles in the diffusion regime (<100 nm).

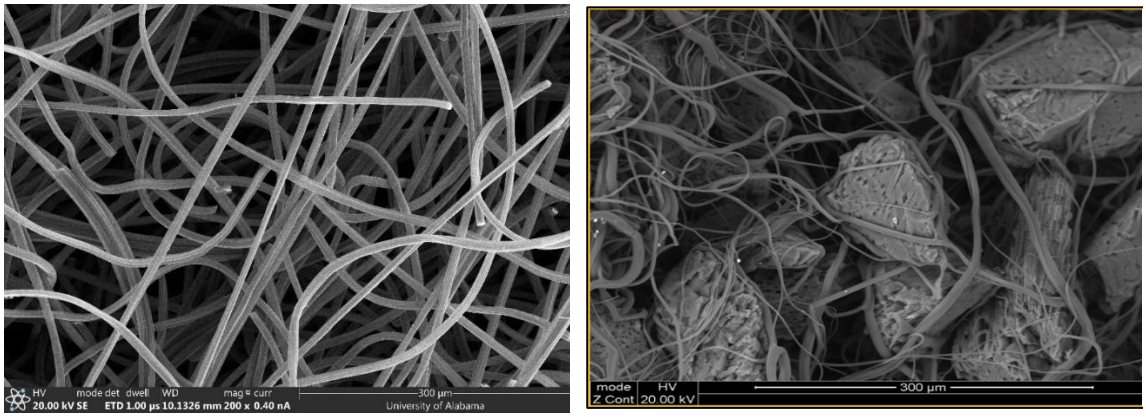

Figures 32 and 33. SEM images of ACFF 1200 (left) and the 3M™ 2097 adsorbent (right) at 200x magnification.

Surface Area Analysis

Surface area analysis (Table 20) shows that the carbon material used in the 3M™ 2097 Adsorbent has a high BET surface area (1120.65 m^2/gram) and a similar percentage of micropores by volume (78.73%) when compared to ACFF 1200 (78.70%). Surface area analysis from the intact 3M™ 2097 shows a BET surface area of 860.72 m^2/g, much

less than the surface area of the carbon material alone, and reflective of the fact that the carbon been blended with a relatively non-adsorbent filter material (polypropylene).

Table 20. Results surface area analysis for ACFF 1200 and 3M™ 2097 adsorbent.

Parameters	3M™ 2097 Adsorbent (Intact)	3M™ 2097 Adsorbent (Carbon Only)	ACFF 1200
BET Surface Area (m^2/g)	860.72	1120.65	1205.97
Micropore area (m^2/g)	724.05	882.3137	1015.25
% Micropore by area	84.18	78.7323	78.70
Pore Volume (cm^3/g)	0.3599	0.5211	0.58
Micropore Volume (cm^3/g)	0.2845	0.3567	0.42
Micropore by volume (cm^3/g)	79.05	68.4508	72.96
Pore Size (nm)	1.67	1.8601	1.82

Breakthrough Time Analysis

Breakthrough curves for ACFF 1200 and the 3M™ 2097 adsorbent were compared for all three representative organic vapors (toluene, MEK, and hexane) at single and multiple layers. Summary graphs appear in Figures 34A – 36B below. For all depths and adsorbates, ACFF 1200 showed longer breakthrough times at $C_o/C_i = 0.10$ than the 3M™ 2097 adsorbent. Additionally, ACFF 1200 breakthrough curves for hexane and toluene appear to have steeper slope than those of the 3M™ 2097 adsorbent. The comparative shape of these breakthrough curves suggest that ACFF 1200 has less resistance to mass transfer for toluene and hexane than the 3M™ 2097 adsorbent under the experimental conditions described in Chapter 3.

Table 21. ACFF vs. 3M 2097 $t_{b\ 10\%}$ (min) for single and multiple media layers.

Adsorbate	ACFF 1200 $t_{b10\%}$ (min)	3M™ 2097 $t_{b\ 10\%}$ (min)
Toluene, Layer 1	7.67	6.92
Toluene Layer 4	30.5	28.17
MEK, Layer 1	5.33	3.5
MEK, Layer 4	27.67	22.17
Hexane, Layer 1	6.00	2.67
Hexane, Layer 3	15.83	12.67

34A. *34B.*

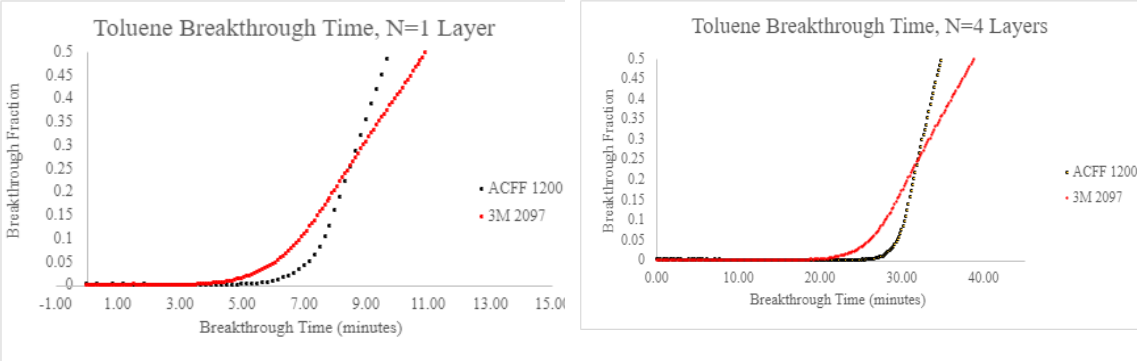

Figure 34A and 34B. Toluene breakthrough curves for ACFF 1200 and 3M™ 2097 adsorbent for N=1 and N=4 layers of media.

35A. *35B.*

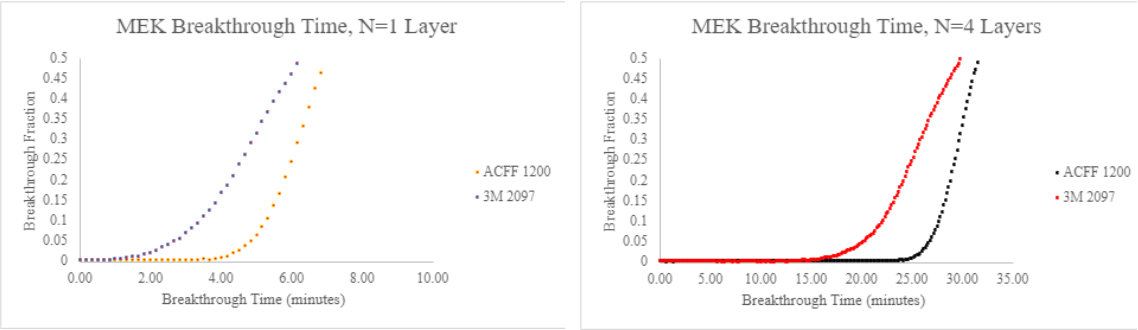

Figure 35A and B. MEK breakthrough curves for ACFF 1200 and 3M™ 2097 adsorbent for N=1 and N=4 layers of media.

36A. *36B.*

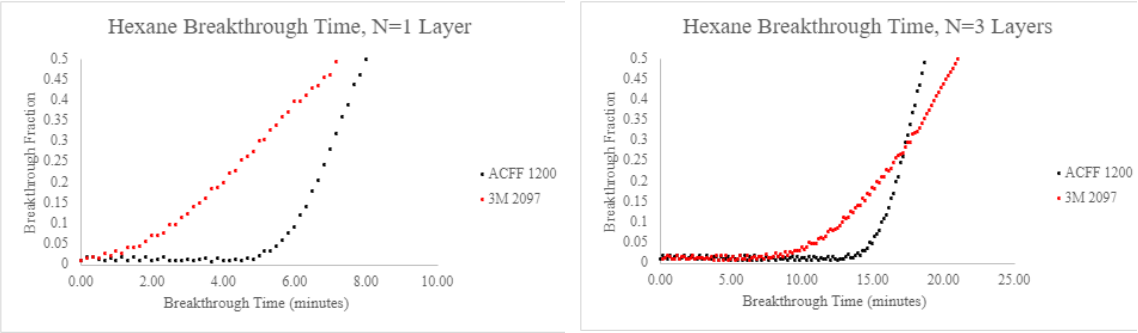

Figure 36A and B. Hexane breakthrough curves for ACFF 1200 and 3M™ 2097 adsorbent for N=1 and N=3 layers of media.

Filtration Efficiency, Pressure Drop, and Quality Factor

In comparison to the 3M™ 2097 adsorbent media, a single layer of ACFF consistently demonstrated higher global filtration efficiency and higher size-resolved filtration efficiency, as per Figure 37. The 3M™ 3097 media was demonstrably thinner and exhibited a lower pressure drop at N=1 layer. When these results were analyzed in terms of quality factor (qF), the 3M™ 2097 media showed a qF an order of magnitude higher that the ACFF 1200 (0.125 mm^{-1} H_2O vs. 0.025 mm^{-1} H_2O, respectively) (Table 22).

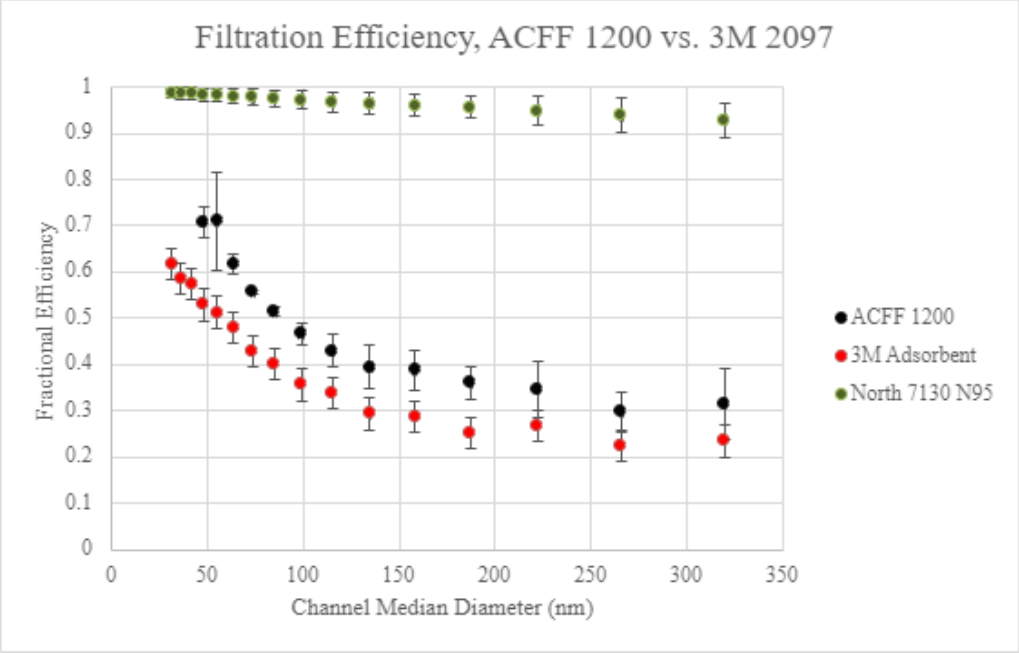

Figure 37. Filtration Efficiency for ACFF 1200 and 3M™ 2097 at 10 cm/s face velocity and N=1 Layer.

Table 22. Results from single layer testing of ACFF and 3M™ 2097 media at 10 cm/s (64 LPM scaled flow rate) using the experimental set-up described previously.

Media Type	Pressure Drop (mm H_2O)	Instantaneous Filter Efficiency (%)	Instantaneous Penetration (%)	Quality Factor (mm H_2O^{-1})
ACFF 1200	3.40	56.75	43.25	0.02513
3M™ 2097	2.24	44.18	55.82	0.12520

Discussion

Performance testing of the 3M™ 2097 adsorbent media was done to support the premise that ACF materials perform on par with the current media used as thin, nuisance-level OV adsorbents.

ACFF 1200 was selected for comparison because its bulk properties (i.e., depth and grammage) aligned more closely with the 3M™ 2097 nuisance OV adsorbent than the other ACF types (ACFF 1800 and ACFF 2000) evaluated in previous chapters. As demonstrated by breakthrough testing, ACFF 1200 was capable of preventing 10% breakthrough of a challenge contaminant for a longer period of time than the 3M™ 2097 adsorbent for all challenge contaminants (toluene, MEK, and hexane) and at all tested depths. The slope of the toluene and hexane breakthrough curves for ACFF 1200 were steeper than those of the 3M™ 2097 adsorbent, indicating rapid adsorption and less resistance to mass transfer. Unfortunately, calculation of adsorption capacity for the 3M™ 2097 could not be completed without a more accurate estimate of this media's carbon content by weight.

A comparison of the filtration performance of ACFF 1200 vs. the 3M™ 2097 adsorbent indicate that single layer ACFF 1200 has higher overall filtration efficiency than the 3M™ 2097 adsorbent; however, when a comparison was made based on filter quality factor, the 3M™ 2097 adsorbent greatly outperformed the ACFF 1200. This was an expected finding based on 3M™ 2097's status as a NIOSH-approved P100 respirator and the likelihood that each individual component thereof has been optimized for filtration.

This Aim was exploratory in nature and is obviously limited by lack of statistical analysis comparing the performance of the two media types. For adsorption behavior, the performance of successive breakthrough trials (rather than N=1 at each depth) would allow for means testing (i.e., paired t-test) of single-layer $t_{b10\%.}$ times Expanded surface area analysis (to include D-R analysis of the ACFF 1200 and nuisance organic vapor adsorbent) at N=3 trials would also allow for comparison of carbon properties (limiting micropore volume; characteristic energy of adsorption) and estimation of equilibrium adsorption capacities, as described in Chapter 4.

CHAPTER 7

CONCLUSION AND FUTURE RESEARCH DIRECTION

Our studies demonstrate that ACF has properties (i.e., high specific surface area (m^2/g), high adsorption capacity, and rapid adsorption kinetics) that make it a good candidate for use in thin, N95-style respirators for nuisance-level organic vapors. We also found that ACFF 1200, the lowest surface area ACF used in our laboratory, had greater 10% breakthrough times for a 200 ppm challenge of toluene, hexane and MEK (respectively) than the nuisance odor adsorbent from a commercially available respirator (3M™ 2097). It appears to be possible to use the D-R equation and nitrogen adsorption isotherms to predict equilibrium adsorption capacities and 10% breakthrough times for the tested adsorbates, although future studies should focus on optimizing this predicted model. Based on our research, a lightweight adsorbent such as ACF, if incorporated into an N95-style respirator, could potentially provide low-level OV protection in a physical form that is accessible to workers and consistent with OSHA's voluntary use provisions for facepiece respirators. In this context, and supported by our research, ACF would provide an advantage over the existing adsorbent used in such respirators: ACF's fiber diameter (in comparison to carbon granule diameter) suggests much higher adsorption rate coefficients; ACF used in our laboratory shows higher BET surface area and limiting micropore volume, and ACF is self-supporting and composed entirely of adsorptive

elements, unlike the polypropylene matrix used in commercially available nuisance odor adsorbents. It would be interesting to see if the advantages of ACF relative to existing nuisance OV adsorbents are maintained at a wider range of use conditions, in particular, conditions of high heat and humidity. It would also be interesting to test the performance of ACF relative to the nuisance odor adsorbent at much lower ppmv (or ppmb) concentrations.

Per our findings, ACF's performance as a particulate filter appears to be less than competitive. This is a predictable consequence of the ACF's bulk properties, which were not tailored or optimized for respiratory protection in our studies. Additionally, the presence of a lower limit on ACF fiber diameter may hinder its use as an exclusive particulate filter. Most activated carbon fibers are typically created from polymer precursors that exhibit a fiber diameter between 4 and 10 μm.[2] Activated carbon fibers smaller than 4 μm show diminished tensile strength and have a tendency to rapidly degrade and form powders.[67] As filtration by diffusion and interception both show dependence on fiber diameter, this "lower limit" on ACF diameter could limit or at least discourage its use in advanced filtration media. Based on the results presented in Chapter 5, it appears that off-the-shelf ACF felts can participate in but not exclusively support respirator filtration applications, as one might expect (and in fact predict) based on the fiber diameter and packing density of these media. Additionally, ACF displays an electrical conductivity several orders of magnitude larger than traditional electret media, and could, in theory, hasten the decay of the embedded electrical charge on electret media. This could present a practical barrier to its use in proximity to electrically-active N95 media.

To overcome these limitations, it would be worthwhile to investigate the filtration performance of ACF when blended with cellulose, glass fiber, or polypropylene fiber. However, as described by previous researchers, it is possible that blending the ACF with other media may improve filtration efficiency but interfere with adsorption performance by occluding micropore space.[3] It would be interesting to re-assess breakthrough curves and adsorption capacity of ACFs that are blended with other relatively non-adsorbent filter media.

Based on the proposed use of ACF, future research should also examine whether the presence of a dual airborne contaminant (i.e., representative VOC plus solid aerosol) produces a measurable change in either the filtration or adsorption abilities of the ACF media. This research direction would have two main goals: to determine if an ACF in the presence of a dual airborne contaminant shows any significant difference in adsorption capacity when compared with the adsorption capacity of ACF challenged with VOC alone; and to determine if ACF in the presence of a dual airborne contaminant shows any significant difference in initial penetration when compared with ACF presented with a test aerosol alone.

The presence of a solid aerosol in the challenge airstream could potentially impact the ACF's adsorption behavior in several ways. First, the deposition of particles on the surface of the media may occlude the pore structure and impact the equilibrium adsorption capacity of the media by decreasing the micropore volume available for adsorption. Furthermore, the deposition of solid particles on the filter surface could potentially change the flow profile through the filter over time. Filter loading with solid particles occurs in a staged manner. In the first stage, referred to as the "stationary

phase," solid particles are deposited on the filter at numbers that have no apparent effect on filter behavior. As more particles are deposited, however, modification of the filtration mechanisms may occur. In this second stage ("non-stationary phase"), the accumulation of solid particles form aggregates that serve as collection sites for additional particles.[68] If the collected particles are smaller than the apparent inter-fiber pore size of the filter, an increase in filter solidity and pressure drop will gradually develop. If such particle accumulations ultimately result in an increased linear velocity through the media, it is conceivable that an impact on breakthrough time could be also be observed. Studies examining the effect of particle loading on the adsorptive capacity of ACF are sparse in the literature, probably because in most applications, the carbon media is, *by design*, protected from particle loading by the presence of a coarse upstream filter.[47,69]

Some models of N95 and P100 style respirators experience an initial decrease in filtration efficiency in the presence of organic vapors and oil aerosols, most likely through shielding or redistribution of surface electrical charge[70, 66,71] Based on our review of the literature and ACF's non-conductive properties, the presence of a non-polar VOC in the challenge airstream is *not* anticipated to cause an increase in initial penetration for an activated carbon fiber filter. Filtration by interception and diffusion are the two most important filtration mechanisms in the particle range of minimal efficiency,[16] and examination of the expressions for single fiber efficiency by diffusion and interception do not necessarily reveal any parameters that are likely to be impacted by the presence of a non-polar VOC either in the airstream or within the pore structure of the media. [73]It seems unlikely that any such change in ACF surface electric properties will be of practical import for global filtration efficiency, as most activated carbon fiber is several

orders of magnitude more conductive than most standard electret filter media and does not generally exhibit filtration by electrostatic deposition.[72] Nevertheless, if ACF intended as a filter media for both particulates and VOCs, it would be necessary to determine if particulate filtration efficiency of ACF is any way degraded by the presence of an organic vapor.

LIST OF REFERENCES

1. Plog, B., Niland, J. & Quinlan, P. *Fundamentals of Industrial Hygiene, 4th Edition*. (National Safety Council, 1996).
2. Hayes, J. *Activated Carbon Fibers and Textiles: Properties and Applications; American Kynol, Inc., Pleasantville, NY*. (1994).
3. Rochereau, A. et al. Combined air treatment: Effect of composition of fibrous filters on toluene adsorption and particulate filtration. *Chem Eng Res Des* **86**, 577–584 (2008).
4. Toku, J. U.S. Patent Number CN201199952Y: Activated Carbon Fiber Respirator.
5. Lillo-Ródenas, M. A., Cazorla-Amorós, D. & Linares-Solano, A. Behaviour of activated carbons with different pore size distributions and surface oxygen groups for benzene and toluene adsorption at low concentrations. *Carbon N Y* (2005) doi:10.1016/j.carbon. 2005.02.023.
6. Occupational Safety and Health Administration. Respiratory Protection Overview. (2022). https://www.osha.gov/SLTC/respiratoryprotection/.
7. Occupational Safety and Health Administration. Respiratory Protection Standard. (2022). https://www.osha.gov
8. Cartier, A. & Bernstein, D. Occupational Asthma: Definitions, epidemiology, causes and risk factors. *Wolters Klower Uptodate* (2018).
9. Zock, J. Exposure to substances in the workplace and new-onset asthma : an international prospective population-based study. The Lancet **370**; 336-341 (2007).
10. Carugno, M. *et al.* Increased Mitochondrial DNA Copy Number in Occupations Associated with Low-Dose Benzene Exposure. *Environmental Health Perspectives* **120**, 210–215 (2011).
11. Kodavanti, P. R. S. *et al.* Acute and subchronic toxicity of inhaled toluene in male Long-Evans rats: Oxidative stress markers in brain. *NeuroToxicology* **51**, 10–19 (2015).

12. Pope, C. A. Mortality effects of longer term exposures to fine particulate air pollution: review of recent epidemiological evidence. *Inhal Toxicol* **19**, 33–38 (2007).

13. Styrene Industry Research Council.(2022). https://styrene.org/

14. ATSDR. *Toxicological Profile for Styrene*. (2010).

15. Hinds, W. *Aerosol Technology: Properties, behavior, and measurement of airborne particles*. (John Wiley and Sons, 1999).

16. Rudnick, S. N. Optimizing the design of room air filters for the removal of submicrometer particles. *Aerosol Science and Technology* (2004) doi:10.1080/027868290503109.

17. Lee, K. W. & Liu, B. Y. H. On the Minimum Efficiency and the Most Penetrating Particle Size for Fibrous Filters. *J Air Pollut Control Assoc* **30**, 377–381 (1980).

18. Code of Federal Regulations, Title 42, Part 84: Approval of Respiratory Protection Devices. https://www.govinfo.gov/content/pkg/CFR-2004-title42-vol1/xml/CFR-2004-title42-vol1-part84.xml (2004).

19. Rengasamy, S., Shaffer, R., Williams, B. & Smit, S. A comparison of facemask and respirator filtration test methods. *Journal of Occupational and Environmental Hygiene* **14**, 92–103 (2017).

20. Zhang, X., Gao, B., Creamer, A. E., Cao, C. & Li, Y. Adsorption of VOCs onto engineered carbon materials: A review. *Journal of Hazardous Materials* Preprint at https://doi.org/10.1016/j.jhazmat.2017.05.013 (2017).

21. Carratalá-Abril, J., Lillo-Ródenas, M. A., Linares-Solano, A. & Cazorla-Amorós, D. Activated carbons for the removal of low-concentration gaseous toluene at the semipilot scale. *Industrial and Engineering Chemistry Research* (2009) doi:10.1021/ie800521s.

22. Wood, G. O. Reviews of models for adsorption of single vapors, mixtures of vapors, and vapors at high humidities on activated carbon for applications including predicting service life of organic vapor respirator cartridges. 1–162 (2000).

23. Webb, P. & Orr, C. *Analytical Methods in Fine Particle Technology*. (Micromeritrics Instrument Corporation, 1997).

24. Lodewyckx, P. Activated Carbon Surfaces in Environmental Remediation. *Interface Science and Technology* **7**, 475–528 (2006).

25. Rozzi, T., Snyder, J. & Novak, D. Pilot study of Aromatic Hydrocarbon Adsorption Characteristics of Disposable Filtering Facepiece Respirators that

Contain Activated Carbon. *Journal of Occupational and Environmental Hygiene* **9**, 624–629.

26. Choi, S. H. *et al.* Activated carbon fiber filters could reduce the risk of surgical smoke exposure during laparoscopic surgery: application of volatile organic compounds. *Surgical Endoscopy and Other Interventional Techniques* (2018) doi:10.1007/s00464-018-6222-0.

27. Reinhardt, T. & Broyles, G. Background and Overview of Wildland Fires and Exposures and Health Effects. in *International Society for Respiratory Protection Conference Proceedings* (2018).

28. Shaffer, R. E. & Janssen, L. Selecting models for a respiratory protection program: What can we learn from the scientific literature? *Am J Infect Control* **43**, 127–132 (2015).

29. Gutierrez, A., Galang, M., Seva, R., Lu, M. & Ty, D. Designing an improved respirator for automotive painters. *International Journal of Industrial Ergonomics* **44**, 131–139 (2014).

30. Braun, D. Particle-Loaded Microfiber Sheet Product and Respirators Made Therefrom; United States Patent Number 3,971,373. 1–12.

31. Anne, J. *et al.* Adsorption Characteristics of Activated Carbon Fibers (ACF) for Toluene. (2011)(Dissertation).

32. Lee, T., Ooi, C., Othman, R. & Yeoh, F. Activated Carbon Fiber - the Hybrid of Carbon Fiber and Activated Carbon. *Rev.Adv.Mater. Sci.* **36**, 118–136 (2014).

33. Li, L., Sun, Z., Li, H. & Keener, T. C. Effects of activated carbon surface properties on the adsorption of volatile organic compounds. *Journal of the Air and Waste Management Association* (2012) doi:10.1080/10962247.2012.700633.

34. Dolidovich, A. F. & Akhremkova, G. S. Theoretical and Experimental Studies of the Porous Structure and Adsorption Properties of Carbofibrous Materials. *Journal of Engineering Physics* **83**, 861–865 (2010).

35. Tsai, J. H., Chiang, H. M., Huang, G. Y. & Chiang, H. L. Adsorption characteristics of acetone, chloroform and acetonitrile on sludge-derived adsorbent, commercial granular activated carbon and activated carbon fibers. *Journal of Hazardous Materials* **154**, 1183–1191 (2008).

36. Zhang, X., Zhao, X., Hu, J., Wei, C. & Bi, H. T. Adsorption dynamics of trichlorofluoromethane in activated carbon fiber beds. *Journal of Hazardous Materials* **186**, 1816–1822 (2011).

37. Balanay, J. A. G., Bartolucci, A. & Lungu, C. T. Adsorption characteristics of activated carbon fibers (ACFs) for toluene: application in respiratory protection. *J Occup Environ Hyg* **11**, 133–43 (2014).

38. Rochereau, A. *et al.* Combined air treatment: Effect of composition of fibrous filters on toluene adsorption and particle filtration efficiency. *Chem Eng Res Des* **86**, 577–584 (2008).

39. Chinn, M. J. & Pears, L. A. Combined Vapor and Particulate Filter; US Patent Number 6,821,321. (2004).

40. Chinn, M., Hindmarsh CJ & Pears, L. Carbon Fibres for Combined Particulate and Vapour Filtration. *JISRP* **28**, (2002).

41. Lorimier, C., le Coq, L., Subrenat, ; Albert & le Cloirec, P. Indoor Air Particulate Filtration onto Activated Carbon Fiber Media. *Journal of Environmental Engineering* **134**, 126–132 (2008).

42. Hayashi, T., Lee, T. G., Hazelwood, M., Hedrick, E. & Biswas, P. Characterization of Activated Carbon Fiber Filters for Pressure Drop, Submicrometer Particulate Collection, and Mercury Capture. *Journal of the Air and Waste Management Association* **50**, 922–929 (2000).

43. Balanay, J. A. G., Bartolucci, A. A. & Lungu, C. T. Adsorption characteristics of activated carbon fibers (ACFs) for toluene: Application in respiratory protection. *Journal of Occupational and Environmental Hygiene* (2014) doi:10.1080/15459624.2013.816433.

44. Balanay, J. A. G., Crawford, S. a. & Lungu, C. T. Comparison of Toluene Adsorption Among Granular Activated Carbon and Different Types of Activated Carbon Fibers (ACFs). *Journal of Occupational and Environmental Hygiene* **8**, 573–579 (2011).

45. Webb, S. W. Gas Transport Mechanisms. in *Gas Transport in Porous Media* doi:10.1007/1-4020-3962-X_2.

46. Giraudet, S. & Le Cloirec, P. Activated carbon filters for filtration-adsorption. in *Activated Carbon Fiber and Textiles* (2016). doi:10.1016/B978-0-08-100660-3.00009-2.

47. Kim, S. Y., Yoon, Y. H. & Kim, K. S. Performance of activated carbon-impregnated cellulose filters for indoor VOCs and dust control. *International Journal of Environmental Science and Technology* **13**, 2189–2198 (2016).

48. Karanfil, T. & Dastgheib, S. A. Trichloroethylene adsorption by fibrous and granular activated carbons: Aqueous phase, gas phase, and water vapor adsorption studies. *Environmental Science and Technology* **38**, 5834–5841 (2004).

49. Hindmarsh, C. J. & Phillips, P. L. Development of Activated Carbon Fibre Mats for Combined Particulate and Vapor Filtration. . *JISRP* **28**, (2002).

50. Wood, G. O. Testing Air-Purifying Chemical Respirator Cartridges: A Review of Options. *JISRP* **34**, (2017).

51. Sullivan, P. *et al.* Physical and chemical properties of PAN-derived electrospun activated carbon nanofibers and their potential for use as an adsorbent for toxic industrial chemicals. *Adsorption* (2012) doi:10.1007/s10450-012-9399-x.

52. National Library of Medicine Hazardous Substances Data Bank: Methyl Ethyl Ketone. (2017).

53. National Library of Medicine Hazardous Substances Data Bank: Toluene. (2017).

54. National Library of Medicine Hazardous Substances Data Bank: n-Hexane. (2017).

55. Lodewyckx, P, Wood, G.O., Ryu, S. K. The Wheeler-Jonas equation a versatile tool for the prediction of carbon bed breakthrough times.pdf. *Carbon N Y* **42**, 1351–1355 (2004).

56. Wood, G. Correlating and Extrapolating Air Purifying Respirator Cartridge Breakthrough Times: A Review. *JISRP* **32**, (2015).

57. Balanay, J. A. G., Floyd, E. L. & Lungu, C. T. Breakthrough curves for toluene adsorption on different types of activated carbon fibers: Application in respiratory protection. *Annals of Occupational Hygiene* (2015) doi:10.1093/annhyg/meu105.

58. Wood, G. O. Review and comparisons of D/R models of equilibrium adsorption of binary mixtures of organic vapors on activated carbons. *Carbon N Y* **40**, 231–239 (2002).

59. Wood, G. O. D-R Plots and Typical Parameters for Several OV and Multigas Cartridges and Cannisters. *JISRP* **26**, (2009).

60. Wood, P. Lodewyckx, G. O. An extended equation for rate coefficients for adsorption of organic vapors and gases on activated carbons in air-purifying respirator cartridges. *Am Ind Hyg Assoc J* **64**, 646 (2003).

61. Wood, G. O. Estimating service lives of organic vapor cartridges II: a single vapor at all humidities. *J Occup Environ Hyg* **1**, 472–492 (2004).

62. Das, D., Gaur, V. & Verma, N. Removal of volatile organic compound by activated carbon fiber. *Carbon N Y* (2004) doi:10.1016/j.carbon.2004.07.008.

63. Huang, Z. H., Kang, F., Liang, K. M. & Hao, J. Breakthrough of methyethylketone and benzene vapors in activated carbon fiber beds. *Journal of Hazardous Materials* **98**, 107–115 (2003).

64. Calgon Carbon Flexzorb: Markets/Applications. https://www.calgoncarbon.com/products/flexzorb/ (2019).

65. Drewnick, F. *et al.* Aerosol filtration efficiency of household materials for homemade face masks: Influence of material properties, particle size, particle

electrical charge, face velocity, and leaks. *Aerosol Science and Technology* **55**, 63–79 (2021).

66. Rengasamy, S., Miller, A., Vo, E. & Eimer, B. C. Filter performance degradation of electrostatic N95 and P100 filtering facepiece respirators by dioctyl phthalate aerosol loading. *Journal of Engineered Fibers and Fabrics* (2013) doi:10.1016/j.jhsa.2012.11.006.

67. Cukierman, A. L. Development and Environmental Applications of Activated Carbon Cloths. *ISRN Chemical Engineering* **2013**, 25–29 (2013).

68. Payet, S., Boulaud, D., Madelaine, G & Renoux, A. Penetration and Pressure Drop of a HEPA Filter During Loading with Submicron Liquid Aerosol. *J. Aerosol Sci* vol. 23 (1992).

69. Kim, C. & Pui, D. Y. H. Experimental study on the filtration efficiency of activated carbons for 3-30 nm particles. *Carbon N Y* **93**, 226–229 (2015).

70. Choi, H. J., Park, E. S., Kim, J. U., Kim, S. H. & Lee, M. H. Experimental Study on Charge Decay of Electret Filter Due to Organic Solvent Exposure. *Aerosol Science and Technology* (2015) doi:10.1080/02786826.2015.1086724.

71. Bergman, M. S. *et al.* Evaluation of Multiple (3-Cycle) Decontamination Processing for Filtering Facepiece Respirators. *Journal of Engineered Fibers and Fabrics* vol. 5.

72. Dascalescu, L. *et al.* Corona Charging of Composite Non-Woven Media for Air Filtration. *Proc. ESA Annual Meeting on Electrostatics*. (2010)

APPENDIX A

BREAKTHROUGH TIME SUMMARY TABLES

Contains summary tables describing organic vapor breakthrough times for each media type, as tested at 10 cm/s face velocity and at varying bed depths.

Appendix Tables A.1. ACFF 1200 Media breakthrough time for toluene at concentrations between 1% and 50% of a 200 ppm challenge for N=4 layers.

ACFF 1200 vs. 200 ppm Toluene Challenge				
	Breakthrough time (min)			
Breakthrough Fraction ($C_{measured}/C_{challenge}$)	*Layer 1*	*Layer 2*	*Layer 3*	*Layer 4*
0.01	6.17	14.83	22.67	27.5
0.05	7.17	16.17	24.17	29.5
0.1	7.67	16.83	25	30.5
0.2	8.33	17.67	26	31.5
0.35	9	18.83	27.17	33.17
0.5	9.83	20.33	28.83	34.83

Appendix Tables A.2. ACFF 1800 Media breakthrough time for toluene at concentrations between 1% and 50% of a 200 ppm challenge for N=4 layers.

ACFF 1800 vs. 200 ppm Toluene Challenge				
	Breakthrough time (min)			
Breakthrough Fraction ($C_{measured}/C_{challenge}$)	*Layer 1*	*Layer 2*	*Layer 3*	*Layer 4*
0.01	9.67	20	30.17	44
0.05	10.42	21.33	31.67	45.67
0.1	10.83	21.83	32.5	46.5
0.2	11.42	22.67	34.17	47.67
0.35	12.08	23.83	36.83	49.67
0.5	12.75	25.17	39	52.83

Appendix Tables A.3. ACFF 2000 Media breakthrough time for toluene at concentrations between 1% and 50% of a 200 ppm challenge for N=4 layers

ACFF 2000 vs. 200 ppm Toluene Challenge				
	Breakthrough time (min)			
Breakthrough Fraction ($C_{measured}/C_{challenge}$)	*Layer 1*	*Layer 2*	*Layer 3*	*Layer 4*
0.01	9.25	19.42	31.75	42.83
0.05	10	20.75	33.17	44.83
0.1	10.42	21.42	33.92	45.67
0.2	11	22.5	34.83	46.5
0.35	11.58	23.67	36	47.67
0.5	12.17	24.75	37.42	49.33

Appendix Tables A.4. 3M™ 2097 Nuisance Adsorbent Media breakthrough time for toluene at concentrations between 1% and 50% of a 200 ppm challenge for N=4 layers.

3M™ 2097 Nuisance Adsorbent vs. 200 ppm Toluene Challenge				
	Breakthrough time (min)			
Breakthrough Fraction ($C_{measured}/C_{challenge}$)	*Layer 1*	*Layer 2*	*Layer 3*	*Layer 4*
0.01	4.67	9.83	12.83	22.33
0.05	6.17	12.17	15.83	26.17
0.1	6.92	13.33	17.33	28.17
0.2	8	14.83	19.33	30.83
0.35	9.42	16.83	22.33	34.83
0.5	10.92	19	25.5	39

Appendix Tables A.5. ACFF 1200 Media breakthrough time for MEK concentrations between 1% and 50% of a 200 ppm challenge. Each media was tested at 4 consecutive layers.

ACFF 1200 vs. 200 ppm MEK Challenge				
	Breakthrough time (min)			
Breakthrough Fraction ($C_{measured}/C_{challenge}$))	*Layer 1*	*Layer 2*	*Layer 3*	*Layer 4*
0.01	4.17	10	17.17	25.17
0.05	4.83	11.33	18.67	26.83
0.1	5.33	12.17	19.5	27.67
0.2	5.83	12.83	20.5	28.83
0.35	6.33	13.67	21.67	30.17
0.5	7	14.67	22.67	31.67

Appendix Tables A.6. ACFF 1800 Media breakthrough time for MEK at concentrations between 1% and 50% of a 200 ppm challenge for N=4 layers.

ACFF 1800 vs. 200 ppm MEK Challenge				
	Breakthrough time (min)			
Breakthrough Fraction ($C_{measured}/C_{challenge}$)	*Layer 1*	*Layer 2*	*Layer 3*	*Layer 4*
0.01	5	11.67	17	25.5
0.05	5.67	12.3	17.83	27.17
0.1	6.17	12.83	18.5	27.83
0.2	6.67	13.17	19	28.67
0.35	7.17	13.67	19.67	30.17
0.5	7.67	14.17	20.33	32.17

Appendix Tables A.7. ACFF 2000 Media breakthrough time for MEK at concentrations between 1% and 50% of a 200 ppm challenge for N=4 layers.

ACFF 2000 vs. 200 ppm MEK Challenge				
	Breakthrough time (min)			
Breakthrough Fraction ($C_{measured}/C_{challenge}$)	*Layer 1*	*Layer 2*	*Layer 3*	*Layer 4*
0.01	4.83	12.17	18.17	23
0.05	5.5	13.17	19.17	24.5
0.1	6	13.67	19.83	25.17
0.2	6.33	14.14	20.33	26.17
0.35	6.83	14.67	21	27.5
0.5	7.33	15.17	22	29.17

Appendix Tables A.8. 3M™ 2097 Adsorbent Media breakthrough time for MEK at concentrations between 1% and 50% of a 200 ppm challenge for N=4 layers.

3M™ 2097 Nuisance Adsorbent vs. 200 ppm MEK Challenge				
	Breakthrough time (min)			
Breakthrough Fraction ($C_{measured}/C_{challenge}$)	*Layer 1*	*Layer 2*	*Layer 3*	*Layer 4*
0.01	1.5	7.5	15.67	16.33
0.05	2.67	9.67	18.33	20.33
0.1	3.5	11	20.83	22.17
0.2	4.33	12.83	23.17	24.17
0.35	5.17	14.67	25.83	26.83
0.5	6.33	17	28.33	30

Appendix Tables A.9-A.12. ACFF 1200 Media breakthrough time for hexane concentrations between 5% and 50% of a 200 ppm challenge. Media were tested at 3 consecutive layers.

ACFF 1200 vs. 200 ppm Hexane Challenge			
	Breakthrough time (min)		
Breakthrough Fraction ($C_{measured}/C_{challenge}$)	*Layer 1*	*Layer 2*	*Layer 3*
0.05	5.67	10.5	15
0.1	6	11.17	15.83
0.2	6.67	12.17	16.67
0.35	7.33	13.17	17.83
0.5	8	14.17	18.83

Appendix Tables A.10. ACFF 1800 Media breakthrough time for hexane at concentrations between 1% and 50% of a 200 ppm challenge for N=3 layers.

ACFF 1800 vs. 200 ppm Hexane Challenge			
	Breakthrough time (min)		
Breakthrough Fraction ($C_{measured}/C_{challenge}$)	*Layer 1*	*Layer 2*	*Layer 3*
0.05	6.45	11.83	23.17
0.1	6.85	12.33	24.17
0.2	7.35	13.7	25.5
0.35	8.05	14.33	27.5
0.5	8.6	15	29.5

Appendix Tables A.11. ACFF 2000 Media breakthrough time for hexane at concentrations between 1% and 50% of a 200 ppm challenge for N=3 layers.

ACFF 2000 vs. 200 ppm Hexane Challenge			
	Breakthrough time (min)		
Breakthrough Fraction ($C_{measured}/C_{challenge}$)	*Layer 1*	*Layer 2*	*Layer 3*
0.05	4.15	12.5	17.83
0.1	4.7	13	18.67
0.2	5.3	13.83	19.5
0.35	6	14.67	20.83
0.5	6.6	15.83	22.3

Appendix Tables A.12. 3M™ 2097 Adsorbent Media breakthrough time for hexane at concentrations between 1% and 50% of a 200 ppm challenge for N=3 layers.

3M™ 2097 Nuisance Adsorbent vs. 200 ppm Hexane Challenge			
	Breakthrough time (min)		
Breakthrough Fraction ($C_{measured}/C_{challenge}$)	*Layer 1*	*Layer 2*	*Layer 3*
0.05	1.83	7.17	11.33
0.1	2.67	8.33	12.67
0.2	4	10	15.33
0.35	5.67	11.67	18.5
0.5	7.33	13.5	21

APPENDIX B

ADSORPTION CAPACITY CALCULATIONS

Contains plots of 10% organic vapor breakthrough time vs. adsorbent weight for each media type, with accompanying adsorption capacity calculations

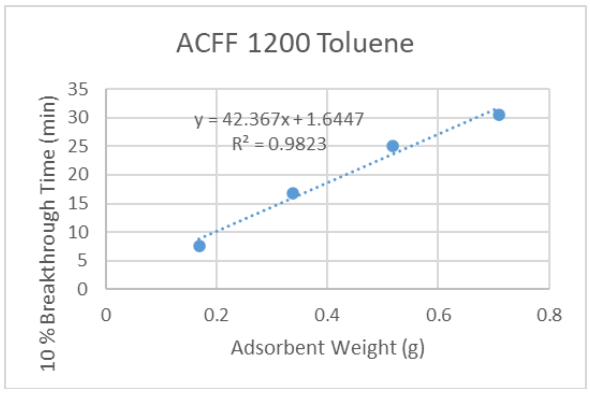

B.1.

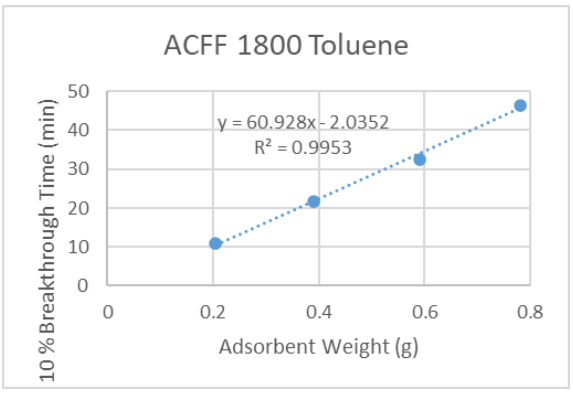

B.2

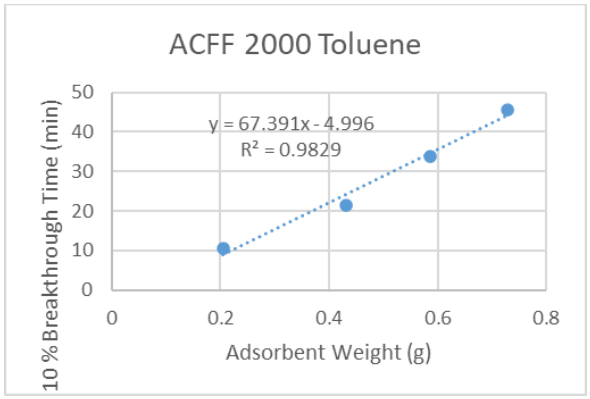

B3.

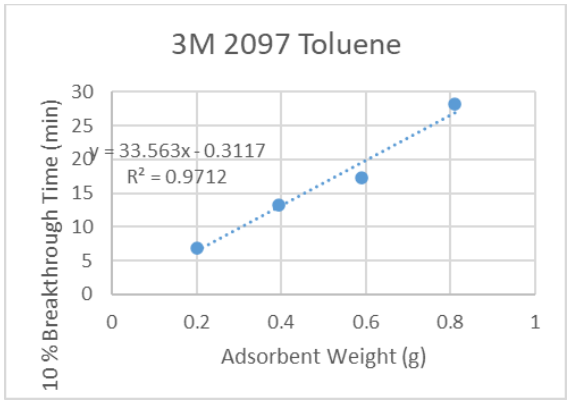

B4.

Appendix Figures B.1-B.4. 10% breakthrough times plotted against adsorbent weight for each adsorbent type (ACFF 1200, ACFF 1800, ACFF 2000 and the nuisance adsorbent from a 3M™ 2097 respirator cartridge). The challenge contaminant was Toluene. Capacity calculations are provided in Table B.1..

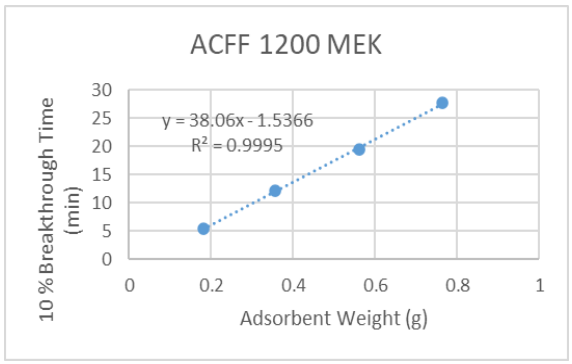

B.5.

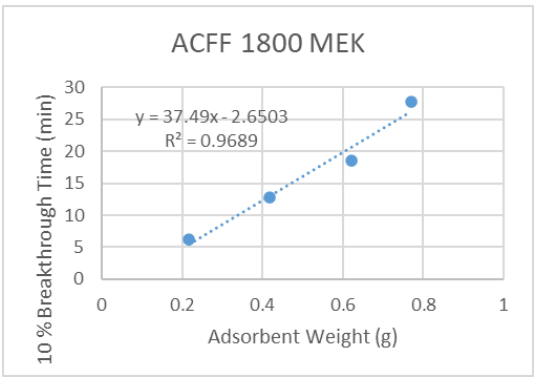

B.6.

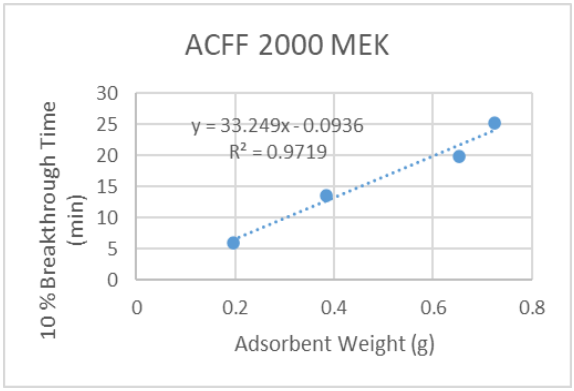

B.7.

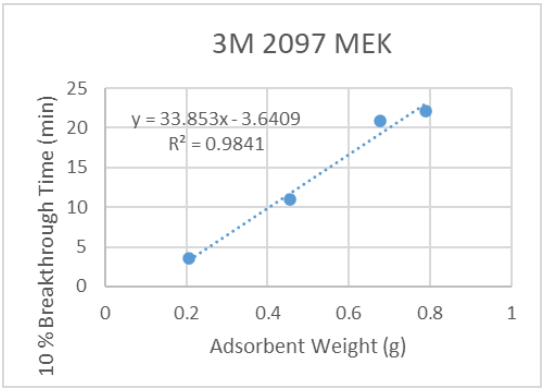

B.8.

Appendix Figures B.5-B.8. 10% breakthrough times plotted against adsorbent weight for each adsorbent type (ACFF 1200, ACFF 1800, ACFF 2000 and the nuisance adsorbent from a 3M™ 2097 respirator cartridge). The challenge contaminant was MEK. Capacity calculations are provided in Table B.2.

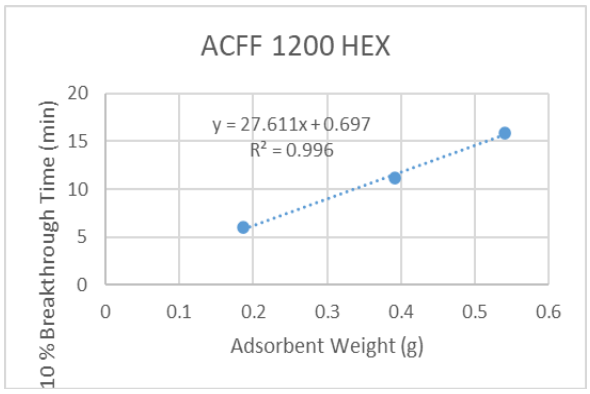

B.9.

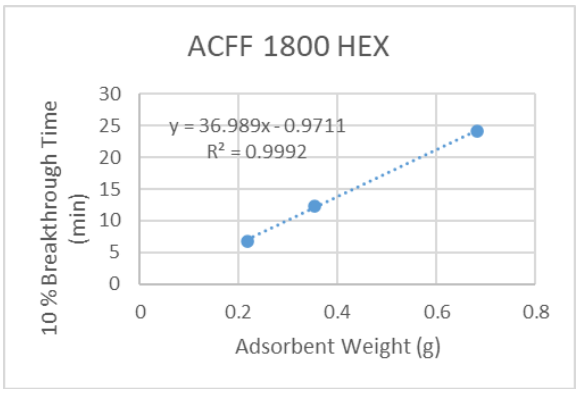

B.10.

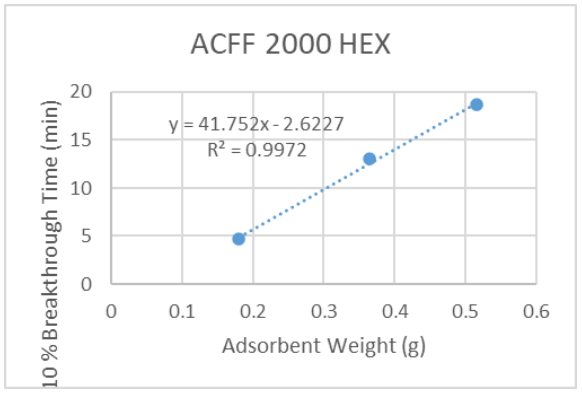

B 11.

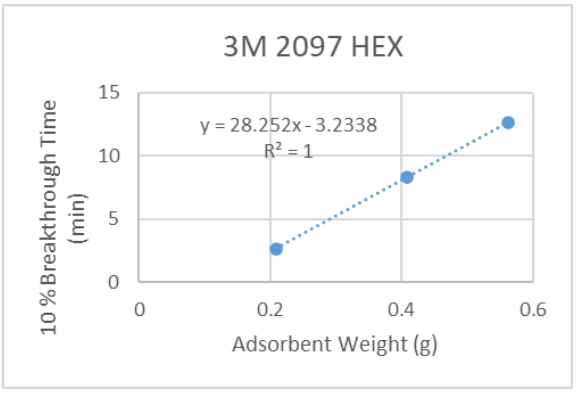

B.12.

Appendix Figures B.9-A.12. 10% breakthrough times plotted against adsorbent weight for each adsorbent type (ACFF 1200, ACFF 1800, ACFF 2000 and the nuisance adsorbent from a 3M™ 2097 respirator cartridge.) The challenge contaminant was Hexane. Capacity calculations are provided in Table B.3.

Appendix Table B.1. Adsorption Capacity Calculation for Toluene. Challenge concentration 200 ppm Toluene is expressed below in units of g/L.

Toluene Adsorption Capacity Calculations				
Media Type	Challenge Concentration (g/L)	Challenge Flow Rate (L/min)	Slope (min/gram)	Capacity (g/g)
ACFF 1200	0.000753	7.5	42.367	0.2393
ACFF 1800	0.000753	7.5	60.928	0.3441
ACFF 2000	0.000753	7.5	67.391	0.3806
3M™ 2097	0.000753	7.5	33.563	0.1895

Appendix Table B.2. Adsorption Capacity Calculation for MEK. Challenge concentration of 200 ppm MEK is expressed below in units of g/L.

MEK Adsorption Capacity Calculations				
Media Type	Challenge Concentration (g/L)	Challenge Flow Rate (L/min)	Slope (min/gram)	Capacity (g/g)
ACFF 1200	0.000589	7.5	42.367	0.2393
ACFF 1800	0.000589	7.5	60.928	0.3441
ACFF 2000	0.000589	7.5	67.391	0.3806
3M™ 2097	0.000589	7.5	33.563	0.1895

Appendix Table B.3. Adsorption Capacity Calculation for Hexane. Challenge concentration of 200 ppm Hexane is expressed below in units of g/L.

Hexane Adsorption Capacity Calculations				
Media Type	Challenge Concentration (g/L)	Challenge Flow Rate (L/min)	Slope (min/gram)	Capacity (g/g)
ACFF 1200	0.000704	7.5	42.367	0.2393
ACFF 1800	0.000704	7.5	60.928	0.3441
ACFF 2000	0.000704	7.5	67.391	0.3806
3M™ 2097	0.000704	7.5	33.563	0.1895

APPENDIX C

ACF SURFACE AREA CHARACTERIZATION

Contains results of ACF surface area characterization, as obtained from nitrogen isotherm data at 77 K.

Appendix Figure C.1. Surface area characterization as determined by nitrogen isotherm data. Where multiple trials were performed, a mean and standard deviation are reported. Carbon was extracted from the adsorbent layer of a 3M™ 2097 respirator for comparison with ACF surface area characteristics.

BET Surface Area, m^2/g				
ACF Type	Sample 1	Sample 2	Sample 3	Mean ± SD
ACFF 1800	1567.0	1435.0	1622.0	1541.34 ± 96.14
ACFF 2000	1919.3	1832.3	1959.6	1903.71 ± 65.01
ACFF 1200	1206.0			
3M™ Nuisance Adsorbent	1120.7			

t-Plot Micropore Area, m^2/g				
ACF Type	Sample 1	Sample 2	Sample 3	Mean ± SD
ACFF 1800	1071.1	994.5	1102.8	1056.14 ± 55.66
ACFF 2000	833.7	803.9	879.1	838.89 ± 37.90
ACFF 1200	1015.3			
3M™ Nuisance Adsorbent				
-	882.3			

% Micropore by Area				
ACF Type	Sample 1	Sample 2	Sample 3	Mean ± SD
ACFF 1800	68.4	69.3	68.0	68.52 ± 0.68
ACFF 2000	43.4	43.9	44.9	44.06 ± 0.73
ACFF 1200	78.7			
3M™ Nuisance Adsorbent				
-	78.7			

Pore Volume, cm^3/g				
ACF Type	Sample 1	Sample 2	Sample 3	Mean ± SD
ACFF 1800	0.71	0.64	0.74	0.69 ± 0.05
ACFF 2000	0.92	0.88	0.93	0.90 ± 0.03
ACFF 1200	0.58			
3M™ Nuisance Adsorbent				
-	0.52			

t-Plot Micropore Volume, cm^3/g				
ACF Type	Sample 1	Sample 2	Sample 3	Mean ± SD
ACFF 1800	0.42	0.39	0.44	0.41 ± 0.05
ACFF 2000	0.32	0.31	0.34	0.32 ± 0.16
ACFF 1200	0.42			
3M™ Nuisance Adsorbent				
-	0.36			

% Micropore by Volume				
ACF Type	Sample 1	Sample 2	Sample 3	Mean ± SD
ACFF 1800	59.27	60.30	59.08	59.51 ± 0.66
ACFF 2000	34.97	35.37	36.78	35.71 ± 0.95
ACFF 1200	72.96			
3M™ Nuisance Adsorbent -	68.45			

Pore Size (nm)				
ACF Type	Sample 1	Sample 2	Sample 3	Mean ± SD
ACFF 1800	1.80	1.80	1.83	1.80 ± 0.02
ACFF 2000	1.92	1.92	1.90	1.91 ± 0.01
ACFF 1200	1.82			
3M™ Nuisance Adsorbent -	1.86			

APPENDIX D

ACF PRESSURE DROP MEASUREMENTS

Contains a summary of pressure drop measurement for each media type. Each media was tested at 3 face velocities for N=1-4 consecutive layers.

Appendix Table D.1 Pressure drop measurements for consecutive layers of ACFF 1200 media, tested at three face velocities.

ACFF 1200 - ΔP (mm H_2O)				
Layer	Depth	ΔP at 7.6 cm/s	ΔP at 10 cm/s	ΔP at 14 cm/s
1	0.25	2.83	3.4	4.9
2	0.5	5.69	6.91	9.84
3	0.75	8.44	10.47	14.9
4	1	11.6	14.41	20.55

Appendix Table D.2 Pressure drop measurements for consecutive layers of ACFF 1800 media, tested at three face velocities.

ACFF 1800 - ΔP (mm H_2O)				
Layer	Depth	ΔP at 7.6 cm/s	ΔP at 10 cm/s	ΔP at 14 cm/s
1	0.30	4.69	5.71	8.05
2	0.6	9.81	12.13	17.3
3	0.9	15.59	19.3	27.18
4	1.2	20.6	25.21	36.13

Appendix Table D. 3 Pressure drop measurements for consecutive layers of ACFF 2000 media, tested at three face velocities.

ACFF 2000 - ΔP (mm H_2O)				
Layer	Depth	ΔP at 7.6 cm/s	ΔP at 10 cm/s	ΔP at 14 cm/s
1	0.3	4.41	5.42	7.66
2	0.6	8.82	10.93	15.67
3	0.9	14.58	18.06	25.6
4	1.2	20.53	25.51	36.82

Appendix Table D.4 Pressure drop measurements for consecutive layers of 3M™ Nuisance Adsorbent media, tested at three face velocities.

3M™ Nuisance Adsorbent Media - ΔP (mm H_2O)				
Layer	Depth	ΔP at 7.6 cm/s	ΔP at 10 cm/s	ΔP at 14 cm/s
1	0.1	1.82	2.24	3.3
2	0.2	3.69	4.59	6.68
3	0.3	5.46	6.85	9.75
4	0.4	7.31	9.01	13.01

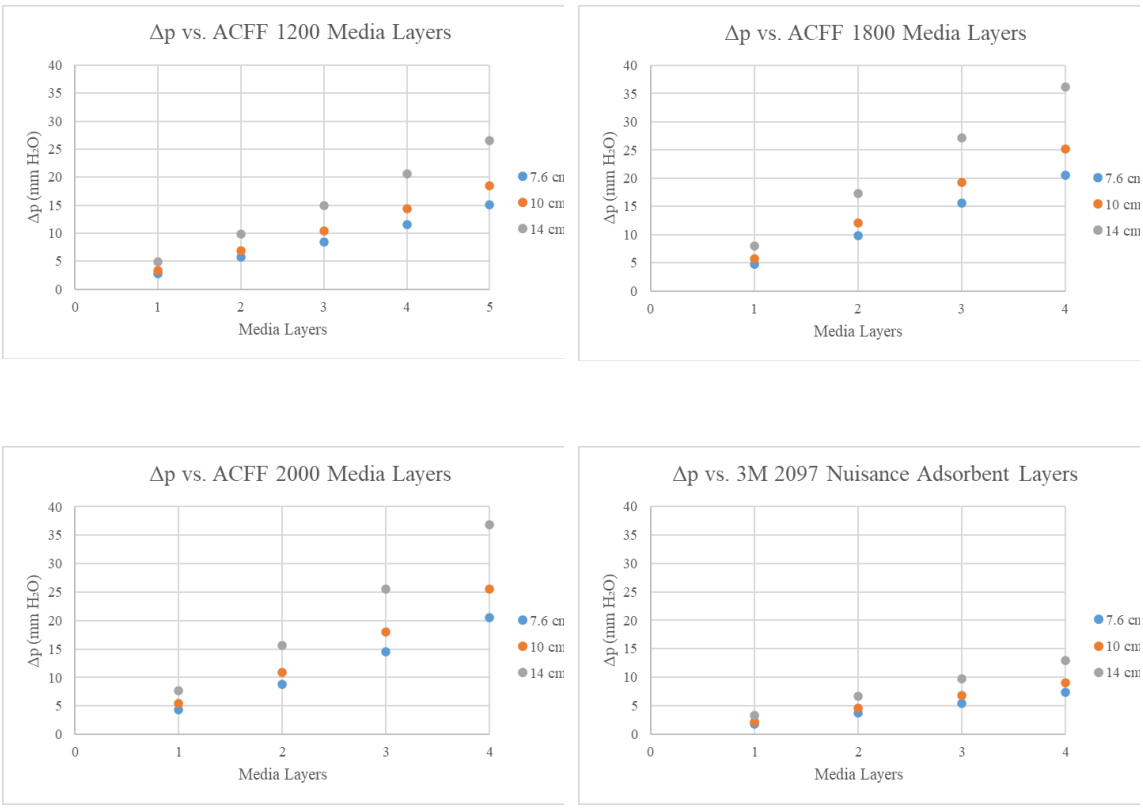

Appendix Figures D.1 – D.4. Pressure drop for each media type (ACFF 1200, ACFF 1800, ACFF 2000, and 3M™ 2097 Nuisance Adsorbent). Measurements were taken for consective media layers at three different face velocities.

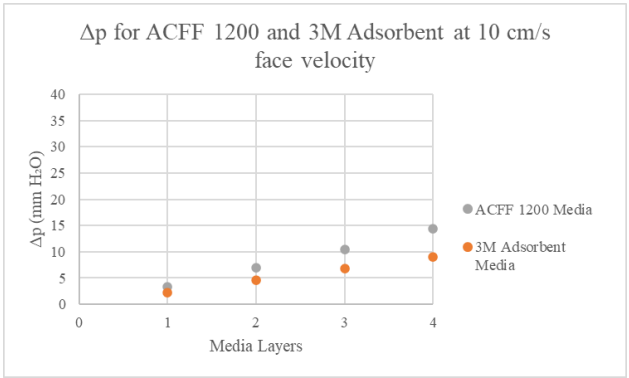

Appendix Figure D.5. Comparison of pressure drop measurements at 10 cm/s face velocity for a single layer of ACFF 1200 and 3M™ 2097 Nuisance Adsorbent media.

APPENDIX E

TEST AEROSOL CHARACTERISTICS

Contains summary statistics for the test aerosol used in filtration studies, to include CMD, GSD, number concentration and mass concentration.

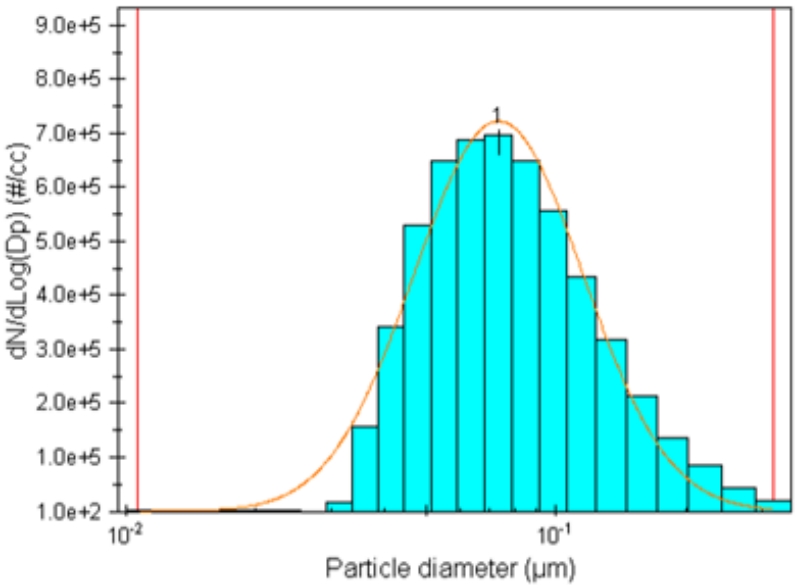

Data Statistics

	Number	Length	Surface	Mass
Mode (µm)	7.313e-2	8.474e-2	1.343e-1	2.212e-1
Mean (µm)	8.533e-2	1.078e-1	1.377e-1	1.716e-1
Std. Dev. (µm)	4.38e-2	5.676e-2	6.835e-2	7.455e-2
G. Mean (µm)	7.671e-2	9.549e-2	1.22e-1	1.548e-1
GSD	1.565e+0	1.625e+0	1.645e+0	1.602e+0
Tot. Conc.	3.577e+5	3.145e+4	1.105e+4	2.638e+2
Tot. Y Value	5.546e+6	4.732e+5	1.603e+5	3.678e+3

Fitting Parameters

Number	Peak #1	Peak #2	Peak #3	Peak #4
G. Mean (µm)	7.345e-2	0.e+0	0.e+0	0.e+0
GSD	1.573e+0	0.e+0	0.e+0	0.e+0
Tot. Area	3.565e+5	0.e+0	0.e+0	0.e+0
Rel. FWHM	1.118e+0	0.e+0	0.e+0	0.e+0
Peak Value	7.226e+5	0.e+0	0.e+0	0.e+0
R^2	9.75e-1			

Appendix Figure E.1. Summary statistics for NaCl test aerosol, as reported by MSP Corporation's Data Commander software. These data are the average of four consecutive measurements. The report shows a polydisperse aerosol with CMD of 76.7 nm and GSD of 1.56. As a validation of the above report, the raw data from the size distribution was used to independently calculate CMD and GSD of the test aerosol (see Appendix Figure E.2).

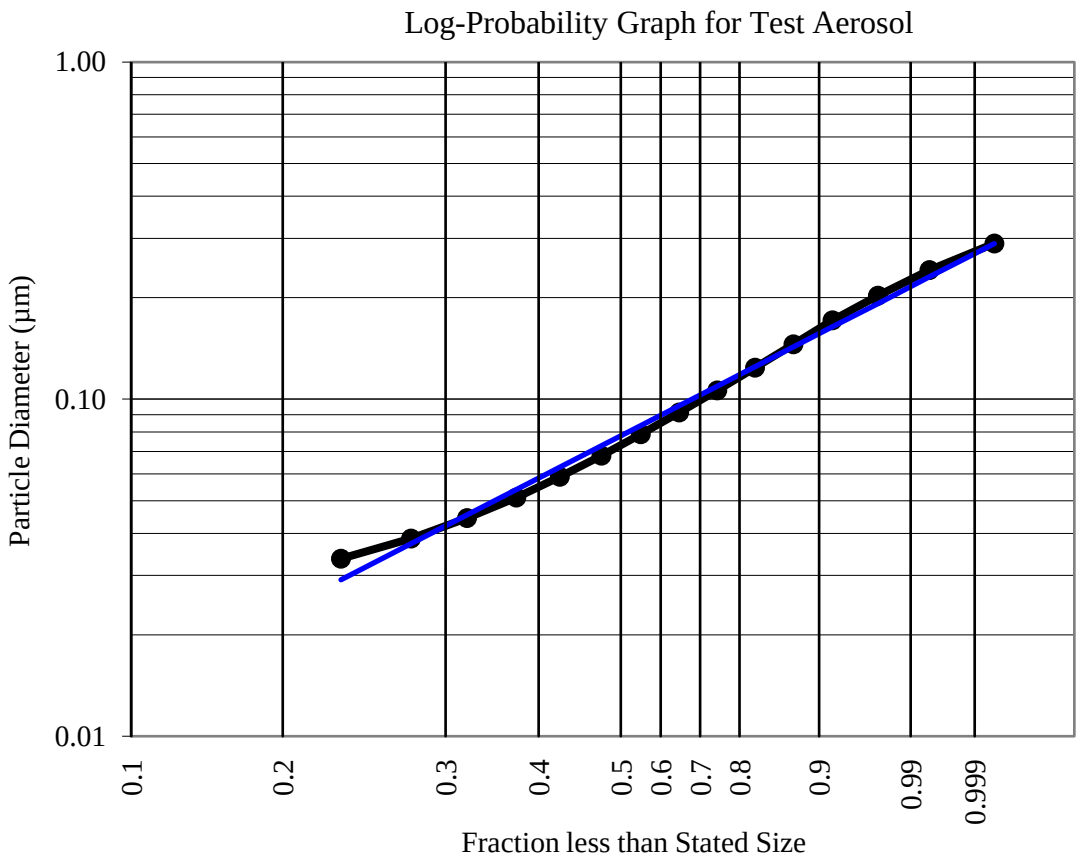

Appendix Figure E.2. Log probability chart for test aerosol. The x-axis is a cumulative fraction scale that is compressed near the median. A cumulative plot of aerosol count data yield a straight line, indicating a lognormal distribution. A best fit line appears above in blue ($R^2 = 0.9970$).

Appendix Table E.1 Data Processing from best fit line on Log-Probability Graph, where CMD is the diameter at 0.50th fraction on the fitted line, and GSD is the ratio of the diameters at 0.50th and 0.84th fractions.

CMD (µm)	73.03
84th percentile size (µm)	150
Percent under 100 nm (%)	72
GSD	1.71
r^2	1

Appendix Table E.2. Log probability chart data inputs.

Channel Median Diameter(nm)	Number concentration (#/cc) (N= 4 scans)	Cumulative Frequency for Log Probability Plot
31.47	17603	0.0433
36.12	24931	0.1046
41.5	33529	0.1871
47.745	40276	0.2862
55.005	41938	0.3893
63.47	43637	0.4966
73.385	41637	0.5990
85.045	37831	0.6921
98.82	33075	0.7734
115.19	27456	0.8410
134.77	21751	0.8945
158.37	16081	0.9340
187.03	12298	0.9643
222.15	7975	0.9839
265.595	4453	0.9948
319.83	2095	1.0000
	Σ = 406568	

APPENDIX F

MEDIA CHARACTERIZATION BY WEIGHT & SOLIDITY

Shows ACFF weight measurements, bulk density and filter solidity (α) calculations for each ACF type.

Appendix Table F. 1. ACFF weight measurements for 6 cm diameter ACFF cuttings. used in Solidity Calculations (Tables E.2 -E.4).

ACFF Weights (mg) per 6 cm diameter cutting			
Measurement	ACFF 1200	ACFF 1800	ACFF 2000
1	447.00	425.18	383.11
2	433.50	409.56	426.86
3	433.67	430.90	401.24
4	430.50	405.75	422.02
5	329.90	416.76	423.32
6	331.87	479.85	424.43
7	338.67	481.00	419.00
8	347.50	480.70	412.99
Mean ± STDEV	386.58±53.49	441.21±33.50	414.12±14.97

Appendix Table F.2. Packing Density (α) calculation for ACFF 1200 media.

Solidity Calculation Attempt - ACFF 1200		
Material Type		ACFF 1200
Literature Skeletal Density for Activated Carbon	2.00	grams/cm³
Filter mass	0.3865	grams
Filter thickness	2.5	millimeter
Filter diameter	6	cm
Filter cross sectional area	28.2743	cm²
Filter volume	7.0686	cm³
solids volume (filter mass/fiber density)	0.1933	cm³
Alpha (solid volume/filter volume)	0.0273	-
Bulk Density (filter mass/filter volume)	0.0547	grams/cm³

Appendix Table F.3. Packing Density (α) calculation for ACFF 1800 media.

Solidity Calculation Attempt - ACFF 1800		
Material Type		ACFF 1800
Literature Skeletal Density for Activated Carbon	2.00	grams/cm³
Filter mass	0.4412	grams
Filter thickness	3	millimeter
Filter diameter	6	cm
Filter cross sectional area	28.2743	cm²
Filter volume	8.4823	cm³
solids volume (filter mass/fiber density)	0.2206	cm³
Alpha (solid volume/filter volume)	0.0260	-
Bulk Density (filter mass/filter volume)	0.0520	grams/cm³

Appendix Table F.4. Packing Density (α) calculation for ACFF 2000 media.

Solidity Calculation Attempt - ACFF 2000		
Material Type		ACFF 2000
Literature Skeletal Density for Activated Carbon	2.00	grams/cm³
Filter mass	0.4141	grams
Filter thickness	3	millimeter
Filter diameter	6	cm
Filter cross sectional area	28.2743	cm²
Filter volume	8.4823	cm³
solids volume (filter mass/fiber density)	0.2071	cm³
Alpha (solid volume/filter volume)	0.0244	-
Bulk Density (filter mass/filter volume)	0.0488	grams/cm³

APPENDIX G

MPPS CALCULATION

Contains a sheet showing input parameters for calculation of Most Penetrating Particle size for each media type when tested at a 10 cm/s airflow.

The MPPS for each media type, given a face velocity of 10 cm/s and assuming 293.K ambient temperature and 101.3 kPa ambient pressure, was determined using Appendix F Equation 1, below:

Appendix F. Equation 1.

$$D_{p,min} = 0.885\left(\left(\frac{K}{1-\alpha}\right)\left(\frac{\sqrt{\lambda}\,kT}{\mu}\right)\left(\frac{D_f^2}{u}\right)\right)^{\frac{2}{9}}$$

where $D_{p,\,min}$= minimum efficiency diameter, or most penetrating particle size
K=Kuwubara hydrodynamic factor
α= solidity, or fiber volume fraction of the material
u= face velocity
λ = mean free path of gas molecules (6.65×10^{-8} m)
k= Boltzmann's constant
μ = gas viscosity (1.80×10^{-5} Pa)
T= absolute temperature

Appendix Table G.1. MPPS calculation sheet for ACFF 1200 media.

Most penetrating size (Hinds 9-34, 9-35) - ACFF 1200		
Temperature	293.15	Kelvin
Pressure	101.3	kPa
Fiber diameter	8	μm
Solidity or packing density (alpha)	0.02734	
Gas velocity	0.1	m/s
Air viscosity =	1.80711E-05	Pa*s
Molecular mean free path =	6.65323E-08	m
K (hydrodynamic factor) =	1.076855355	
Most penetrating size =	0.4350	μm

Appendix Table G.2 MPPS calculation sheet for ACFF 1800 media

Most penetrating size (Hinds 9-34, 9-35) - ACFF 1800		
Temperature	293.15	Kelvin
Pressure	101.3	kPa
Fiber diameter	8	μm
Solidity or packing density (alpha)	0.026	
Gas velocity	0.1	m/s
Air viscosity =	1.80711E-05	Pa*s
Molecular mean free path =	6.65323E-08	m
K (hydrodynamic factor) =	1.10066037	
Most penetrating size =	0.4370	μm

Appendix Table G.3 MPPS calculation sheet for ACFF 2000 media

Most penetrating size (Hinds 9-34, 9-35) - ACFF 2000		
Temperature	293.15	Kelvin
Pressure	101.3	kPa
Fiber diameter	8	µm
Solidity or packing density (alpha)	0.0244	
Gas velocity	0.1	m/s
Air viscosity =	1.80711E-05	Pa*s
Molecular mean free path =	6.65323E-08	m
K (hydrodynamic factor) =	1.130837233	
Most penetrating size =	0.4394	µm

APPENDIX H

FILTRATION AND QUALITY FACTOR SUMMARY TABLES

Contains summary tables describing filtration efficiency for each media type when tested at a 10 cm/s airflow and up to N=1-4 layers of media; contains quality factor calculation sheet and summary table.

Appendix Table H1. ACFF 1200 Media Filtration Summary at 10 cm/s airflow, n=3 filtration trials and N=4 layers of media.

Layers (N)	Fractional Filtration Efficiency (FE)	Stdev	Penetration (P)	$P_{predicted}$, *Layers 2-4*	$FE_{predicted}$, *Layers 2-4*	Percent Difference $FE_{Predicted}$ *vs.* $FE_{Measured}$
1	0.5675	0.0139	0.4325			
2	0.8443	0.0333	0.1557	*0.1871*	*0.8129*	3.7138
3	0.9527	0.0140	0.0473	*0.0809*	*0.9191*	3.5281
4	0.9551	0.0267	0.0449	*0.0350*	*0.9650*	-1.0384

Appendix Table H2. ACFF 1800 Media Filtration Summary at 10 cm/s airflow, n=4 filtration trials and N=4 layers of media.

Layers (N)	Fractional Filtration Efficiency (FE)	Stdev	Penetration (P)	$P_{predicted}$, *Layers 2-4*	$FE_{predicted}$, *Layers 2-4*	Percent Difference $FE_{Predicted}$ *vs.* $FE_{Measured}$
1	0.6684	0.3316	0.3316			
2	0.8662	0.1730	0.1338	0.1099	0.8901	-2.7588
3	0.9400	0.0426	0.0600	0.0364	0.9636	-2.5096
4	0.9853	0.1300	0.0147	0.0121	0.9879	-0.2622

Appendix Table H3. ACFF 2000 Media Filtration Summary at 10 cm/s face velocity, n=3 filtration trials and N=4 layers of media.

Layers (N)	Fractional Filtration Efficiency (FE)	Stdev	Penetration (P)	$P_{predicted}$, *Layers 2-4*	$FE_{predicted}$, *Layers 2-4*	Percent Difference $FE_{Predicted}$ *vs.* $FE_{Measured}$
1	0.6822	0.0415	0.3178			
2	0.9477	0.0112	0.0523	*0.1010*	*0.8990*	5.1365
3	0.9744	0.0131	0.0256	*0.0321*	*0.9679*	0.6651
4	0.9989	0.0001	0.0011	*0.0102*	*0.9898*	0.9071

Appendix Table H.5. 3M™ 2097 Nuisance Adsorbent Media Filtration Summary at 10 cm/s face velocity, n=3 filtration trials, and N=1 layer of media.

Layers (N)	Fractional Filtration Efficiency (FE)	Stdev	Penetration (P)	$P_{predicted}$, *Layers 2-4*	$FE_{predicted}$, *Layers 2-4*	Percent Difference $FE_{Predicted}$ *vs.* $FE_{Measured}$
1	0.4418	0.0127	0.5582	-	-	-

Appendix Table H.6. Filtration Summary for North Brand N95 Respirator (*#7130N95S*) at 10 cm/s face velocity, n=3 filtration trials, and N=1 layer of media.

Layers (N)	Fraction Filtration Efficiency (FE)	Stdev	Penetration (P)	$P_{predicted}$, *Layers 2-4*	$FE_{predicted}$, *Layers 2-4*	Percent Difference $FE_{Predicted}$ *vs.* $FE_{Measured}$
1	0.9741	0.0185	0.0259	-	-	-

Appendix Table H.7. Filter Quality Factor calculation sheet for N=1 layer of media and 10 cm/s airflow.

Media	Fractional FE	Penetration	Pressure drop (mm H_2O)	Quality Factor (mm $H2O^{-1}$)
ACFF 1200	0.6822	0.3178	5.42	0.0215
ACFF 1800	0.6684	0.3316	5.71	0.0197
ACFF 2000	0.5675	0.4325	3.4	0.0251
3M™ 2097 Adsorbent	0.4418	0.0639	2.24	0.1252

APPENDIX I

ACF SEM IMAGES

SEM images (50X – 5000X) of each ACF. Images were taken at University of Alabama Department of Physics and Astronomy using an Apreo™ 2 Scanning Electron Microscope operated at 20 kV voltage and 0.40 nA current.

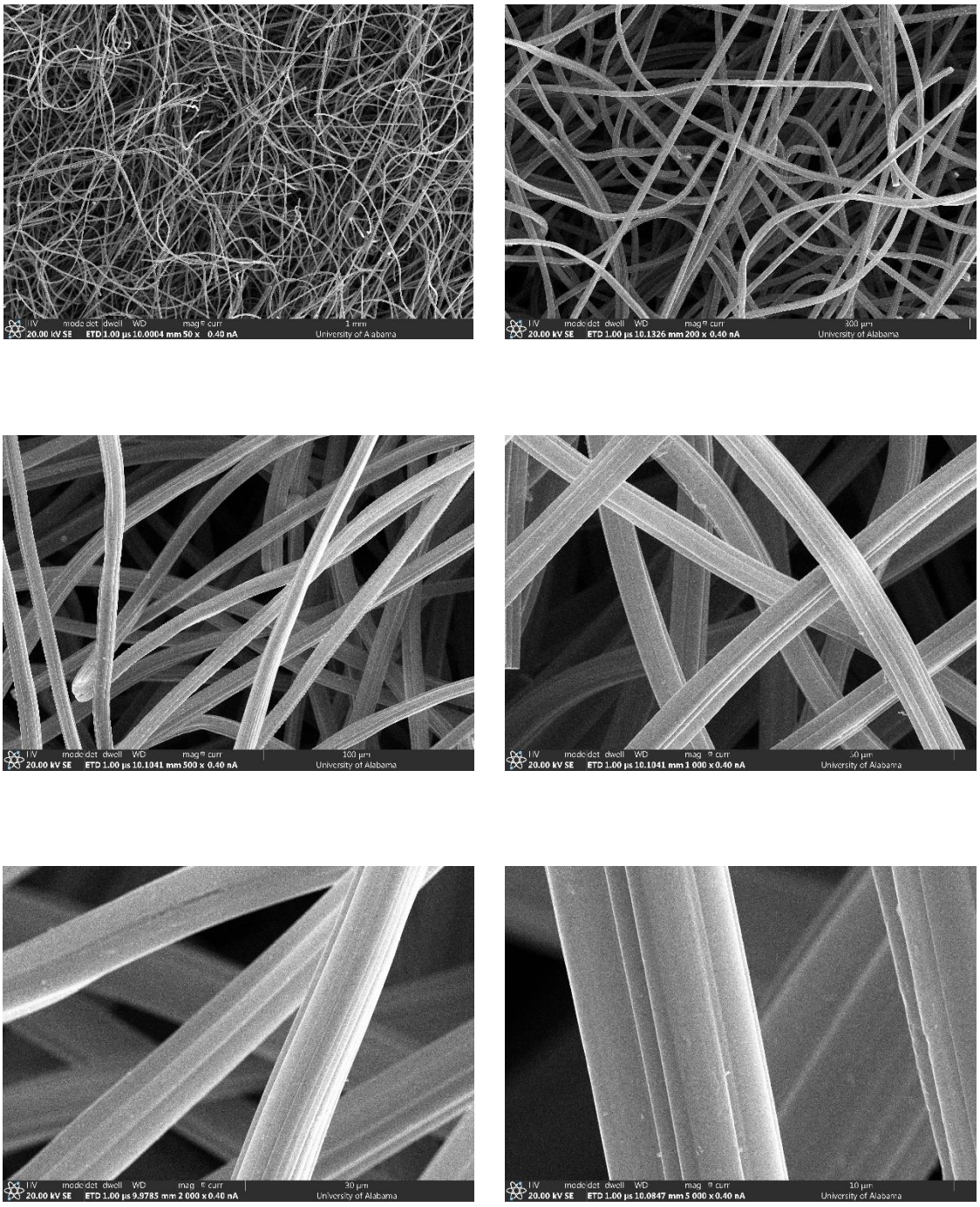

Appendix Figures I.1 – I.6 (left to right). SEM Images of ACFF 1200 at 50X, 200X, 500X, 1000X, 2000X, and 5000X, respectively.

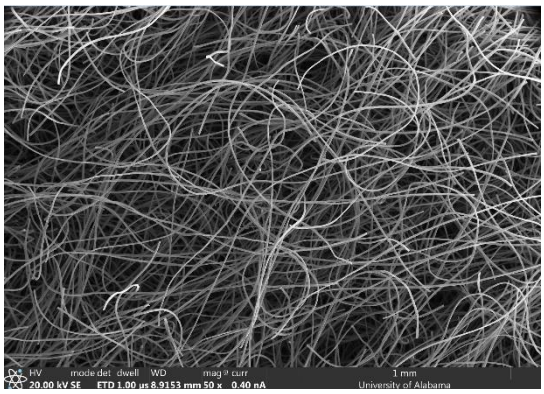

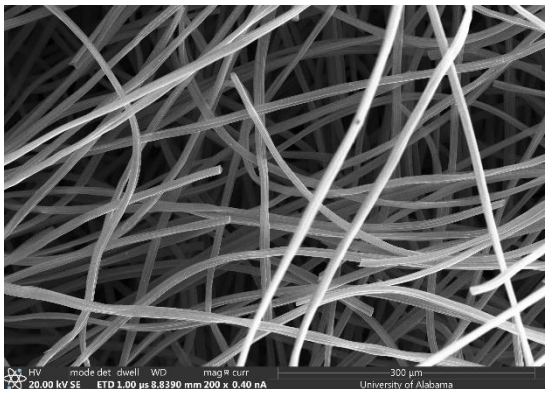

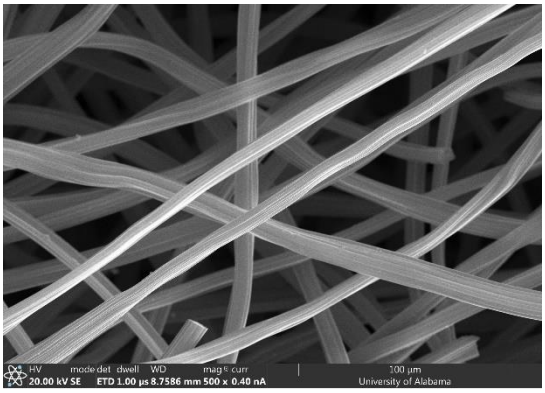

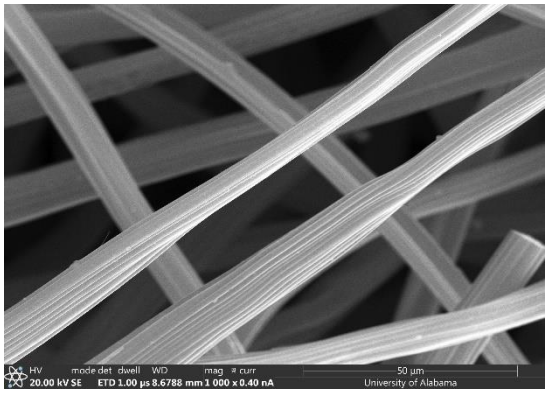

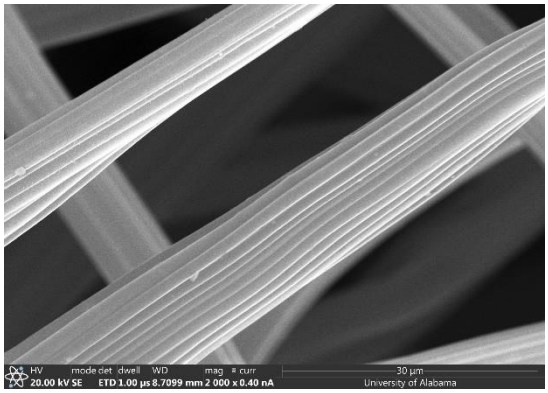

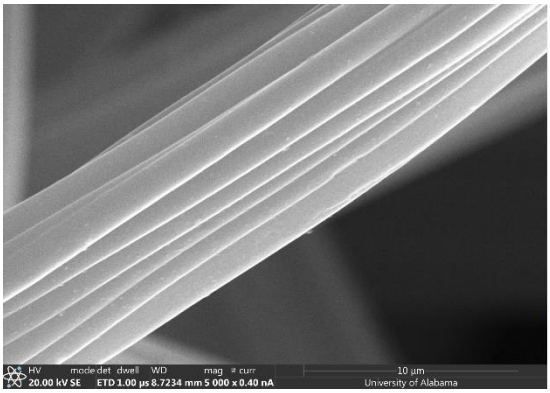

Appendix Figures I.7 – I.12 (left to right). SEM Images of ACFF 1800 at 50X, 200X, 500X, 1000X, 2000X, and 5000X, respectively.

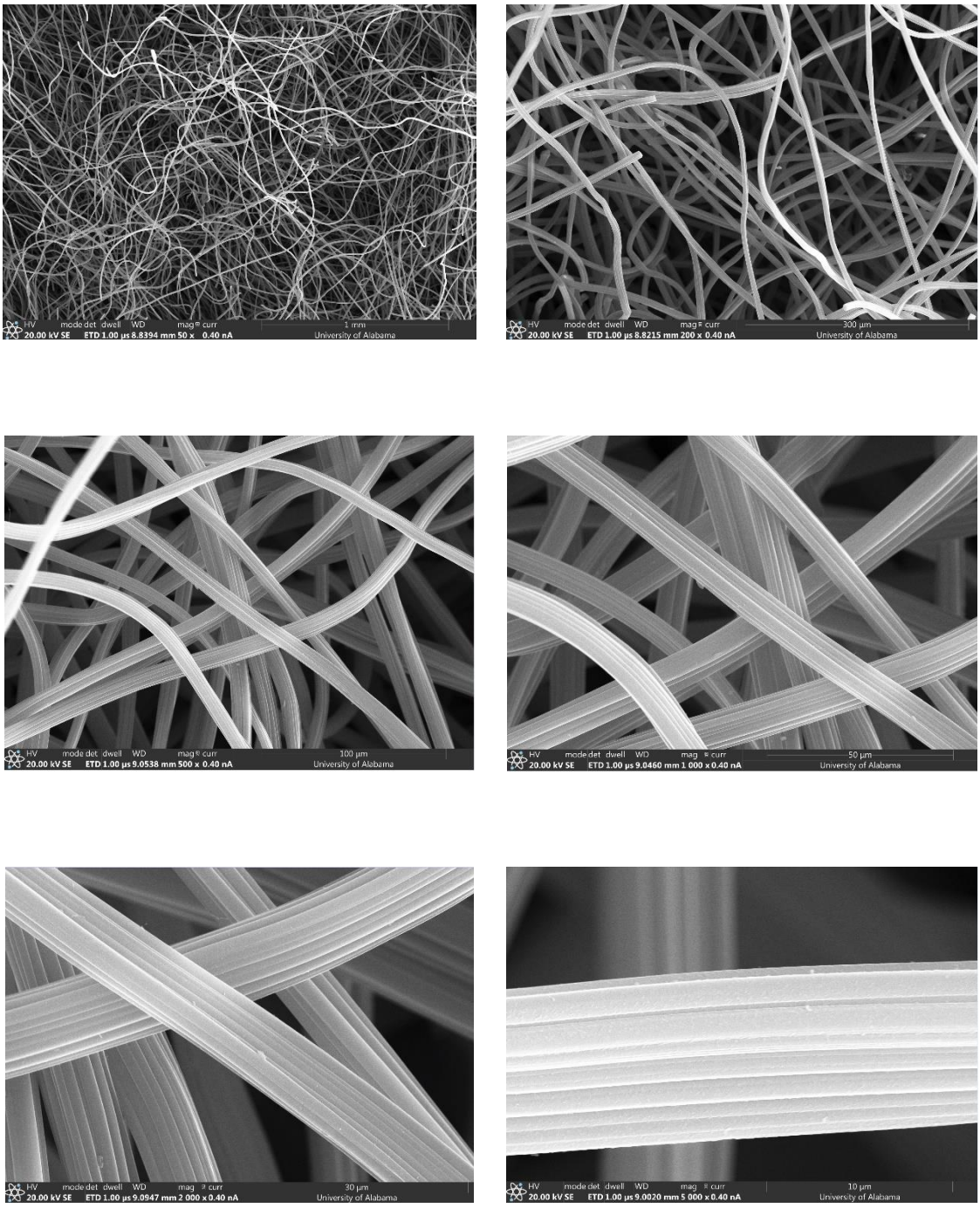

Appendix Figures I.13 – I.18. SEM Images of ACFF 2000 at 50X, 200X, 500X, 1000X, 2000X, and 5000X, respectively.

APPENDIX J

EQUILIBRIUM ADSORPTION CAPACITY CALCULATIONS

Contains calculation worksheets for the determination of ACFF 1800 and ACFF 2000 equilibrium adsorption capacities using D-R equation and carbon parameters derived from N_2 isotherm data.

Appendix Table J.1. ACFF 1800 equilibrium adsorption capacity for toluene, n-hexane, and MEK, based on adsorbate properties and carbon parameters (W_e and E_0) derived from N_2 isotherm data. Experimental capacities are shown below the calculated capacities.

Input Parameters			
Adsorbate	Toluene	n-Hexane	MEK
Molecular weight (g/mol)	92.14	86.16	72.11
Liquid Density (g/cm^3)	0.8669	0.6603	0.8054
Benzene Molecular Polarizability	26.259	26.259	26.259
Adsorbate Molecular Polarizability	31.054	29.877	20.681
β (Affinity Coefficient to Benzene)	1.162934967	1.123189212	0.80661077
P_{sat} in mmHg at 25 ºC	21	124	78
Adsorbate Partial Pressure (mm Hg)	0.152	0.152	0.152
Temperature (K)	298	298	298
Adsorption Energy (kJ/mol)	17.2583	17.2583	17.2583
W_o, micropore capacity (cm^3/gram)	0.5792	0.5792	0.5792
Capacity Calculations			
Ln (W_o)	-0.546107438	-0.546107438	-0.546107438
$P_{sat}/P_{partial}$	138.1578947	815.7894737	513.1578947
$\ln(P_{sat}/P_{partial})$	4.928397196	6.704156324	6.240583585
Gas constant (R)	0.0083145	0.0083145	0.0083145
$RT/\beta E_o$	0.123452236	0.12782078	0.177987856
$(RT/\beta E_o) \cdot \ln (P_{sat}/P_{partial})$	0.608421651	0.856930492	1.110748092
$[(RT/\beta E_o) \cdot \ln (P_{sat}/P_{partial})]^2$	0.370176906	0.734329868	1.233761323
$\ln(W_o) - [(RT/\beta E_o) \cdot \ln (P_{sat}/P_{partial})^2]$	-0.916284344	-1.280437306	-1.779868761
exp(Above Field)	0.400002555	0.27791574	0.168660281
liquid density * Above Field	0.346762215	0.183507763	0.13583899
Calculated Capacity (mg/g)	*346.76*	*183.51*	*135.84*
Experimental Capacity (mg/g)	*344.09*	*195.5*	*165.61*

Appendix Table J.2. ACFF 2000 equilibrium adsorption capacity for toluene, n-hexane, and MEK, based on adsorbate properties and carbon parameters (W_e and E_0) derived from N_2 isotherm data. Experimental capacities are shown below the calculated capacities.

Input Parameters			
Adsorbate	Toluene	n-Hexane	MEK
Molecular weight (g/mol)	92.14	86.16	72.11
Liquid Density (g/cm^3)	0.8669	0.6603	0.8054
Benzene Molecular Polarizability	26.259	26.259	26.259
Adsorbate Molecular Polarizability	31.054	29.877	20.681
β (Affinity Coefficient to Benzene)	1.162934967	1.123189212	0.80661077
P_{sat} in mmHg at 25 ºC	21	124	78
Adsorbate Partial Pressure (mm Hg)	0.152	0.152	0.152
Temperature (K)	298	298	298
Adsorption Energy (kJ/mol)	16.8875	16.8875	16.8875
W_o, micropore capacity (cm^3/gram)	0.6732	0.6732	0.6732
Capacity Calculations			
Ln (W_o)	-0.395712817	-0.395712817	-0.395712817
$P_{sat}/P_{partial}$	138.1578947	815.7894737	513.1578947
$\ln(P_{sat}/P_{partial})$	4.928397196	6.704156324	6.240583585
Gas constant (R)	0.0083145	0.0083145	0.0083145
$RT/\beta E_o$	0.123452236	0.12782078	0.177987856
$(RT/\beta E_o) \cdot \ln (P_{sat}/P_{partial})$	0.608421651	0.856930492	1.110748092
$[(RT/\beta E_o) \cdot \ln (P_{sat}/P_{partial})]^2$	0.370176906	0.734329868	1.233761323
$\ln(W_o) - [(RT/\beta E_o) \cdot \ln (P_{sat}/P_{partial})^2]$	-0.765889723	-1.130042685	-1.62947414
exp(Above Field)	0.464920097	0.323019468	0.196032633
liquid density * Above Field	0.403039232	0.213289755	0.157884682
Calculated Capacity (mg/g)	*403.04*	*213.29*	*157.88*
Experimental Capacity (mg/g)	*380.59*	*220.7*	*146.87*

APPENDIX K

ADSORPTION RATE COEFFICIENT CALCULATIONS

Contains calculation worksheets for the determination of adsorption rate coefficients (k_v) per the semi-empirical relationship described by Lodewyckx and Wood in 2003.

Appendix Table K.1. and K.2 ACFF 1800 and ACFF 2000 k_v calculations.

ACFF 1800 - Input Parameters			
Adsorbate	Toluene	n-Hexane	MEK
Molecular weight (g/mol)	92.14	86.16	72.11
Liquid Density (g/cm3)	0.8669	0.6603	0.8054
Molecular Polarizability of Benzene	26.259	26.259	26.259
Molecular Polarizability of Adsorbate	31.054	29.877	20.681
β (Affinity Coefficient to Benzene)	1.18260406	1.137781332	0.787577592
Linear velocity (v_L) (cm/s)	10	10	10
Fiber diameter (d_p) (cm)	0.001	0.001	0.001
W_e (calculated Capacity)(g/g)	0.346762215	0.183507763	0.13583899
Kinetic Rate Coefficient Calculations			
$\beta^{0.33}$	1.056907526	1.043516704	0.924223072
$v_L^{0.75}$	5.623413252	5.623413252	5.623413252
$d_p^{-1.5}$	31622.7766	31622.7766	31622.7766
W_e/M_w	0.003763428	0.002129849	0.001883775
$(W_e/M_w)^{0.5}$	0.061346781	0.046150284	0.043402473
$\beta^{0.33} v_L^{0.75} d_p^{-1.5} [(W_e/M_w)^{0.5}]$	11529.98576	1459.400112	1372.506703
$800 \cdot [\beta^{0.33} v_L^{0.75} d_p^{-1.5} [(W_e/M_w)^{0.5}]$	9.224E+06		
kv (min^{-1})	*9.224E+06*		

ACFF 2000 - Input Parameters			
Adsorbate	Toluene	n-Hexane	MEK
Molecular weight (g/mol)	92.14	86.16	72.11
Liquid Density (g/cm3)	0.8669	0.6603	0.8054
Molecular Polarizability of Benzene	26.259	26.259	26.259
Molecular Polarizability of Adsorbate	31.054	29.877	20.681
β (Affinity Coefficient to Benzene)	1.18260406	1.137781332	0.787577592
Linear velocity (v_L) (cm/s)	10	10	10
Fiber diameter (d_p) (cm)	0.001	0.001	0.001
W_e (calculated Capacity)(g/g)	0.403039232	0.213289755	0.157884682
Kinetic Rate Coefficient Calculations			
$\beta^{0.33}$	1.056907526	1.043516704	0.924223072
$v_L^{0.75}$	5.623413252	5.623413252	5.623413252
$d_p^{-1.5}$	31622.7766	31622.7766	31622.7766
W_e/M_w	0.004374205	0.002475508	0.002189498
$(W_e/M_w)^{0.5}$	0.066137772	0.049754475	0.046792069
$\beta^{0.33} v_L^{0.75} d_p^{-1.5} [(W_e/M_w)^{0.5}]$	2091.459973	1573.374663	1479.695153
$800 \cdot [\beta^{0.33} v_L^{0.75} d_p^{-1.5} [(W_e/M_w)^{0.5}]$	1.673E+06		
kv (min^{-1})			